EPRI
Electric Power
Research Institute

Keywords:
Fourier Transform Infrared Analysis
Coal Devolatilization
Coal Pyrolysis
Coal Gasification
Entrained Flow Laboratory Reactor
Infrared Spectroscopy

EPRI AP-2603
Project 1654-8
Final Report
July 1983

EPRI-AP--2603

DE83 902950

Analysis of Coal Devolatilization in a Laboratory-Scale Entrained Flow Reactor

Prepared by
Advanced Fuel Research, Inc.
East Hartford, Connecticut

Analysis of Coal Devolatilization in a Laboratory-Scale Entrained-Flow Reactor

AP-2603
Research Project 1654-8

Final Report, July 1983

Prepared by

ADVANCED FUEL RESEARCH, INC.
87 Church Street
East Hartford, Connecticut 06108

Principal Investigators
P. R. Solomon
D. G. Hamblen

Prepared for

Electric Power Research Institute
3412 Hillview Avenue
Palo Alto, California 94304

EPRI Project Manager
G. H. Quentin

Clean Gaseous Fuels Program
Advanced Power Systems Division

ORDERING INFORMATION

Requests for copies of this report should be directed to Research Reports Center (RRC), Box 50490, Palo Alto, CA 94303, (415) 965-4081. There is no charge for reports requested by EPRI member utilities and affiliates, U.S. utility associations, U.S. government agencies (federal, state, and local), media, and foreign organizations with which EPRI has an information exchange agreement. On request, RRC will send a catalog of EPRI reports.

NOTICE

Prepared by
Advanced Fuel Research, Inc.
East Hartford, Connecticut

ABSTRACT

The objective of this program is to develop the techniques to predict the pyrolysis behavior of a coal under conditions typical of entrained-flow gasifiers. To achieve this objective, measurements of coal pyrolysis were made in a dilute-phase, lab-scale entrained-flow reactor which has the capacity for in-situ analysis by FT-IR. These data were used to modify and validate a general coal-pyrolysis theory under development at Advanced Fuel Research, Inc. The theory predicts pyrolysis product yields and compositions in detail, and provides a foundation for modeling phenomena such as ignition, swelling, char reactivity, methane yield, and the formation and gasification of tar and soot.

Six coals (Pittsburgh #8, two Illinois #6 and a Utah bituminous, a Wyoming subbituminous and a Montana lignite) were pyrolyzed at temperatures from 700°C to 1200°C for times from 6 to 660 milliseconds. Data were obtained for char and tar composition and gas yields as functions of reaction time and temperature. Material balances near 90% were obtained for the most recent tests.

Results from the entrained-flow-reactor experiments indicate that FT-IR is an excellent way to measure gas evolution (including in-situ measurements of species and temperature) and functional group changes in the reactants. The measurements have yielded additional evidence that coal-pyrolysis kinetics are insensitive to coal rank. Good agreement between theory and experiment have been obtained using a set of distributed kinetic rate coefficients which fit experiments differing substantially in configuration, temperature and reaction time.

EPRI PERSPECTIVE

PROJECT DESCRIPTION

This final report, Analysis of Coal Devolatilization in a Laboratory-Scale Entrained Flow Reactor, describes a study of thermal decomposition of coals of different rank using in situ measurement of gas composition by Fourier transform infrared (FTIR) spectroscopy (under RP1654-8).

In a prior study (see EPRI Report AP-2602), Advanced Fuel Research, Inc., (AFR) used FTIR for off-line analysis of coal and char samples from another laboratory-scale entrained flow reactor operated by Combustion Engineering, Inc. (C-E). Those samples were prepared under various operating conditions during the study of combustion and gasification by C-E (see EPRI Report AP-2601).

In a coal gasifier, the release of volatile matter from coal (devolatilization) and subsequent gas-phase reactions are integral phenomena that occur as coal initially decomposes (see EPRI Report AP-1803). The yield and fate of volatile matter vary greatly with coal type and can affect the design and operation of a gasification reactor. Therefore, computer simulation models of large-scale gasifiers (see EPRI Reports AF-590, AF-1179, AP-2576, and AP-2740) generally include experimental correlations for such phenomena since they are not readily described from first principles.

Existing correlations of coal devolatilization rates have been based on experiments in a heated grid apparatus in which evolving gases are promptly removed from the decomposing coal char, thereby inhibiting secondary reactions. Effective experimental methods for more immediate analysis of devolatilization and other reaction phenomena in a realistic gasification environment are therefore essential for developing improved correlations.

PROJECT OBJECTIVES

This study is a pioneering effort to scrutinize devolatilization closely by means of laboratory experiments that feature in situ FTIR measurement in a small-scale

entrained flow reactor. It represents an attempt to distinguish between the effects of primary reactions (release) and secondary (gas-phase) reactions of volatile matter during coal gasification. The ultimate intent is to obtain improved correlations of devolatilization.

Another goal is to evaluate on-line gas-phase measurement of composition and temperature in a laboratory-scale reactor using FTIR analysis for possible application of such methods in larger pilot plant reactors.

PROJECT RESULTS

The experimental reactor was newly constructed for this study to permit in situ FTIR measurement. It proved capable of yielding data under conditions of interest for coal gasification studies. The reactor was designed for complete collection of devolatilization products (i.e., char, tar, and gases) to provide accurate mass balances and a sufficient data base for improved rate correlations. However, following the initial operation of the reactor in this study, modifications to the apparatus were necessary to improve solids collection. Typical closure of material balances was in the range of 80 to 95% during later stages of the work.

On-line gas composition was compared at two points. FTIR analysis was made both at the in situ port where the gas could be measured at reactor conditions and at a downstream cell where a gas sample could be collected and measured at ambient conditions. An initial comparison based on a single run indicated that the in situ and the downstream composition measurements were similar, although not identical. Additional comparisons were made in a subsequent study for the DOE; they revealed no substantial difference between the in situ and the downstream gas composition measurements. The downstream cell offered an advantage for FTIR analysis because the signal could be enhanced (e.g., greater path length) to reduce noise levels, allowing additional trace species (e.g., hydrogen cyanide) to be identified.

The gas temperature was calculated from the FTIR spectra for carbon monoxide and was measured by suction pyrometer at the in situ optical port for comparison. The FTIR calculated value was 1050°C compared with 930°C for the pyrometer; however, some cooling is suspected in the latter. Although this indicates some potential for the FTIR technique, solids loading in a larger gasifier is an order of magnitude higher, and this generally creates problems for optical measurements (e.g., slag tends to obscure optical ports). Considerable development would be necessary to apply the

FTIR analysis for temperature measurement in a larger reactor. Other techniques (e.g., laser measurements) may have a greater chance for success, with the additional prospect for precise resolution in space and time.

The experimental results determined kinetic rate coefficients for the pyrolysis of a number of coal components (or functional groups). These data agreed well with prior correlations developed by AFR from heated grid experiments. In those empirical correlations, the rate coefficients are essentially independent of coal rank. The entrained flow reactor did provide a more comprehensive data base for the devolatilization correlations than the heated grid apparatus, since the evolving gases remained in contact with the solids phase, which allowed further (secondary) gas-solids reaction. However, the in situ FTIR measurement did not provide the anticipated resolution between the primary (release) and secondary (decomposition) reactions of volatile matter during coal gasification. Here again, laser techniques that are being applied elsewhere (i.e., for molecular-scale studies of pyrolysis and free radical reactions under sponsorship of the Gas Research Institute) may ultimately resolve these devolatilization phenomena for even more meaningful correlations.

In summary:

- The entrained flow reactor was an excellent means for experimental studies of devolatilization under realistic gasifier conditions, as it was for the earlier gasification studies by C-E (see EPRI AP-2601).

- The in situ FTIR measurement successfully measured gas composition and temperature in the presence of solids, i.e., at moderate loadings.

- However, the in situ gas composition measurement was not substantially different from a downstream cell measurement and therefore did not resolve primary and secondary devolatilization reactions.

- The higher solids loading in larger pilot plant reactors is generally a serious impediment for application of such optical measurements of temperature. However, the use of FTIR measurement of gas composition may be more conveniently applied to a slipstream after the gasifier, with appropriate cooling and filtering, as was used in this study. The additional information that FTIR can produce on key functional groups present in the heavier devolatilization species is a distinct advantage over more conventional analytic techniques.

- The experimental data base for coal devolatilization kinetics was extended by use of the entrained flow reactor, which allowed further gas-solids reaction than the heated grid apparatus. Results from

this study agreed well with the earlier heated grid correlations. Such empirical correlations appear suitable for inclusion in comprehensive gasifier simulation models (see EPRI AP-2740).

- This study was conducted at atmospheric pressure; it appears that further gasification studies in a high-pressure laboratory entrained flow reactor would provide conditions more nearly approximating those in larger pressurized gasifiers currently under development. For example, the cracking of methane is one reaction whose rate might be correlated with pressure.

This report is of particular interest for the coal gasification research community. The information produced by such experiments should be useful to developers of mathematical models for coal gasification reactor simulation studies in the course of gasifier design and development.

George H. Quentin, Project Manager
Advanced Power Systems Division

ACKNOWLEDGMENT

The authors would like to thank N. Y. Nsakala, G. J. Goetz, R. W. Seeker, Eric Suuberg and R. C. Flagan for their advice on various details of the experiment. The authors also express their appreciation for the encouragement given to this program by J. Yerushalmi, George Quentin and Leonard Naphtali.

CONTENTS

ILLUSTRATIONS

TABLES

SUMMARY

The objective of this program is to develop the techniques to predict the pyrolysis behavior of a coal under conditions typical of entrained flow gasifiers. To achieve this objective, measurements of coal pyrolysis were made in a dilute-phase, lab-scale entrained flow reactor which has the capacity for in-situ analysis by FT-IR. These theory under development at Advanced Fuel Research, Inc. The theory predicts pyrolysis product yields and compositions in detail, and provides a foundation for modeling phenomena such as ignition, swelling, char reactivity, methane yield and the formation and gasification of tar and soot.

The experimental facility provides control and measurement of process conditions, has provisions for collecting all pyrolysis products (i.e. char, tar, soot and the following gases: CO, CO_2, H_2O, CH_4, C_2H_2, C_2H_4, C_2H_6, C_3H_6, C_3H_8, C_4H_8, C_6H_6, NH_3, HCN, SO_2, COS, CS_2, CH_3OH, CH_3COOH, CH_3COCH_3, and achieves good material balance. It has optical access to the reaction zone and employs FT-IR for in-situ analysis of gas species and gas temperature. Coal pyrolysis data have been obtained at temperatures between 700°C and 1200°C and particle heating rates between 5,000 and 100,000°C/sec. at atmospheric pressure. The reactor is unique in the completeness of the pyrolysis data obtained, thus providing an adequate test of the pyrolysis predictions.

Four coals (Pittsburgh #8 and Illinois #6 bituminous coals, a Wyoming subbituminous coal and a Montana lignite) were tested during the initial operation of the reactor. Data were obtained for char composition and gas yields as functions of reaction time and temperature. Results from these tests suggested modifications to the sample collection procedures to improve mass balance. The modifications were made under DOE Contract #DE-AC21-81-FE05122. The reactor was subsequently used to study pyrolysis of a second Illinois #6 and a Utah bituminous coal under this project. These data have been compared with the pyrolysis model.

Results from the entrained flow reactor experiments indicate that FT-IR is an excellent way to measure gas evolution (including in-situ measurements of species and temperature) and functional group changes in the reactants. The measurements

have yielded additional evidence that coal pyrolysis kinetics are insensitive to coal rank. Good agreement between theory and experiment have been obtained using a set of distributed kinetic rate coefficients which fit experiments differing substantially in configuration, temperature and reaction time.

An assessment has been made of the application of the correlations obtained under this program to large scale gasifiers. There are three applications which have been identified. First, the correlations may be used to infer reactor conditions from the composition of chars, tars and gases sampled from the gasifier. Second, given the approximate conditions of the gasifier, predictions can be made for volatile yields, compositions and physical properties and their dependence on variations in coal or operating conditions. Third, the model can be integrated with previously developed computer codes for fluid mechanics and reaction chemistry to provide a truly predictive capability for gasifiers. The model appears capable of predicting the thermal decomposition phenomena which are of importance in coal gasification, but additional work is needed on volatile oxidation, swelling and char reactivity.

Section 1

INTRODUCTION

A key element in predicting coal gasification behavior is pyrolysis. This is the initial step in gasification, the step which controls the amount, physical structure and reactivity of the char and the step which is most dependent on the properties of the coal. Recent reviews of coal pyrolysis (1,2,3) conclude that the pyrolysis product distribution and apparent kinetic rates vary widely with the experimental measurement. Analysis of the reported data shows that the wide variation cannot be explained by variations in coal rank. It is clear that to establish a true predictive capability, additional work is needed to understand pyrolysis reactions, to separate chemical kinetics from heat and mass transfer effects and to define accurate rates.

Useful experiments for investigating pyrolysis have been performed with the captive sample, heated grid devices which have achieved good mass and elemental balances and have provided data on individual species evolution (4-15). An extensive set of heated grid data provided the basis for developing a general kinetic model of coal pyrolysis (11-15). The model considers the coal to be an ensemble of functional groups. During pyrolysis the functional groups decompose with rate coefficients which are insensitive to coal rank to form light gas species. Simultaneously, a representative sampling of functional groups evolves without decomposition. They evolve as constituents of coal molecule fragments which break off to form tar. Pyrolysis is viewed as "depolymerization" in parallel with thermal decomposition of the "monomers". The model predicts the time-and temperature-dependent evolutions of the products of thermal decomposition using: 1) a coal independent set of kinetic rate coefficients, 2) the coal's structural composition and 3) the time-temperature history of the coal. While the heated grid experiments are excellent for obtaining material balance and for minimizing secondary reactions, the heating of the coal is slower than in gasifiers so that the kinetic data is difficult to extrapolate to gasifier conditions.

Entrained flow reactors provide more realistic particle heating but have been employed primarily to study pyrolysis weight loss (16-23). In a separate complementary program (see EPRI Final Report, AP 2602) (21), the pyrolysis model under development at Advanced Fuel Research, Inc. (AFR) was compared with

experimental studies of coal pyrolysis performed at Combustion Engineering, using a laminar entrained flow reactor (called the Drop Tube Furnace system, DTFS) (16), similar to the one described by Badzioch and Hawksley (17). These experiments provided char samples reacted at various distances and temperatures. Analyses of the functional group composition of chars by Fourier Transform Infrared (FT-IR) Spectroscopy and analysis of physical properties by optical microscopy were performed at AFR and these data plus elemental analysis were compared with the theoretical predictions. The results of the study indicate that the AFR coal pyrolysis model could be used to predict char composition as a function of time and temperature in the entrained flow reactor. Full validation of the model, however, requires more complete pyrolysis data such as char, tar and gas yields and compositions.

A new reactor was proposed to obtain such data to overcome several limitations in the Combustion Engineering DTFS Reactor. The DTFS was not operated to provide quantitative feeding and collection of the coal and products. The char yield for example, was done by ash tracer which has potential inaccuracies. Only a limited number of gases were analyzed and it was difficult to determine the gas yields as a weight percent of the feed coal. The DTFS heat exchanger was not adequate to preheat nitrogen to the furnace temperature and there was an unheated connection to the test section which allowed the gas to cool.

The purpose of the present study was to build a reactor in which it was possible to measure the total distribution of pyrolysis products among char, tar and gas and the composition of each product and to use these data to test the additional predictions of the model.

The program was divided into seven tasks. Task 1 was the assembly and testing of the reactor. Section 2 describes the new apparatus which was designed to combine the advantage of the controlled rapid heating offered by the Badzioch and Hawksley reactor with the advantage of optical access available in recently developed laboratory reactors (24,25). The new reactor: 1) injects coal into a preheated gas stream in a hot furnace to provide rapid particle heating, 2) provides for optical access, 3) employs FT-IR to measure species concentration and temperature, both in-situ and in an external cell, 4) has provisions for collecting all the pyrolysis products to obtain mass balances and 5) is designed for 2 atm pressure.

Under Tasks 2 and 3 the reactor was used to study pyrolysis and secondary reactions of interest in gasification. Pyrolysis measurements were performed on 6 coals with

variations in temperature, gas feed composition and coal type. Section 4 presents the data obtained with four coals (Pittsburgh #8 and Illinois #6 bituminous coals, a Wyoming subbituminous coal and a Montana lignite) pyrolyzed in helium at furnace temperatures from 700°C to 1200°C, during initial operation of the reactor. Additional data are presented for a second Illinois #6 and a Utah bituminous coal in nitrogen at 1100°C obtained after modifications had been made to the reactor to improve the sampling system. All runs were made at 1 atm.pressure.

Under Tasks 4-6 the previously developed pyrolysis model (26-30) was improved and generalized for application in the entrained flow reactor. It has also been applied for other reactor geometries. A discussion of this work is presented in Section 3.

Task 7, the assesment of the application of the results to large-scale gasifiers is presented in Section 5. At the present stage of development, the model and experimental data provide a strong foundation for interpreting results in large scale gasifiers. Additional work to couple the model with accurate codes for fluid mechanics, heat transfer and reaction chemistry could provide a powerful tool for modeling gasifier performance in design or development. The conclusions and recommendations are presented in Section 6.

Results from the entrained flow reactor experiments indicate that FT-IR is an excellent way to measure gas evolution (including in-situ measurements of species and temperature) and functional group changes in the reactants. The measurements have yielded additional evidence that coal pyrolysis kinetics are insensitive to coal rank. Good agreement between theory and experiment have been obtained using a set of distributed kinetic rates which fit experiments differing substantially in configuration, temperature and reaction time. The model appears capable of predicting thermal decomposition phenomena which are of importance in gasification. Additional work is needed on volatile oxidation, swelling and char reactivity, as well as the incorporation of the pyrolysis component into a comprehensive computer code simulating fluid mechanics, heat transfer and chemical reactions in an entrained flow gasifier.

Section 2

EXPERIMENTAL

ENTRAINED FLOW REACTOR

The reactor has been designed to study coal behavior under conditions of temperature and heating rate encountered in an entrained flow gasifier. The schematic of the experiment is presented in Fig. 2-1. The reactor itself is shown in Fig. 2-2 and views during various stages of assembly are shown in Figs. 2-3 to 2-5. The reactor consists of a heat exchanger and test section contained in a 30 cm diameter by 60 cm long hot section of a furnace. The furnace is heated with Kanthal Super 33 electrical heating elements. These are the U-shaped rods shown in Fig. 2-3b. The electrical connections are shown in Fig. 2-4. The hot section is insulated with 1.2 to 2.5 cm of Zircar type Sali and type Al 30 refractories in the hot section, 5 cm of Babcock and Wilcox Safil bulk alumina fiber in the middle and 5 cm of Combustion Engineering Cer-wool-2700 in the coolest section. The layers of insulation can be seen in Fig. 2-3.

The heat exchanger (visible in Fig. 2-3) consists of a 10 cm diameter alumina cylinder filled with alumina chips. The test section (also visible in Fig. 2-3) consists of a 5 cm diameter alumina tube. The heat exchanger and test section are connected with the Zircar type Sali U-tube shown in Fig. 2-4a. The furnace is enclosed in a gas tight steel enclosure.

To operate the reactor, a gas stream of predetermined composition is heated during transit through the heat exchanger (maintained at furnace temperature). Prior to heating, the gas composition can be analyzed by routing the stream through an infrared cell. The gas stream then turns through the U-tube and enters a test section, maintained at the furnace temperature. Coal is introduced into the test section at variable positions through a movable water cooled injector.

The coal is fed using a modification of a MIT entrainment system (31) illustrated in Fig. 2-6. In the modified system, the feeder tube, which extends up through the coal bed, is slowly lowered as the feed gas (injected above the bed) exits through the tube. When the tube feeder entrance is at the level of the bed, coal is entrained in the gas and enters the tube. The rate for coal feeding is controlled by the rate at which the tube is lowered.

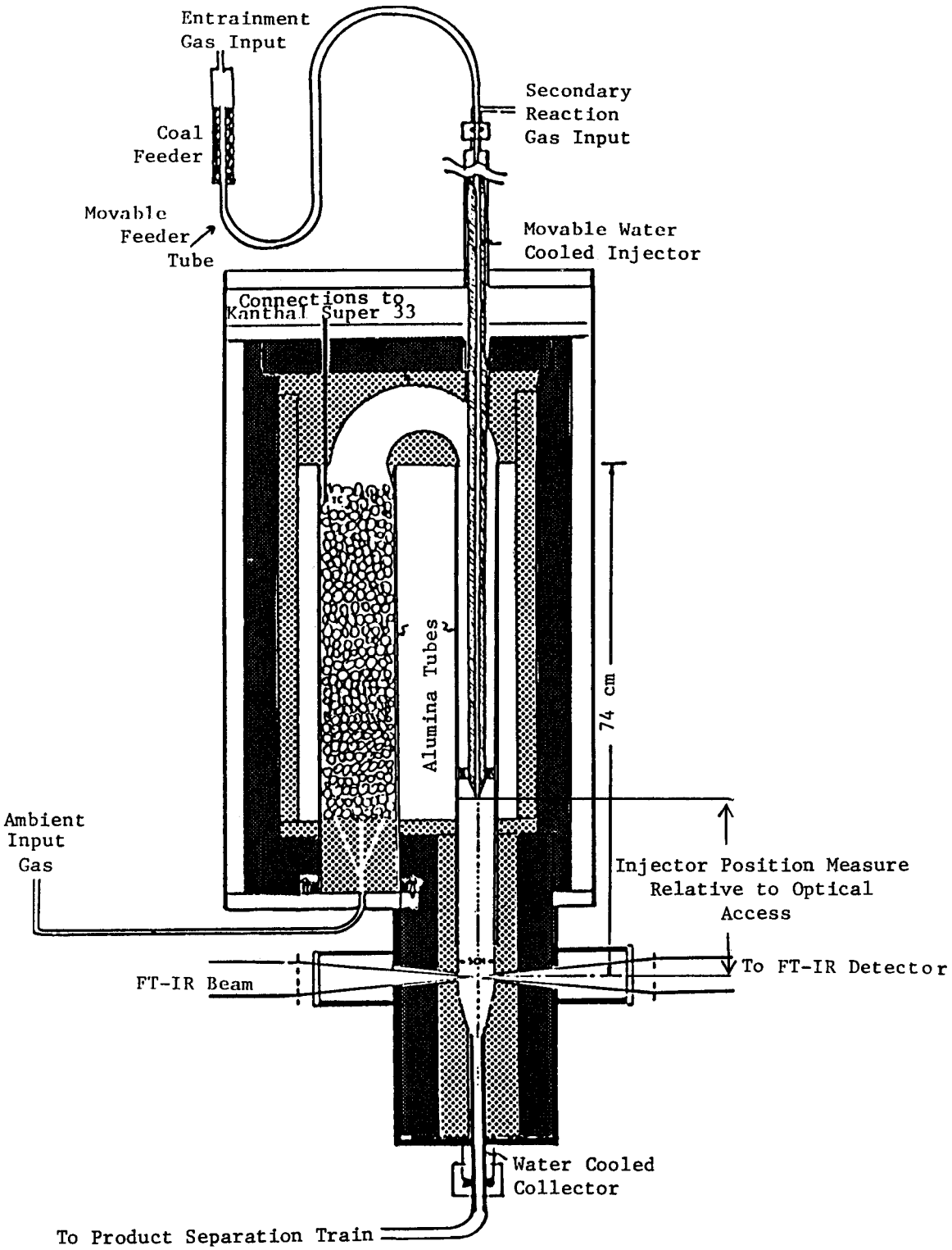

Figure 2-1. Schematic of Entrained Flow Reactor.

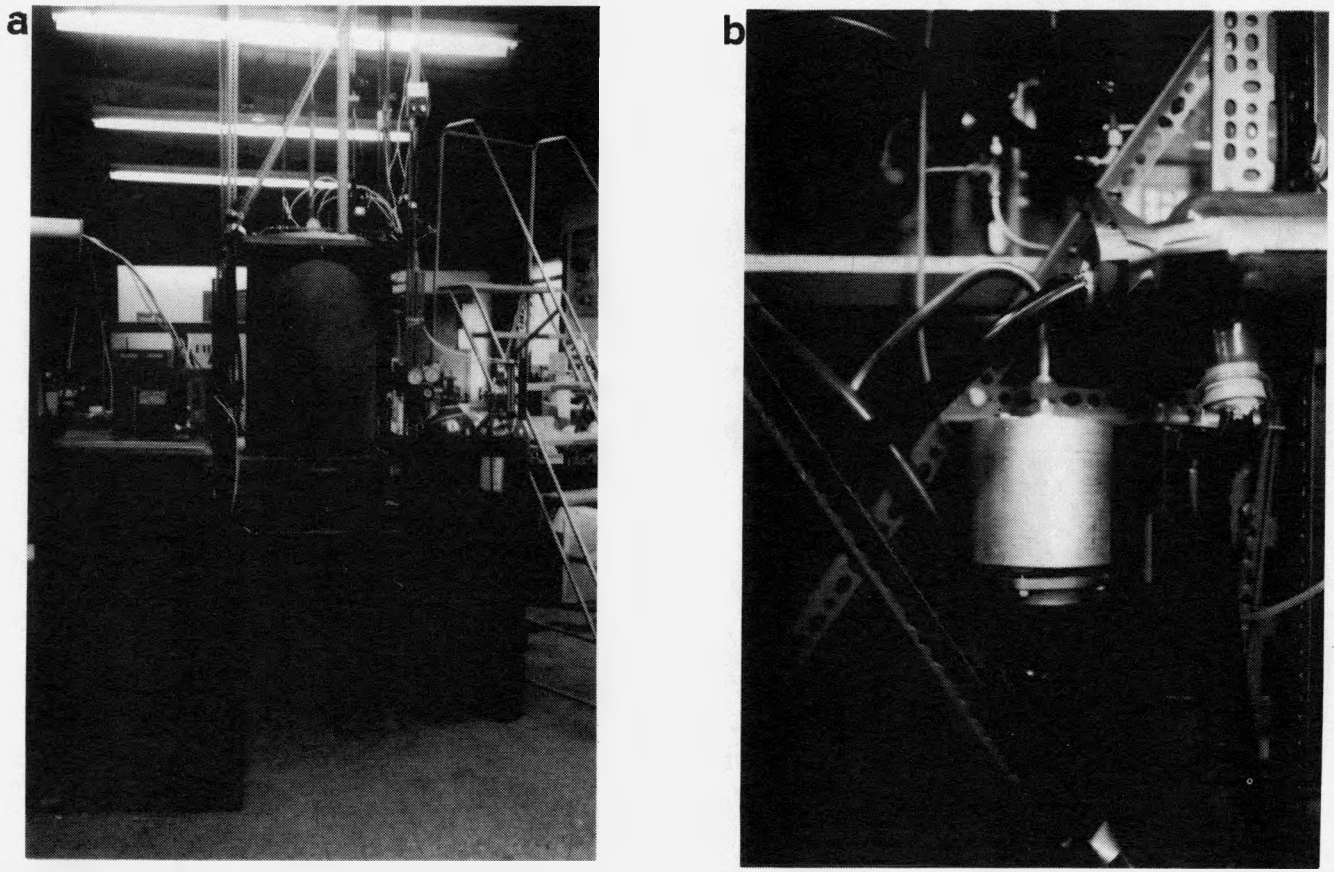

Figure 2-2. Entrained Flow Reactor. a) Reactor, b) Close-up of Char Separation Cyclone.

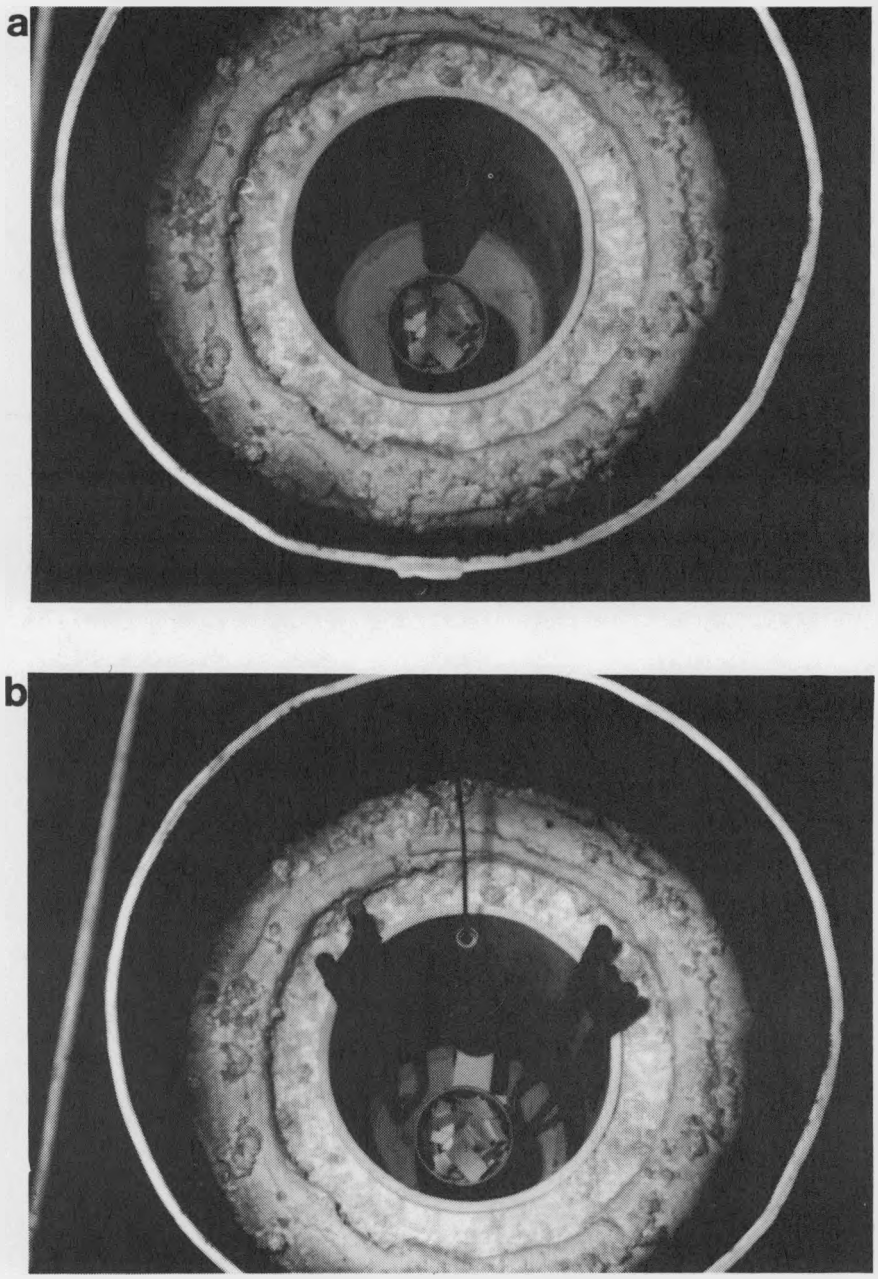

Figure 2-3. Hot Section of Furnace During Assembly. a) Heat Exchanger and Test Section, b) Kanthal Heating Elements Added.

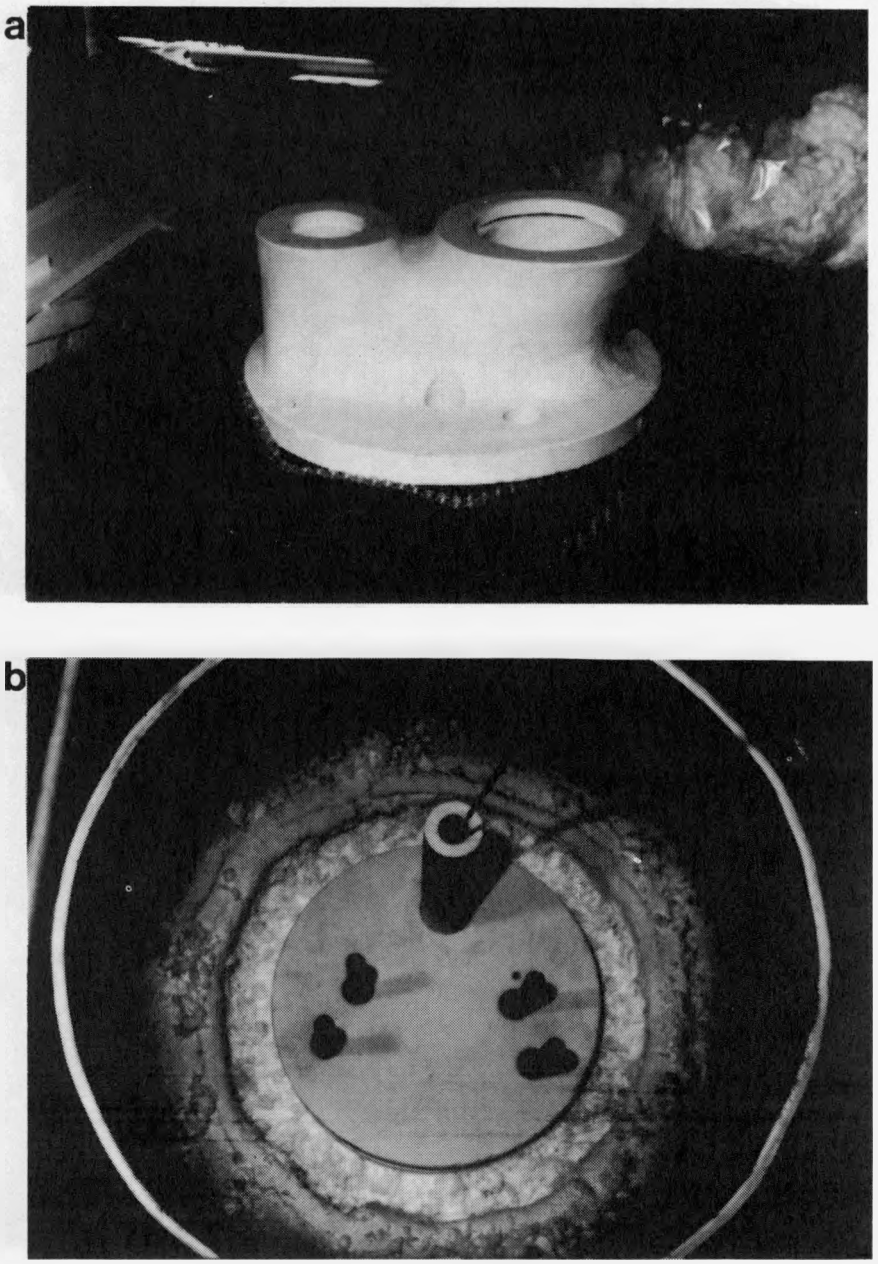

Figure 2-4. Furnace During Assembly. a) Gas Path "U" Tube, b) U-Tube in Place.

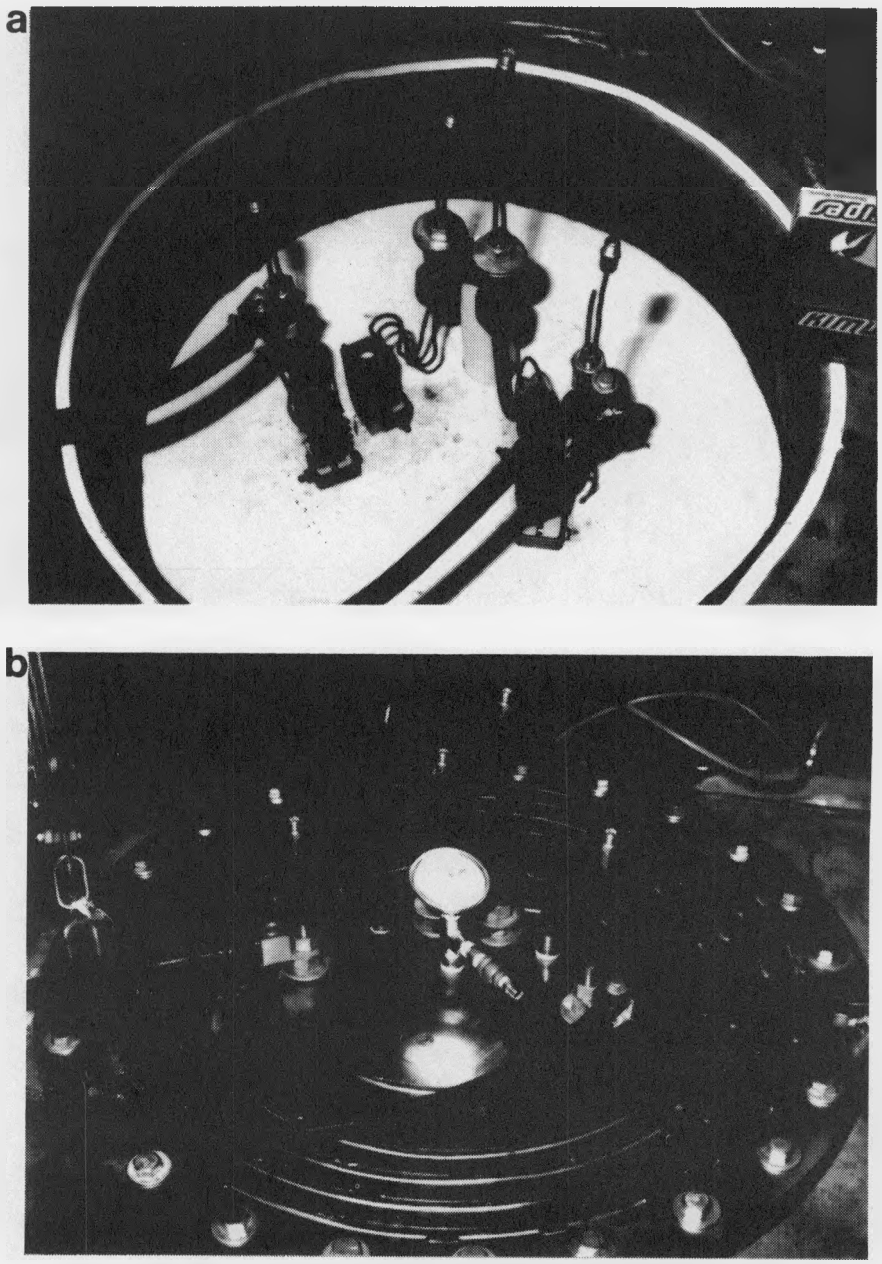

Figure 2-5. Electrical Connectors During Assembly. a) Internal Connection b) External Connection.

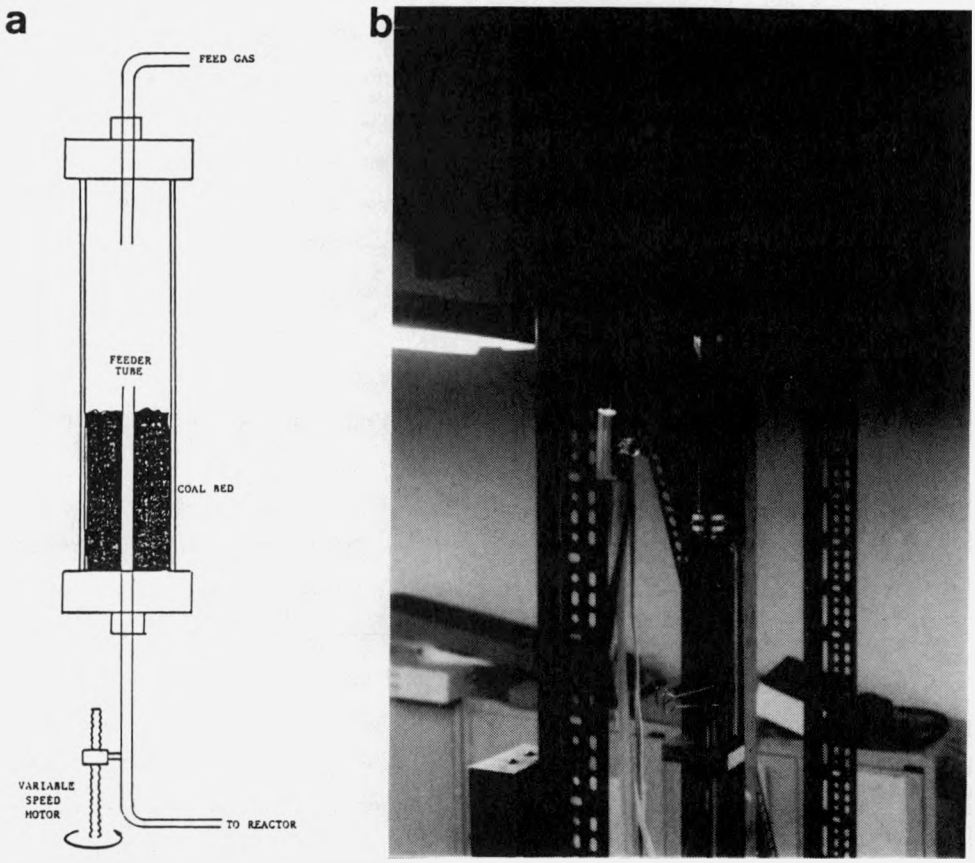

Figure 2-6. Coal Feeder. a) Schematic, b) Feeder in Place.

After a variable residence time, the reacting stream passes optical access ports and immediately downstream is quenched in a water cooled collector. There are five optical access ports, two of which are presently employed for the FT-IR beam. The other three ports are available for additional diagnostics.

GAS ANALYSIS BY FT-IR

The FT-IR can quantitatively determine many gas species observed in coal pyrolysis including CO, CO_2, H_2O, CH_4, C_2H_2, C_2H_4, C_2H_6, C_3H_6, C_3H_8, C_4H_8, C_6H_6, NH_3, HCN, SO_2, COS, CS_2 and heavy paraffins and olefins. Infrared spectra were obtained with a Nicolet model 7199 FT-IR using a globar source and a mercury-cadmium telluride detector. For obtaining the spectra within the furnace and within the cell, 100 scans at 0.5 wavenumber resolutions were accumulated in 140 seconds and transformed in under 2 minutes. The instrument can take spectra every 80 msec to follow rapid changes in the reactor or co-add spectra for long periods of steady state flow to increase signal to noise ratio. FT-IR is well suited to in-situ furnace experiments since the FT-IR system operates by coding the infrared source with an amplitude modulation which is unique to each infrared frequency. The detector is sensitive to the modulated radiation so that unmodulated stray radiation is eliminated from the experiment.

Figure 2-7 compares the gas analysis spectrum from the in-situ port with that of the sampled gas (analyzed in the room temperature cell) with the coal injector at 66 cm above the optical port and the furnace at 1100°C. The in-situ spectrum shows an acceptable noise level and no drastic effects from the particle scattering. The species which can be easily seen are CO, CO_2, H_2O, CH_4, and heavy paraffins. Additional species could be observed through the use of software signal enhancement techniques (32). The room temperature cell spectrum shows lower noise which permits the measurement of additional species including C_2H_2, C_2H_4, C_2H_6, C_3H_6, HCN, NH_3, COS, CS_2, SO_2, and heavy paraffins and olefins.

Several comparisons have been made between the in-situ spectra and the cell spectra to determine whether there are any substantial differences in species concentration due to reactions within the sample collector. For the conditions used so far, no such variations have become appearant and so the room temperature cell spectra have been used for gas analysis.

Figure 2-8 compares the room temperature cell spectra for pyrolysis gases from

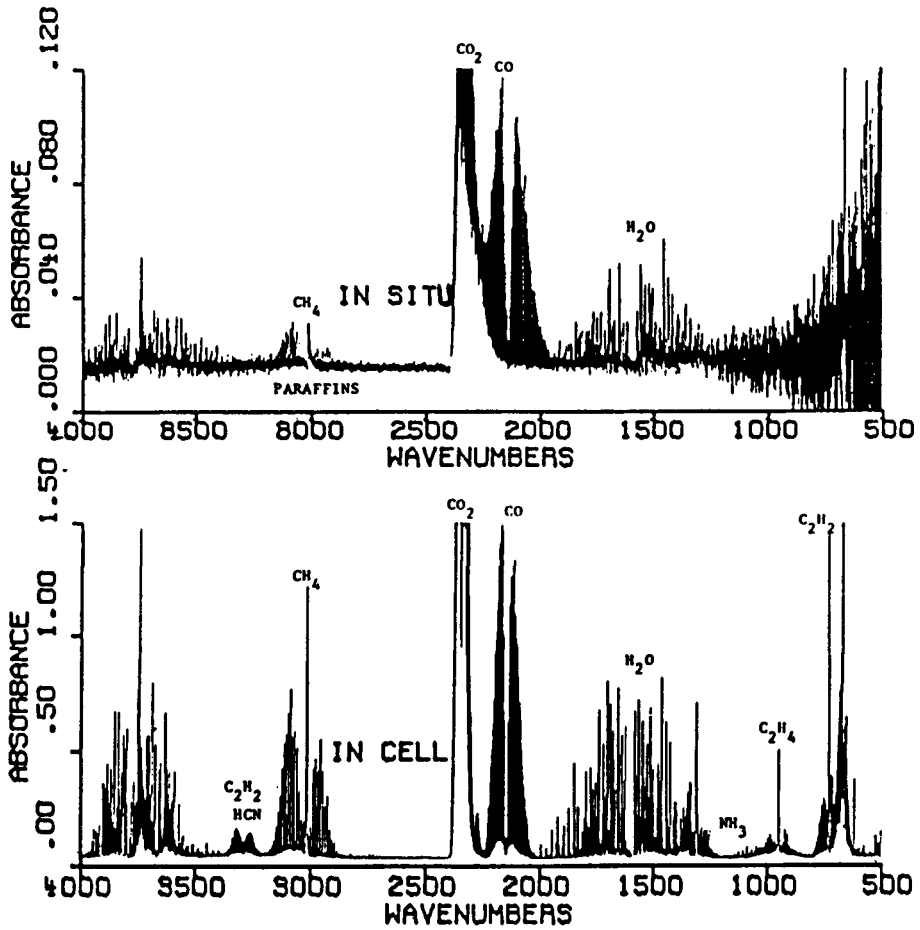

Figure 2-7. FT-IR Spectra of Gases from Beulah, North Dakota Lignite Pyrolyzed at 1100°C in Nitrogen. a) In-Situ Spectrum, b) Room Temperature Cell Spectrum.

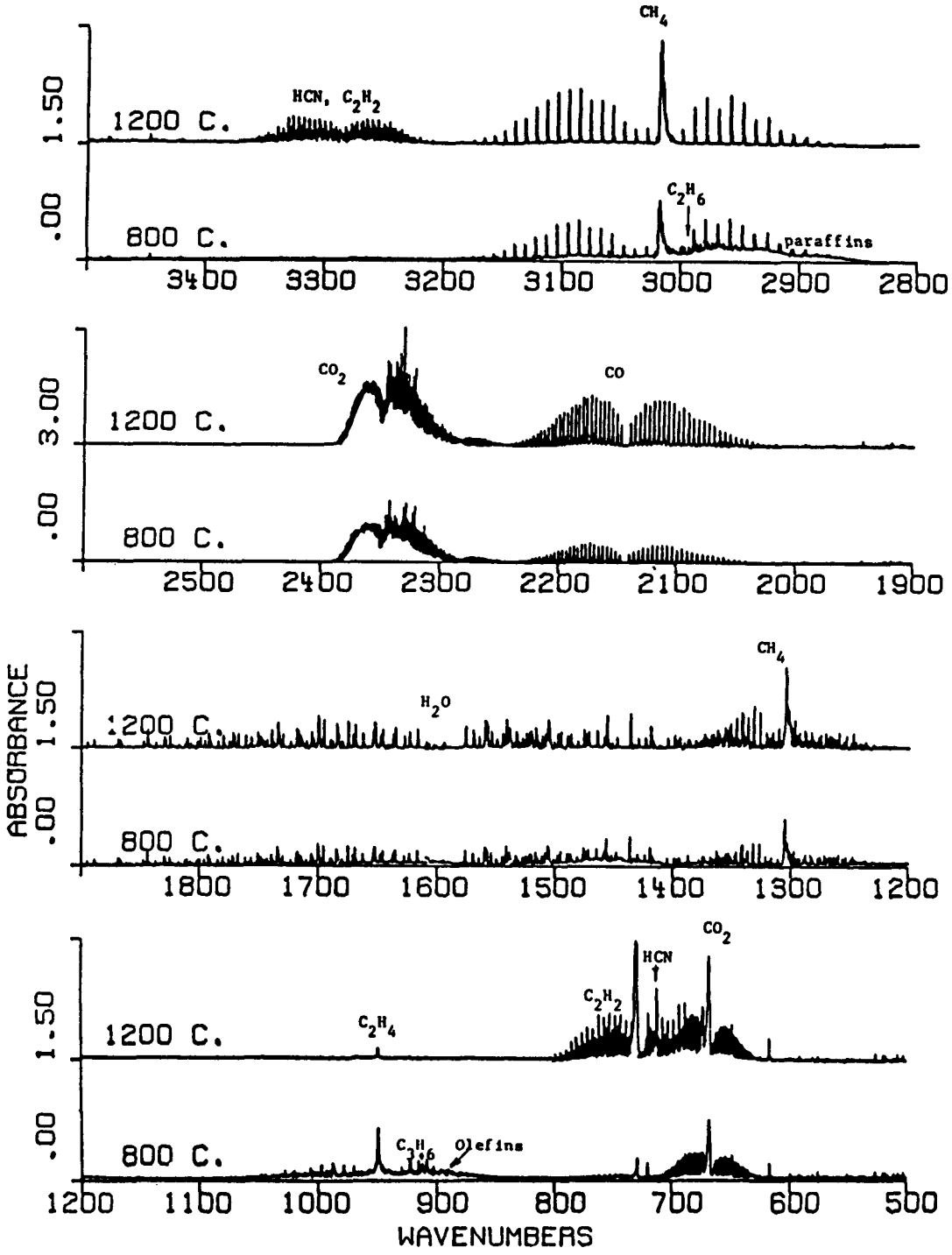

Figure 2-8. FT-IR Spectra from Jacob's Ranch Coal at 800°C and 1200°C from Room Temperature Cell.

Jacob's Ranch coal injected at 66 cm above the optical port at furnace temperatures of 800 and 1200°C. Important differences in the product mix at these two temperatures can be observed. The top pair of spectra show the region between 3500 and 2800 cm^{-1}. At 1200°C there is HCN, C_2H_2 and CH_4. At 800°C there is less methane and little HCN or C_2H_2 but significant amounts of ethane and heavy paraffins (indicated by the broad background). This observation is consistent with the cracking of paraffins to form olefins, acetylene and soot which has been discussed previously (12-14, 30). The region between 2600 and 1900 cm^{-1} shows the CO_2 and CO. The CO_2 increases by 50% but the CO increases by a factor of 3 in going from 800°C to 1200°C. This is consistent with previous observations of low temperature production of CO_2 and high temperature production of CO (11-15, 30).

TEMPERATURE MEASUREMENT BY FT-IR

The relative intensities of the hot CO absorption lines can be used for measuring gas temperature. An initial assessment of temperature measurement from CO intensities was performed under the EPRI program and continued under DOE contract #DE-AC21-81-FE05122 (30). Figure 2-9 compares the in-situ FT-IR spectra of CO taken at furnace temperatures of 20°C and 1100°C. The major lines result from transitions between rotational fine structure of the lowest two vibrational levels. The theoretical absorptions at an absolute temperature T are given by a degeneracy term times a Boltzman distribution (33):

$$A = C\ (2J+1)\ e^{-\left[\frac{J(J+1)B}{KT}\right]}$$

where A is the integrated absorbance of the line, J is the rotational quantum number of the initial state, B is the rotational constant for CO, K is the Boltzman constant, and C is a constant.

Plotting ln(A)/(2J+1)) vs J(J+1) gives a straight line with slope -B/KT = -2.76/T. The low temperature spectrum yields a reasonable straight line with a slope corresponding to a calculated temperature of 303K (30°C). The high temperature spectrum is not linear. One contribution comes from lower temperature CO which may exist near the reactor tube walls or windows. A second factor is possible saturation effects in the high intensity lines. A third nonlinear contribution is interference from the next highest vibrational transition. A portion of these lines, labled $V_1 \rightarrow V_2$ in the diagram, can be seen between the major lines from 2000

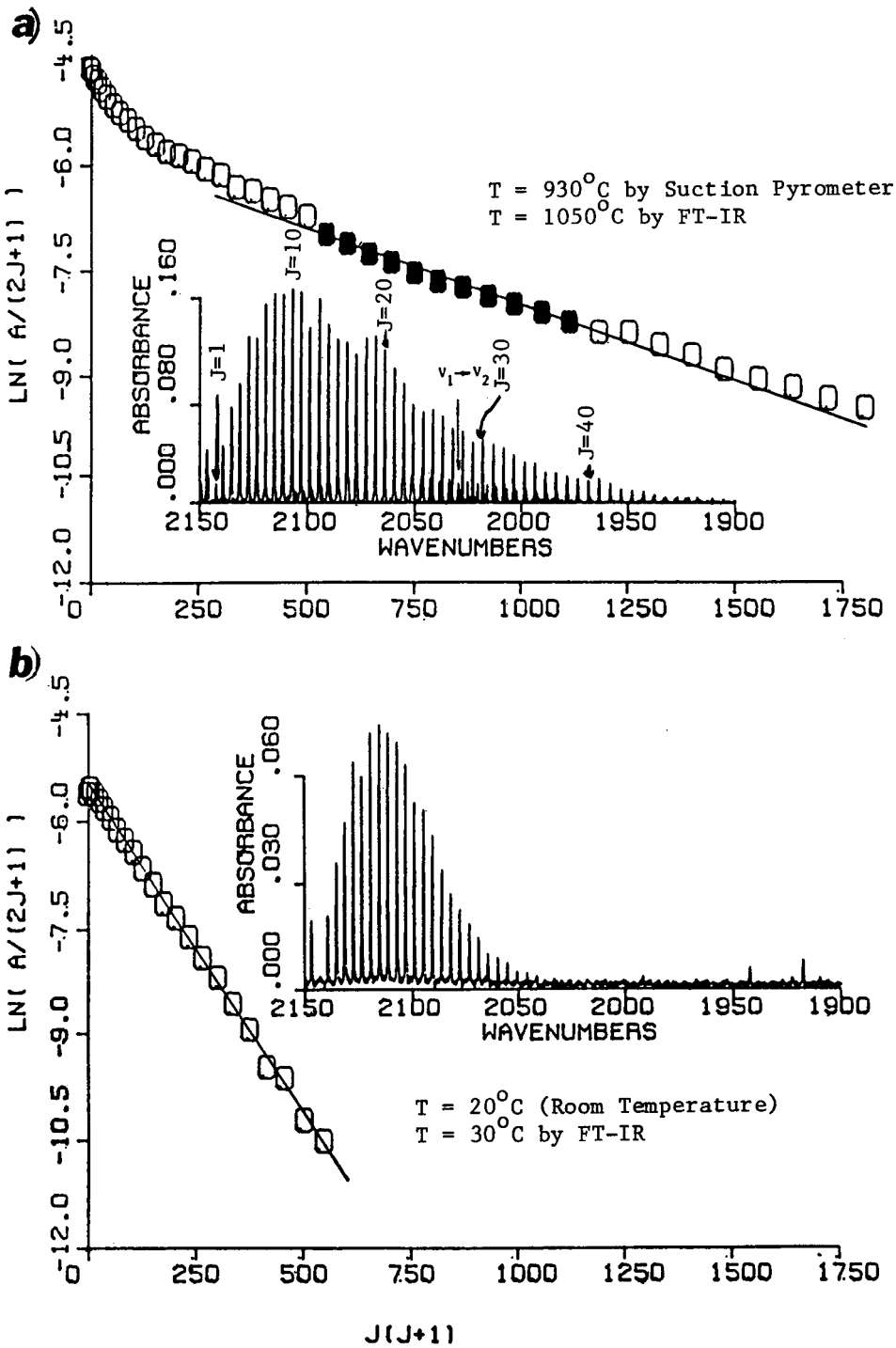

Figure 2-9. Determination of Gas Temperature from CO Rotational Lines. a) Furnace at 1100°C, b) Furnace at 20°C. Inserts Show Experimental Absorbance vs Wavenumber providing Data for Temperature Measurement.

to 2050 wavenumbers (34). The relative intensity of these lines with respect to the ground state transitions can also be used for measuring temperature. The solid data points have been chosen to minimize the non-linearites. The slope of the solid points gives T = 1323K (1050°C) compared to T = 1203K (930°C) as measured with a suction pyrometer at the optical port. This is not unreasonable since the suction pyrometer measures the average gas temperature, while the lines used for the FT-IR determination ignore the cooler gas near the walls.

PRODUCT COLLECTION AND SEPARATION

A great deal of effort was expended under the present project and under DOE contract #DE-AC21-81-FE05122 to establish an acceptable product collection and separation scheme.

The schematic for the presently used procedure is illustrated in Fig. 2-10. The determination of the pyrolysis product distribution is as follows:

- The amount of coal fed is determined by weighing the feeder before and after a run. This procedure eliminates problems originally experienced in determining the coal feed rate from the rate at which the feeder tube is lowered. That method suffers because of variations in bed density, or surface geometry and start up or shut off transients.

- All the pyrolysis products are collected and quenched in a water-cooled collector at the bottom of the reactor. An improvement in this procedure which is being planned is to use a gas quench to a temperature of 400-500°C. This procedure would prevent possible condensation of the tar on the collection walls and on the char.

- Char is collected in a cyclone and weighed. The cyclone pictured in Fig. 2-2b is designed to separate particles larger than 4 microns (35). Tests of the cyclone performed under DOE contract #DE-AC21-81-FE01522 demonstrated that 97% of -200 +325 mesh coal fed to the cyclone was collected. Plans have been made to maintain the cyclone at 400-500°C to avoid tar condensation.

- Gas, fine solids (e.g. soot) and condensed tar vapor which pass through the cyclone are collected in an initially evacuated polyethylene bag. The use of the bag allows the volume of gas collected during the run to be determined directly.

- The pyrolysis gases are quantitatively determined by drawing off a sample from the bag through a teflon filter into a FT-IR cell where the volume percent of gases are determined. The total quantitiy of each gas collected is determined from the volume percent and total volume of gas collected. Sampling from the bag allows mixing of the gases produced during the run, thus eliminating problems due to fluctuations in feed.

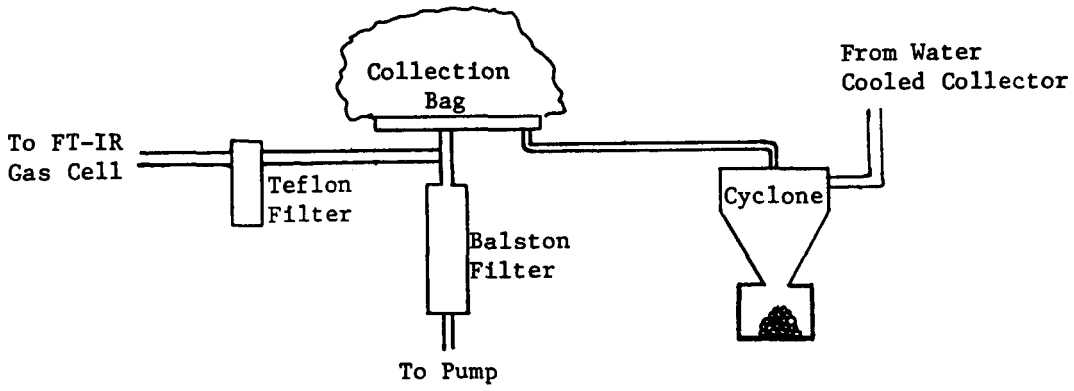

Figure 2-10. Schematic of Pyrolysis Product Separation Train.

TABLE 2-1

Sample of Data from Pyrolysis Run

PYROLYSIS SUMMARY REPORT - FUHRUN 474 10 - 6 - 82

RUN CONDITIONS

4690 mg. VACDRY COAL - Coal Fed During Run
0 sec. @ 0 Amps
0 sec. @ 0 Amps
1100 Degrees C. @ 0 torr with ALTUBE grid - (Furnace Temperature)
758.600 mm. Final Pressure for 102.506 liters - Pressure and Total Gas Collected

COAL

Name : PITT - 24 - Pittsburgh Seam - (injector position in inches measured from 6 cm above the optical point)
% ASH = 11.4000

PYROLYSIS PRODUCT YIELDS, AS WEIGHT PERCENT OF COAL

		Dry Wt. % coal basis	DAF Wt. % coal basis
	Char	46.5735	39.6992
	Tar	9.83368	11.0989
DRY	Gas	22.9596	25.9138
	Water	21.5857	24.3631
	Missing	-.95268	-1.07526

WET GAS COMPONENT YIELDS

	Dry Wt. %	DAF Wt. %	Volume %
Methane	5.89695	6.65570	.41196
CO	7.31954	8.26133	.29219
Hydrogen	0	0	0
CO2	1.89857	2.14285	4.82309E-2
Acetylene	1.58567	1.78970	.06816
Ethylene	1.21460	1.37089	4.84875E-2
Ethane	1.92009E-4	2.16714E-4	7.15406E-6
Propylene	.07908	.08926	2.10485E-3
Paraffins	0	0	0
Olefins	1.60490	1.81139	2.13560E-2
HCN	2.84679	3.21308	.11785
Ammonia	3.61833E-3	4.08390E-3	2.37909E-4
COS	5.29156E-3	5.97241E-3	9.85790E-5
CS2	.45010	.50801	6.61988E-3
SO2	5.43422E-2	6.13343E-2	9.49093E-4
Water	21.5857	24.3631	.92799
OTHER	0	0	.29219
Gas Total:	44.5454	50.2770	

- Tar and soot is collected in two places. Most is collected by pumping the bag contents through a Balston filter lined with a filter paper. The filter is weighed before and after sample collections. A sample of tar or soot is extracted from the filter paper for FT-IR and elemental anlaysis. Some additional tar or soot sticks to the walls of the collection bag. The bag is weighed before and after collection to determine solids collected on its interior.

- Hydrogen is determined in some cases gravimetrically. A sample of gas is drawn through a liquid nitrogen trap into a gas bulb. The gas bulb is weighed to determine the volume percent hydrogen.

The data analysis is presented in table form as illustrated in Table 2-1. The pyrolysis products are presented as a weight percent of the feed coal on a dry and dry ash free basis. Material balances range from 80 to 100%. Generally, cases in which tar yields are low (such as with lignites or with high temperature reaction conditions) produce good material balance. Cases in which tar yields are high result in unmeasured heavy hydrocarbon and tar deposition on walls. Then, material balances as low as 80% are observed.

The run tables are stored on magnetic disks and may be used for data presentation utilizing a routine which will plot designated items in the table as functions of reaction conditions. An example of the distribution of ethane and ethylene from pyrolysis of four coals is illustrated in Fig. 2-11. Little scattering is observed in the gas data.

FOURIER TRANSFORM INFRARED (FT-IR) SPECTROSCOPY ANALYSIS OF SOLIDS

Methods for preparing quantitative FT-IR spectra and determining functional group concentrations have been described in the EPRI Final Report AP2602 (21) and in a number of previous publications (13,26,36,37). Using these techniques, FT-IR spectra were prepared for the chars obtained in the entrained flow reactor. Figure 2-12 shows the FT-IR spectra for a feed coal, a char and a tar. The spectra were obtained using KBr pellets which were dried after preparation to remove water and corrected for scattering. The functional groups associated with the absorption bands are indicated in the figures.

To get a quantitative measure of the functional group concentrations, a curve analysis program developed at Advanced Fuel Research, Inc. was used to synthesize the IR spectra. The synthesis is accomplished by adding 45 absorption peaks with Gaussian shapes, fixed position and width, and variable height. The technique is described in more detail in other references (21 and 37). Figure 2-13 illustrates the synthesis for a coal. The top of the figure compares the coal and the simulated

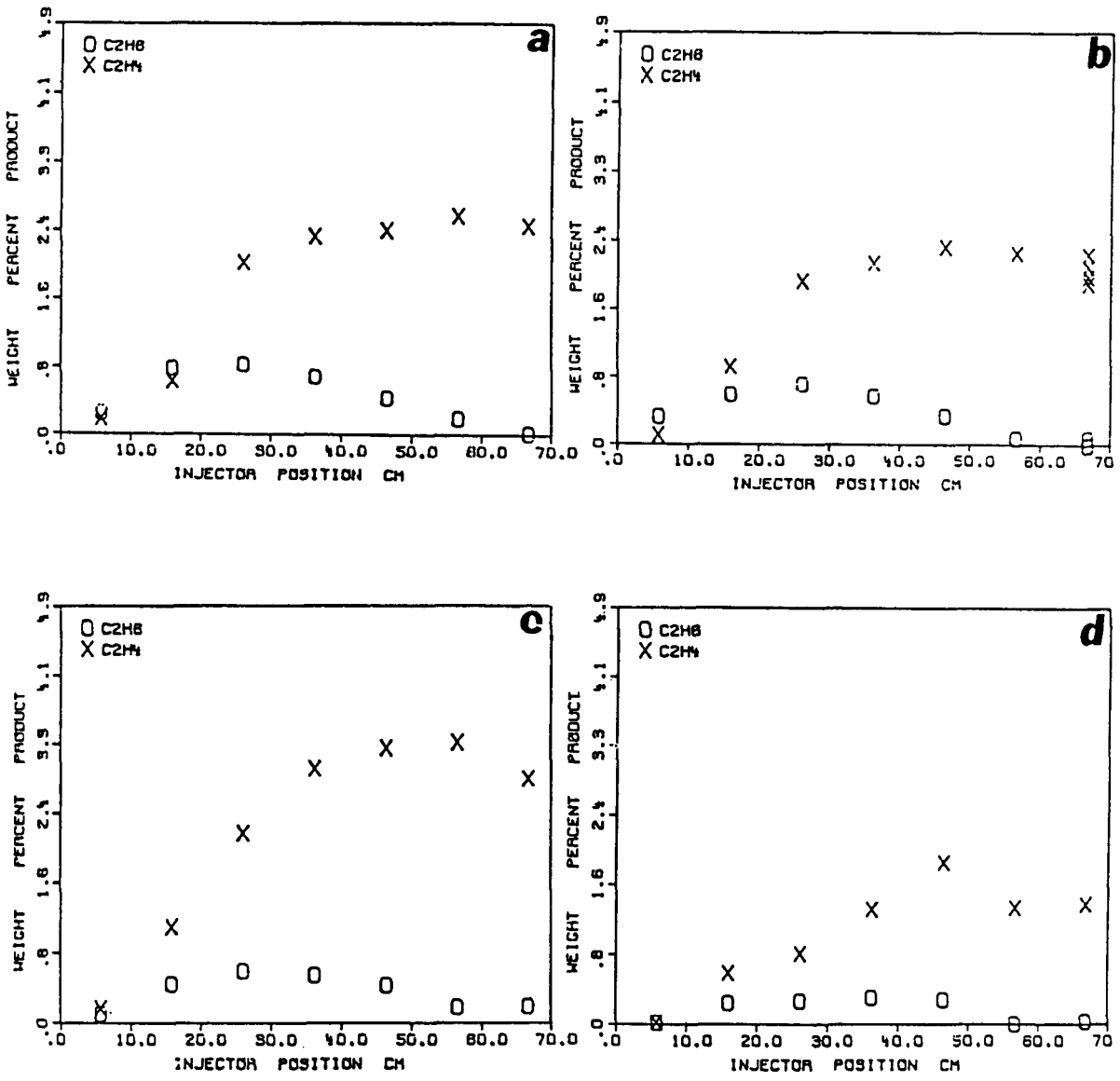

Figure 2-11. Ethane and Ethylene as Weight Percent of DAF Coal for 4 Coals in Nitrogen at 1100°C. a) Pittsburgh #8 Bituminous Coal, b) Kentucky #9 Bituminous Coal, c) Gillette, Wyoming Subbituminous Coal and d) Beulah, North Dakota Lignite.

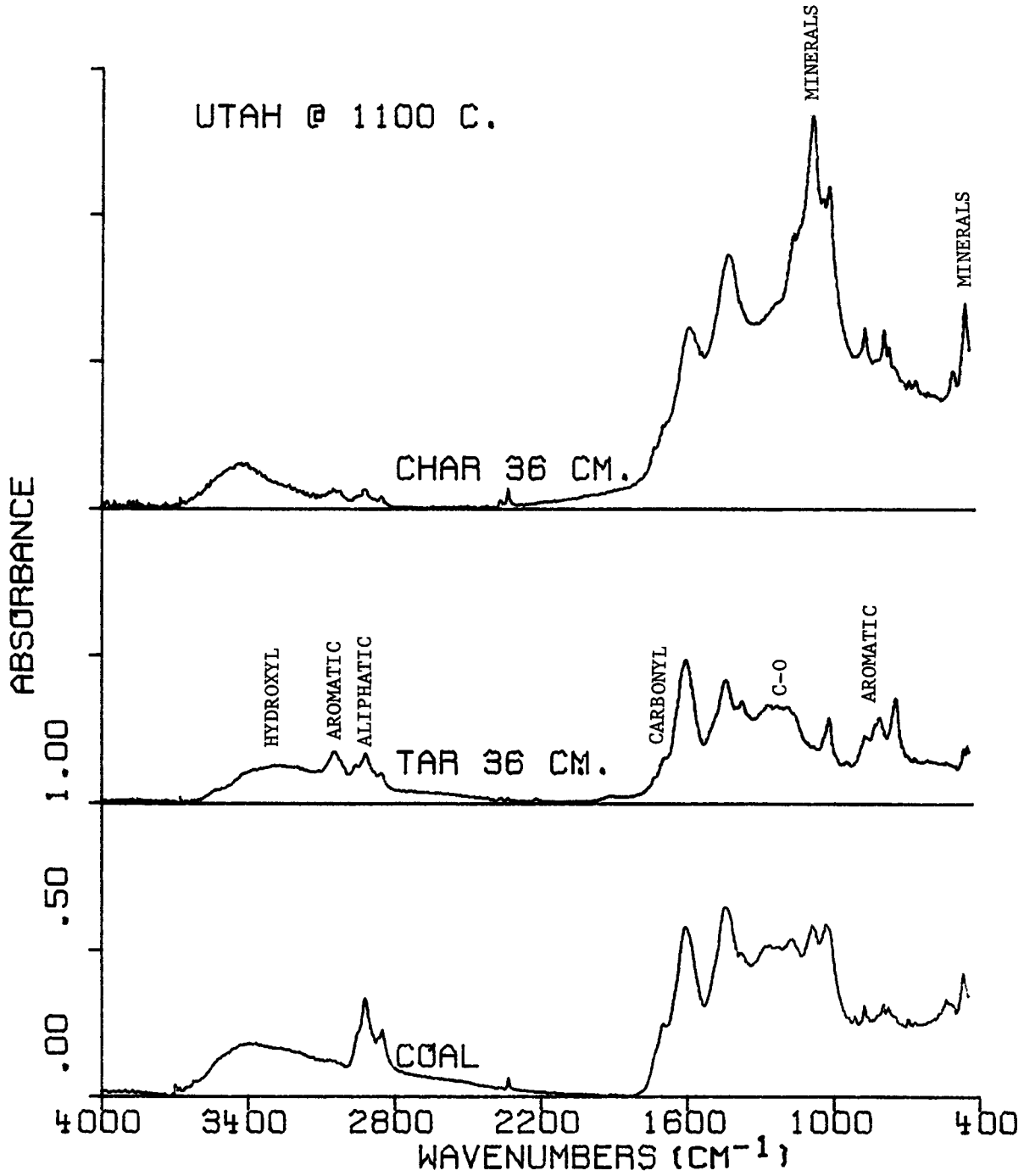

Figure 2-12. Quantitative FT-IR Spectra of Coal, Tar and Char.

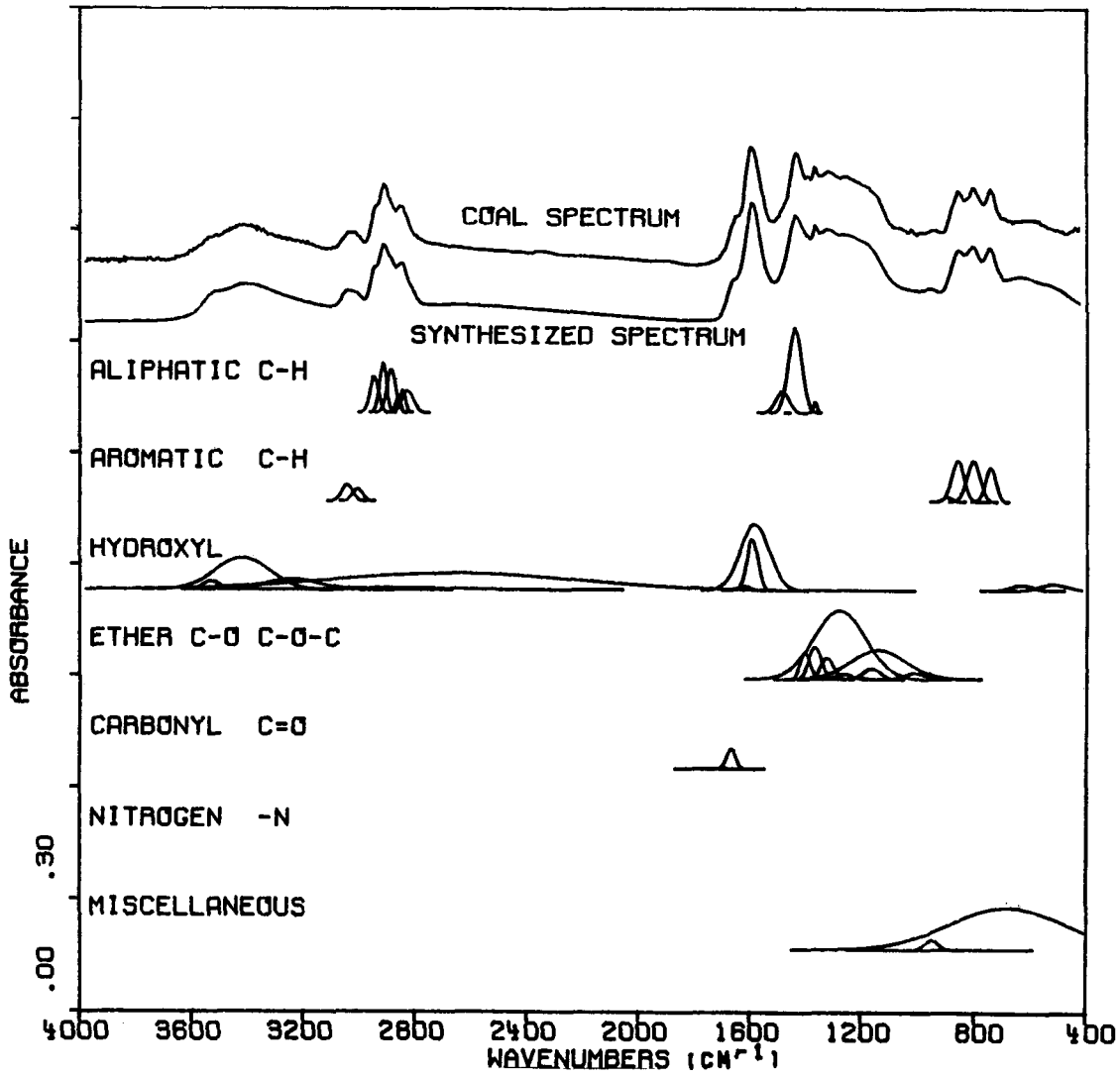

Figure 2-13. Synthesis of FT-IR Spectrum.

spectra. In most cases the two can't be distinguished. The peaks which are used for the functional groups are indicated in the lower part of the figure.

Section 3
THEORY

Aspects of the Advanced Fuel Research coal pyrolysis model have been presented previously (11-16,26-30). The important features of the model and its application are reviewed in this section.

MODEL ASSUMPTIONS

The coal pyrolysis model employs the following three primary assumptions:

(a) Coal consists of an ensemble of functional groups, most of which decompose independently to produce light gas species at rate coefficients which depend on the functional group but are insensitive to coal rank.

(b) Simultaneous with the production of light gas species is the thermal cleavage of bridge structures in the coal to release molecular fragments of the coal (tar) which consist of a representative sampling of the functional group ensemble.

(c) The tar competes with the light hydrocarbons and other light species for the coal's donatable hydrogen (hydroaromatic or aliphatic) to stabilize free radicals. When the internal donatable hydrogen has been consumed, tar and light hydrocarbon evolution ceases.

Pyrolysis is viewed as "depolymerization" in parallel with thermal decomposition of the "monomers" with the products competing for the donatable hydrogen for stabilization.

Assumption (a) is based on a striking feature of thermal decomposition which was observed for a variety of coals. That is, the temperature-and time-dependent evolution rate coefficient of a particular species and the normalized time-temperature-dependent decrease in the functional group concentration is similar for all coals. This is true even though the amount of the species or the functional group composition may vary substantially from one coal to another. An example of this behavior is illustrated in Fig. 2-11. The maximum yield of each species varies from coal to coal, but if the yields are compared on a normalized basis

(i.e. fraction of maximum yield), the dependence on reaction distance is quite similar. This is consistent with kinetic rate coefficients which are independent of coal rank. Additional experimental evidence which appears to support assumption (a) are found in (11-14,21,30,38-43).

The evidence for assumption (b) (that the tar consists of minimally disturbed fragments of the parent coal) is the striking similarity between the two materials which has been observed in elemental composition, FT-IR spectra and NMR spectra (11,13,14,16,28,44,and 45). An example of FT-IR spectra for a tar and its parent coal is presented in Fig. 3-1. For most bituminous coals the two materials are almost identical, suggesting that the tar is a representative sampling of the coal molecular structure (such as "oligomers" from the depolymerized coal "polymer"). The tar differs slightly from the parent coal in that it has a higher concentration of aliphatic hydrogen, especially methyl groups. This extra hydrogen is presumably abstracted from the char to stabilize the free radical sites formed when the bridges were broken.

Assumption (c) is that the simultaneous evolution of tar and light gases creates a competition for donatable hydrogen to stabilize free radical sites. This hydrogen is likely to come from the aliphatic or hydroaromatic portion of the coal H(al). Supporting evidence comes from the observation that tar evolution ceases when the aliphatic peak in the FT-IR spectra of chars goes to zero. (Note that at this point there is still aromatic hydrogen left in the char). If this argument is correct, it is reasonable to expect the tar yield to depend on H(al). Indeed, there is a correlation between tar yield and H(al) (27, 28, 46).

A number of results indicate that the conditions of coal conversion may influence the competition for hydrogen. Some conditions preferentially inhibit the evolution of the large molecules, allowing the light species to escape with most of the H(al). An example is pyrolysis in thick beds as in the determination of "proximate analysis fixed carbon". Under thick bed conditions the tar has opportunity to repolymerize as it percolates through the bed. This results in substantially lower tar yields than the corresponding yield for vacuum pyrolysis in a thin bed. Since the most important mechanism for removing aromatic carbon from the coal is tar evolution, the low tar yield means that most of the aromatic carbon will be retained in the "fixed carbon". This results in the near equality between "proximate analysis fixed carbon" and "aromatic carbon" reported by van Krevelen and Schuyer, (47) and recently studied by Solomon, (26). High pressures also inhibit tar yields by reducing the evaporation and diffusion of heavy molecules, as discussed in Sec.5.

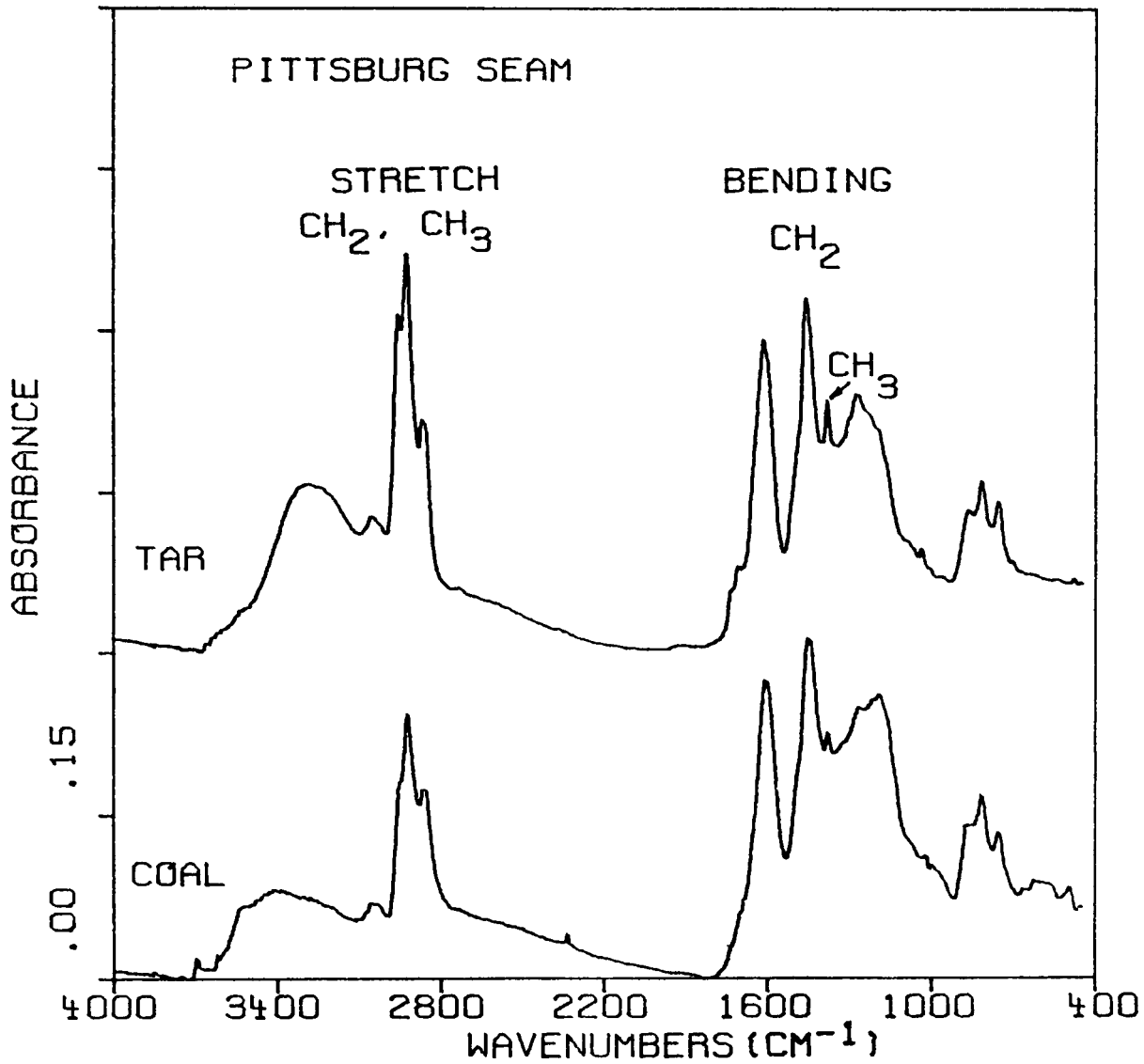

Figure 3-1. Comparison of FT-IR Spectra of Tar and Parent Coal.

Some recent results from the Mobil liquefaction research program (48,49) seem to show the opposite effect. Under certain mild liquefaction conditions the soluble products are very similar in composition to the parent coal and the yield shows a rank dependence which is similar to what is observed in thermal decomposition except that the yields are higher by a factor of two and a half (50). Under the conditions of these experiments, there is little or no hydrogen donated from the solvent so the hydrogen for stabilizing free radicals comes from the coal. The solvent may act, however, to retain and transfer H(al) from the coal and to transport the heavy molecules into solution. Both conditions presumably make more H(al) available for tar formation.

In addition to the basic assumption, there are several additional assumptions included in the model.

(d) Under conditions where pyrolysis products remain hot (such as in the entrained flow reactor) pyrolysis of the functional groups continues at the same rates used for that functional group in the char, (e.g., the rate for methane formation from methyl groups in tar is the same as from methyl groups in the char). For the entrained flow reactor all the products react for the same time. For heated grid pyrolysis simulations, it is assumed that gases and tars are at the grid temperature for 10 milliseconds.

(e) The use of a donatable (hydroaromatic) hydrogen to stablize a tar molecule is assumed to create a methyl group in the tar and to convert another donatable hydrogen to an aromatic.

(f) First order rates are assumed for the following cracking processess paraffins to olefins and hydrogen; olefins to acetylene and hydrogen.

(g) Other than cracking reactions, gas phase chemistry is ignored.

(h) Reactions between gases and char are ignored.

(i) Cracking of the aromatic nuclei of the tar to form smaller molecules is not considered.

(j) Possible rank dependent variations in the tar rate have been ignored. This is one of the most controversial features of the model.

The tar evolution rate is believed to be influenced by transport effects which chould be different for swelling and non swelling coals. For the present these effects are ignored and the amount of tar is a parameter of the model. Improvement in the tar evolution model are discussed in Section 5.

CHEMICAL DESCRIPTION OF PYROLYSIS MODEL

The relationship between a coal molecule and its thermal decomposition products has been discussed previously (11-16, 21, 26-30, 50). The relationship is illustrated in Figs. 3-2 and 3-3, taken from (28), which shows a hypothetical molecule of a Pittsburgh Seam coal (PSOC 170) and its decomposition products. The corresponding structure parameters and the source for the data are summarized in (28).

The decomposition products in Fig. 3-3 are obtained after the weak links in the structure are ruptured. For example, the bond between aliphatic carbons (A) or between the oxygen and an aliphatic carbon (B) are most likely to break. The breaking of these bonds releases the ring clusters with their attached functional groups. These large molecules comprise the coal tar.

Simultaneous with the evolution of tar molecules is the competitive cracking of the bridge fragments, attached functional groups and ring clusters to form the light molecules of the gas. A given species, a methyl group for example, may evolve as part of the tar without rupture of its local bonds or may evolve into the gas as methane with local bond rupture and the addition of a hydrogen.

Thermal decomposition results suggest the following relationship between the components of coal and the evolved light species. At low temperatures there is very little rearrangement of the aromatic ring structure. There is, however, decomposition of the substituted groups and aliphatic (or hydroaromatic) structures resulting in CO_2 release from the carboxyl, H_2O from hydroxyl, hydrocarbon gases from aliphatics, H_2S from mercaptans and some CO from weakly bound ether groups (see Fig. 3-3).

At high temperature there is breaking and rearrangement of the aromatic rings. In this process, H_2 is released from the aromatic hydrogen, CS_2 from the thiophenes, HCN from ring nitrogen and additional CO from tightly bound ether linkages. As this process continues the char becomes more graphitic.

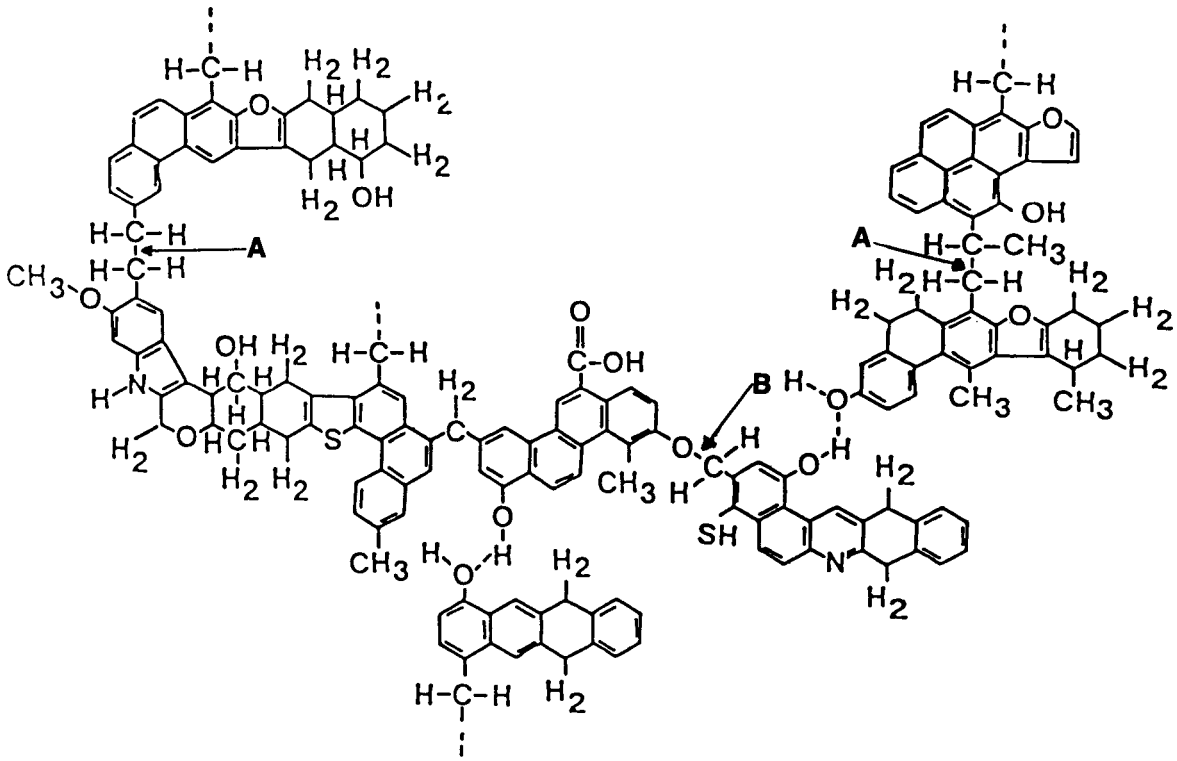

Figure 3-2. Summary of Coal Structure Information in a Hypothetical Coal Molecule.

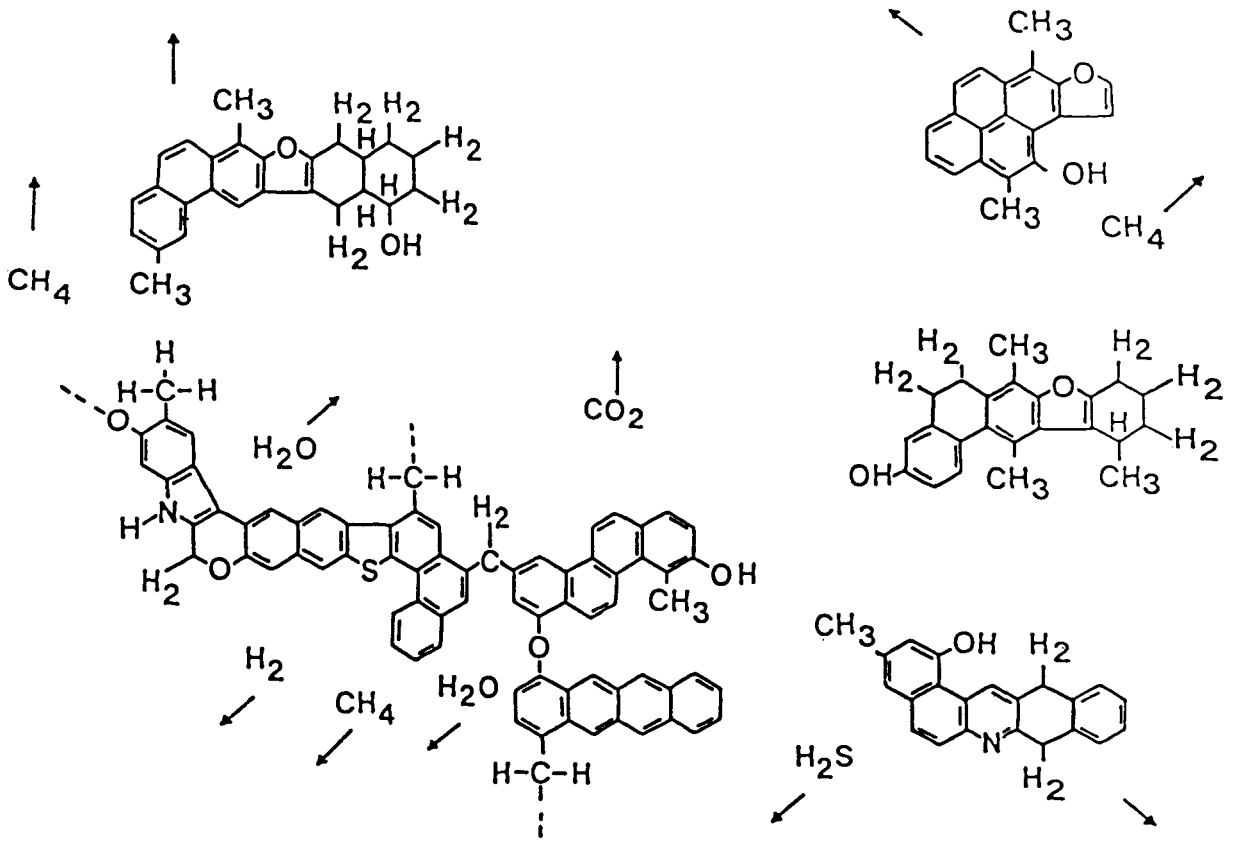

Figure 3-3. Cracking of Hypothetical Coal Molecule During Thermal Decomposition.

MATHEMATICAL DESCRIPTION OF PYROLYSIS MODEL

The mathematical description of the pyrolysis model has been presented previously (11-15,21,26-30). The evolution of tar and light species provides two competing mechanisms for removal of a functional group from the coal: evolution as a part of a tar molecule and evolution as a distinct gas species with cracking of the molecule. The model considers the removal of functional groups by the parallel independent evolution of the light species in competition with tar evolution.

To model these two paths, with one path yielding a product which is similar in composition to the parent coal, the dry ash free coal is represented as a rectangular area with X and Y dimensions. As shown in Fig. 3-4, the Y dimension is divided into fractions according to the chemical composition of the coal. Y°_i represents the initial fraction of a particular component (carboxyl, aromatic hydrogen, etc) and the sum of the Y°_i's equals one. The evolution of each component into the gas (carboxyl into CO_2, aromatic hydrogen into H_2, etc) is represented by the first order diminishing of the Y_i dimension, $Y_i=Y^\circ_i \exp(-k_i t)$. The X dimension is divided into a potential tar forming fraction X° and a non-tar forming fraction $1-X^\circ$. The evolution of the tar is represented by the first order diminishing of the X dimension $X=X^\circ \exp(-k_x t)$. The fractional amount of a particular component in the char is,

$$W_i(\text{char}) = (1-X^\circ+X)Y_i$$

and the amounts in the gas and tar may be obtained by integration with respect to time starting from t = 0.

$$W_i(\text{tar}) = (X^\circ Y^\circ_i - XY_i)\, k_x/(k_i + k_x)$$

$$W_i(\text{gas}) = (1 - X^\circ)\,(Y^\circ_i - Y_i) + W_i(\text{tar})\, k_i/k_x$$

$$\sum_i W_i(\text{char}) + W_i\,(\text{tar}) + W_i(\text{gas}) = 1$$

Further decomposition of aliphatic species to form olefins, acetylene and soot and other model assumptions modify the basic equations.

Figure 3-4a shows the initial state of the coal. Values for Y° are obtained from elemental and FT-IR analysis and from the heated grid pyrolysis experiment. The value of X° is at present a parameter of the model. It is controlled by the oxygen

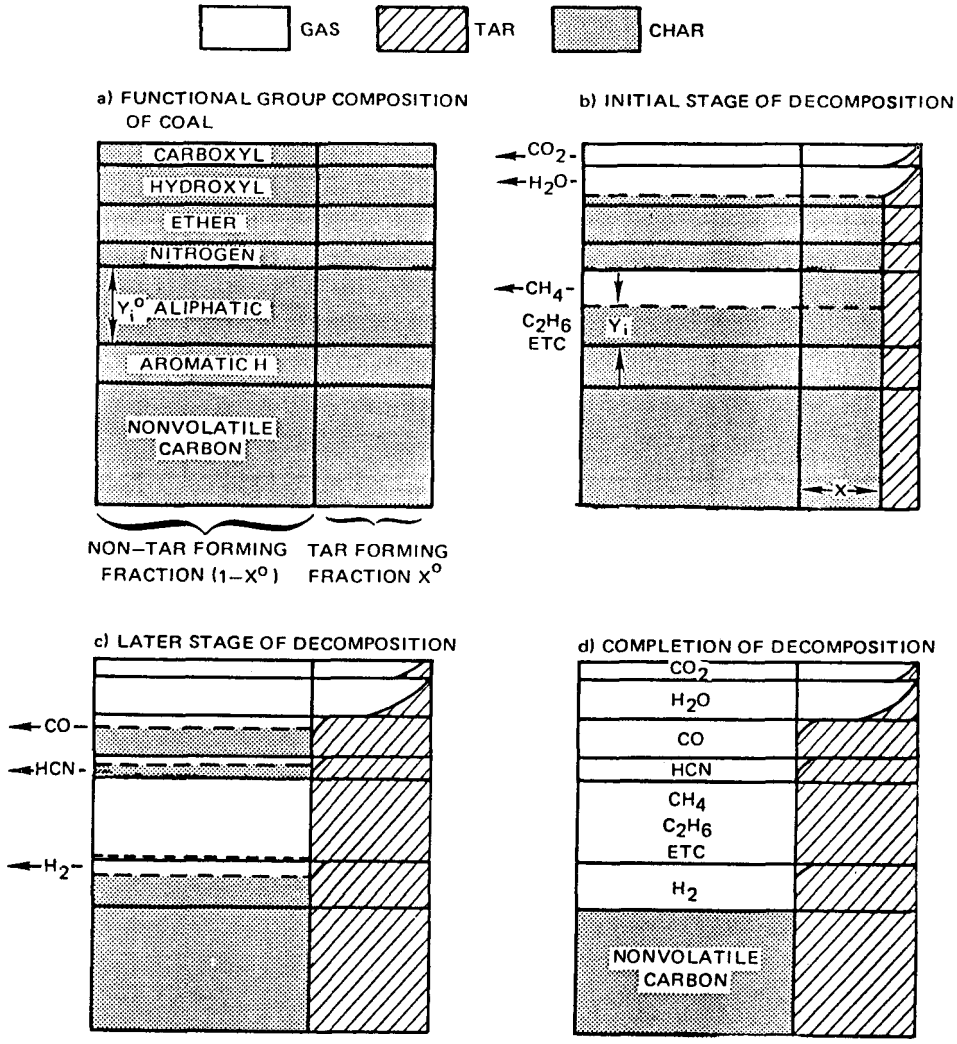

Figure 3-4. Progress of Thermal Decomposition According to Model.
a) Functional Group Composition of Coal, b) Initial Stage of Decomposition,
c) Later Stage of Decomposition, d) Completion of Decomposition.

and donatable hydrogen content of the coal and can be influenced by pressure, particle size, bed geometry and the transport properties of the pyrolysis medium.

Work is presently in progress (51) to compute the tar yield by employing a theory of depolymerization, vaporization and diffusion similar to that of Unger and Suuberg (52). This approach is discussed in Section 5.

Figure 3-4b shows the initial stage of thermal decomposition, during which the most volatile components H_2O, CO-loose and CO_2 evolve from the hydroxyl, ether-loose and carboxyl groups, respectively, along with aliphatics and tar. At a later stage (Figure 3-4c) CO-tight, HCN and H_2 are evolved from the ether-tight, ring nitrogen and aromatic hydrogen. Figure 3-4d shows the final state of the char, tar and gas.

KINETIC RATE COEFFICIENTS

To define kinetic rate coefficients k_i, for various species as a function of reaction temperature, it is important to consider the possible causes for the wide variations (up to 5 orders of magnitude for CO_2) in reported rates (15). For coal pyrolysis in the absence of external reacting gas species, such variations may be caused by:

- Coal type.
- Reaction conditions (pressure, heat & mass transfer rates).
- The assumptions used for deriving a kinetic expression.

Of these three causes, it is the last two which appear to produce most variations.

Variations in reacting conditions lead to problems because coal pyrolysis often occurs during coal heating. The transient conditions are often poorly known and so, while pyrolysis rates may be reasonably well determined, the temperatures to which they apply are not.

The assumptions used for deriving kinetic rates in coal are troublesome because of the coal's inhomogeniety which typically produces a distribution of rates rather than a single sharp rate for any chemical reaction. Such variations can be understood from the work of Stein et al. (53) and Vernon (54) which suggest a variation in bond energies with the degree of ring condensation. Most investigators have assumed a first order process and a rate constant with an Arrhenius temperature dependence. Using a two parameter fit to define the rate when three parameters

(e.g., frequency factor, k_o, activation energy, E_o and a distribution parameter, σ) are required has contributed to the wide variation in published rates.

Examples of the variability in kinetic rate coefficients which can result from the assumptions of the analysis are illustrated in Fig. 3-5 which shows numerical fits to the pyrolysis data of Campbell (55) for CO_2. The simulations are performed assuming $\sigma = 0$ (Campbell's assumption) and a large σ. Both values of σ produced good fits with the data. The resulting kinetic rate coefficients were are follows:

$\sigma = 0$

$k_{loose} = 550 \exp(-9815/T)$

$k_{tight} = 230 \exp(-11582/T)$

Large σ (3-10% of activation energy)

$k_{loose} = 1.0 \times 10^{21} \exp(-(40100 \pm 4000)/T)$

$k_{tight} = 2.4 \times 10^{11} \exp(-(30100 \pm 1000)/T)$

It is obvious that the experimental data from one constant heating rate experiment is insufficient to uniquely determine the σ values and hence the rate coefficients. At least one more experiment with a different heating rate, to adequately shift both peaks of Fig. 3-5, is necessary to enable a unique determination of σ.

Weimer and Ngan (39) obtained useful kinetic rate coefficients by using a three parameter fit to simulate both their own low heating rate experiment and the rapid heating rate experiments of Suuberg, et al. (6,7). The simulations for two experiments at substantially different temperatures can differentiate between the ambiguous choices of the kind presented in Fig. 3-5. Using 3 parameters, it is possible to fit both the high and low heating rate experiments reasonably well. Use of Campbell's $\sigma = 0$ would provide a terrible fit to Suuberg's high heating rate data and Suuberg's $\sigma = 0$ fit does not work well for Campbell's or Weimer and Ngan's low heating rate data.

On the basis of these results a distributed activation energy model was used for species evolution kinetics. A more complete discussion of the distributed activation energy model is contained in the EPRI final report AP2602 (21). The

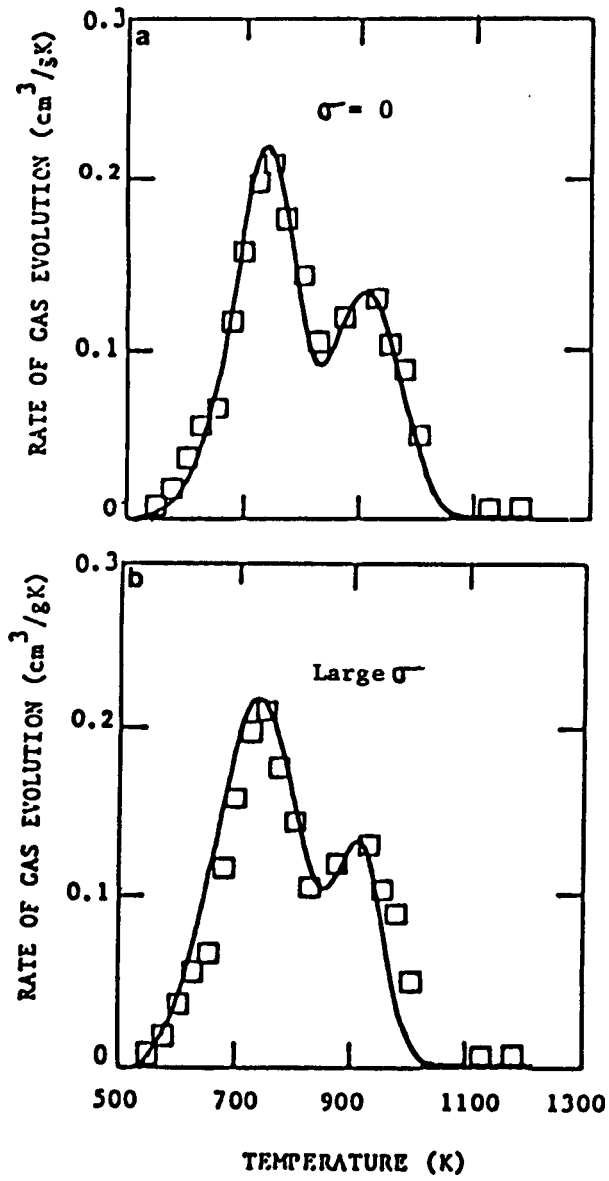

Figure 3-5. Effect on Variations of Distribution Parameter, σ on the Kinetic Rate Coefficients. Constant Heating Rate m = .055°C/sec. (Data of Campbell (55)).

product sources $W_i(E)$ for each species i as a function of activation energy E is assumed to be

$$W_i(E) = \frac{W_{io}}{\sigma\sqrt{2\pi}} \exp\left(-(E-E_{io})^2/2\ \sigma_i^2\right)$$

where σ_i is the width of the distribution and E_{io} is the average activation energy. For computation purposes this distribution is represented by 21 components. Each part of the distribution evolves with a kinetic rate coefficient $k_i = k_{io} \exp(-E/RT)$ where k_{io} is the frequency factor. Experiments at several heating rates are used to define the kinetic rate parameters. Such a kinetic description allowed the simulation of CO_2 evolution from coal in a wide variety of experiments without varying the kinetic rate coefficients (15,21,50).

COAL PARTICLE TEMPERATURES

The model requires coal particle time-temperature histories as input. The calculations are discussed in detail in (21). For the entrained flow reactor, particle temperatures have been calculated, given the reactor wall temperature as a boundary condition, by considering the following: a) radiative heat transfer between the coal particles and the wall; b) convective heat transfer between the coal and the gas; c) conductive heat transfer within the gas. Calculations were performed numerically on a PDP/11 computer using a Runge-Kutta integration scheme to determine the temperature of tubular shells at progressive cross sections of the flow path. Instant mixing of the feed gas with the preheated gas was assumed. The coal particle weights have been measured, and the absorptivity and heat capacities were assumed to be 0.7 and 0.3 cal/gram°C respectively.

The methods of calculation are described in reference 21. A modification has been made in calculating the mass of gas contained in any one volume element. Presently, the mass contained in a volume element is fixed at the value it would have at the nominal average temperature, (and therefore the pressure varies from point-to-point within the reactor). This change allows the average temperatures to be calculated correctly, but ignores variations in mass flow with radius. Previously the pressure was fixed and the mass within an element varied.

Calculations for coal particle temperatures vs the distance travelled (for the injector 66cm above the port) are presented in Fig. 3-6a and b with helium and nitrogen for the ambient gas, respectively, for furnace temperatures of 700 and 1200°C. Calculations for a furnace temperature of 1100°C and for various parametric

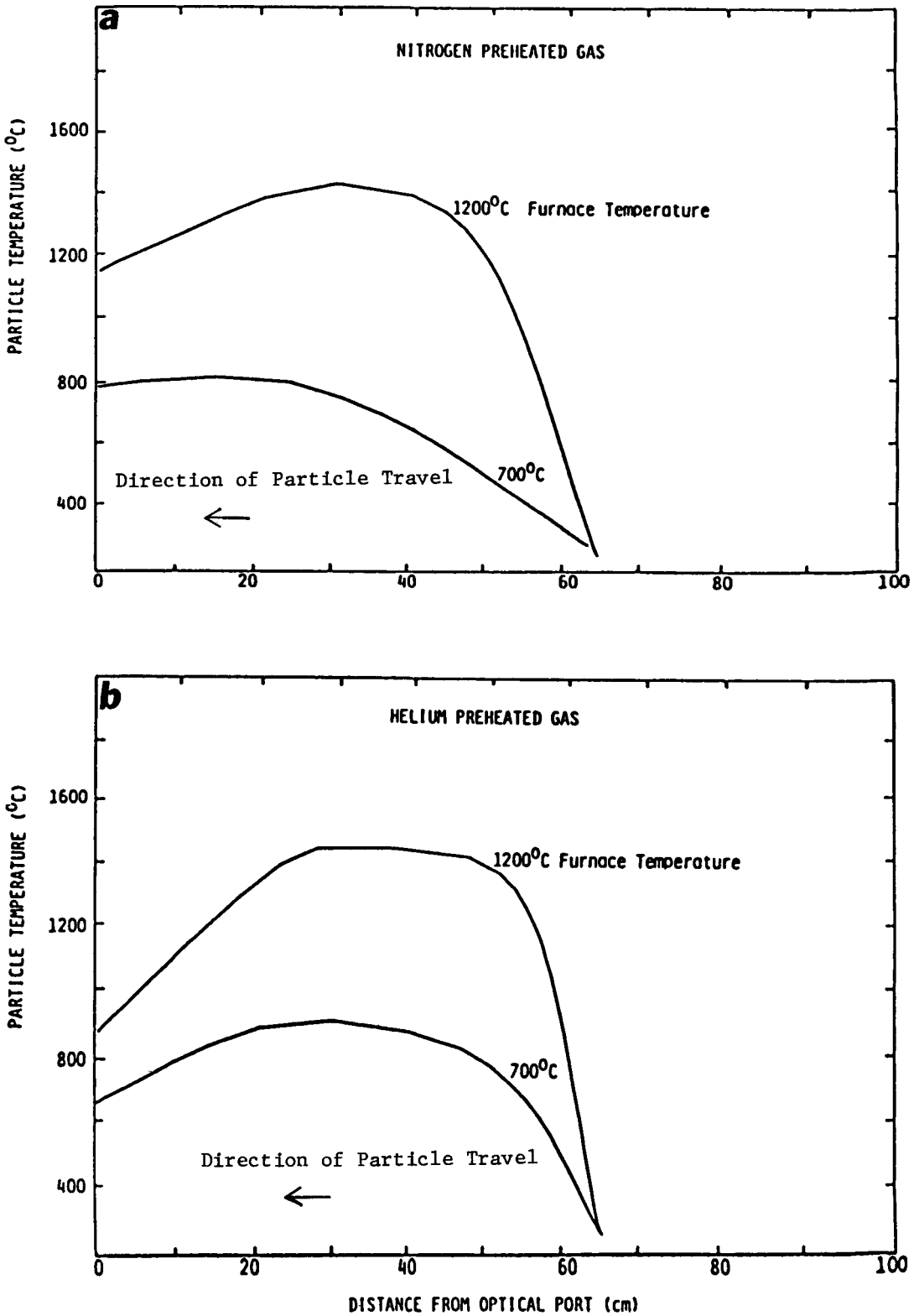

Figure 3-6. Calculated Coal Particle Temperatures in a) Nitrogen, b) Helium for Furnace Temperatures of 700°C and 1200°C with Injector at 66 cm from the Optical Port.

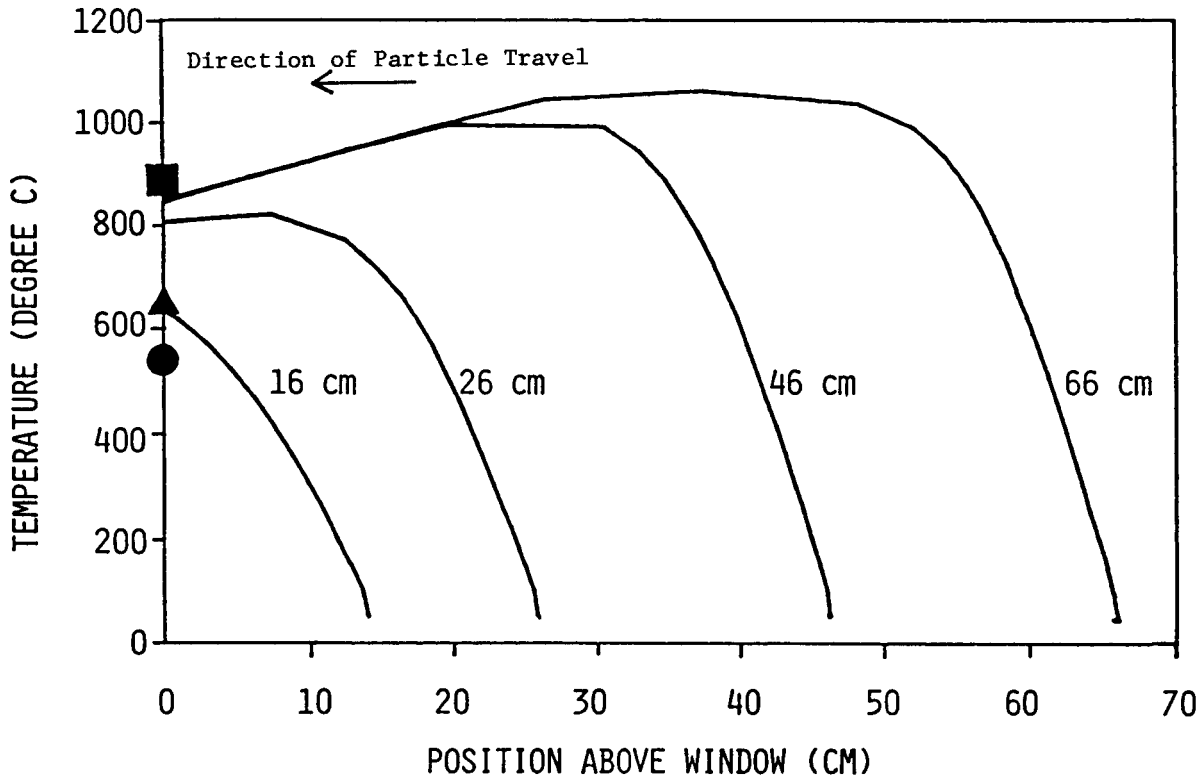

Figure 3-7. Calculated Coal Particle Temperatures in Nitrogen for a Furnace Temperature of 1100°C with Injector Position as a Parameter.

values of the distance between the injector and the optical port are illustrated in Fig. 3-7 where nitrogen is the ambient gas.

For the heated grid flash pyrolysis simulations (Fig. 3-10) a model assuming radiative heat transfer is used to calculate particle temperatures from the grid temperature.

SAMPLE CALCULATIONS

The theory was recently compared to results from the entrained flow reactor and to heated grid pyrolysis experiments (30). The entrained flow reactor data for pyrolysis in one atmosphere of nitrogen of a Beulah (Zap) North Dakota lignite are compared with the pyrolysis model simulation in Figs. 3-8 and 3-9. The coal composition parameters and kinetic rate coefficients are presented in Table 3-1.

To test the generality of the model, the simulation using the same kinetic rate coefficients has also been applied to data for the pyrolysis for 10 seconds in vacuum of a Pittsburgh seam coal in a heated grid. The results are presented in Fig. 3-10 The experimental apparatus and the data have been presented previously (12). The coal composition parameters are presented in Table 3-1.

The overall pyrolysis product distributions are presented in Figs. 3-8a and 3-10a. The model does a good job of simulating the total weight loss. The gas content for the lignite is much higher than for the bituminous coal because of the higher amount of oxygen containing species. The tar content for the lignite is much lower with substantial scatter in the data because of tar collection on walls mentioned in Section 2. The tar is presented in Fig. 3-9c. The highest tar values appear at 16 and 26cm (also see Fig. 4-32). These are also the reaction distances at which the missing material (which is probably tar) is the highest. It seems that the tar is cracking at longer reaction distances as the measured tar is lower and there is little missing material. Cracking of tar has not been incorporated in the model.

Char compositions are presented in Figs. 3-8b and c and 3-10b. There is good agreement between the theory and the data except for the prediction of nitrogen in the bituminous coal and aromatic hydrogen in the lignite. The nitrogen in the bituminous coal disappears less rapidly than predicted. A previous study (38), suggests that the difficulty of nitrogen removal from char goes up with rank. Under these circumstances a rank dependent rate would have to be used for the HCN-tight component. The predicted trend for the aromatic hydrogen (Fig. 3-8c) is accurate

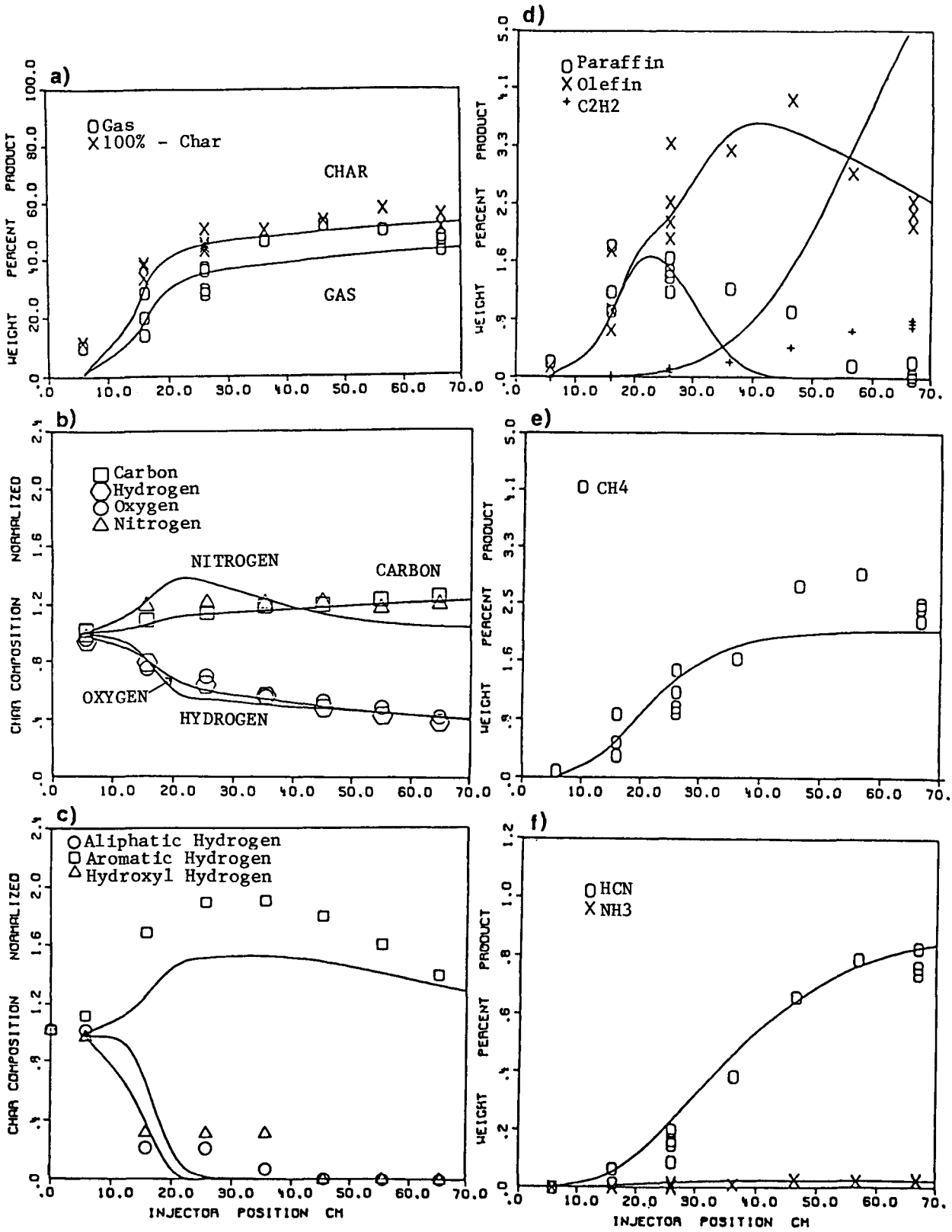

Figure 3-8. Pyrolysis Product Distribution for North Dakota Lignite in Nitrogen at 1100°C in an Entrained Flow Reactor. (30).

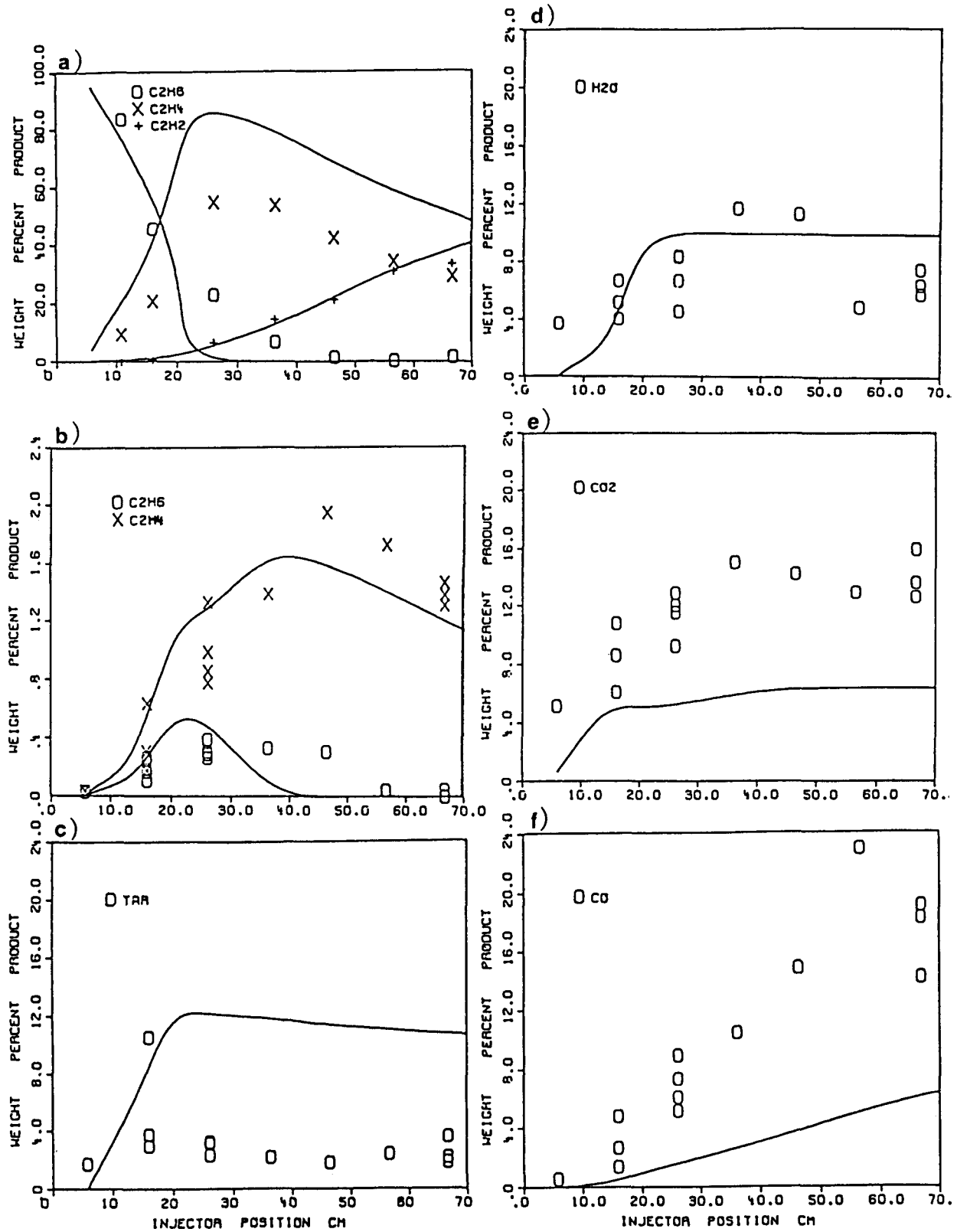

Figure 3-9. Pyrolysis Product Distribution for North Dakota Lignite in Nitrogen at 1100°C in an Entrained Flow Reactor. (30).

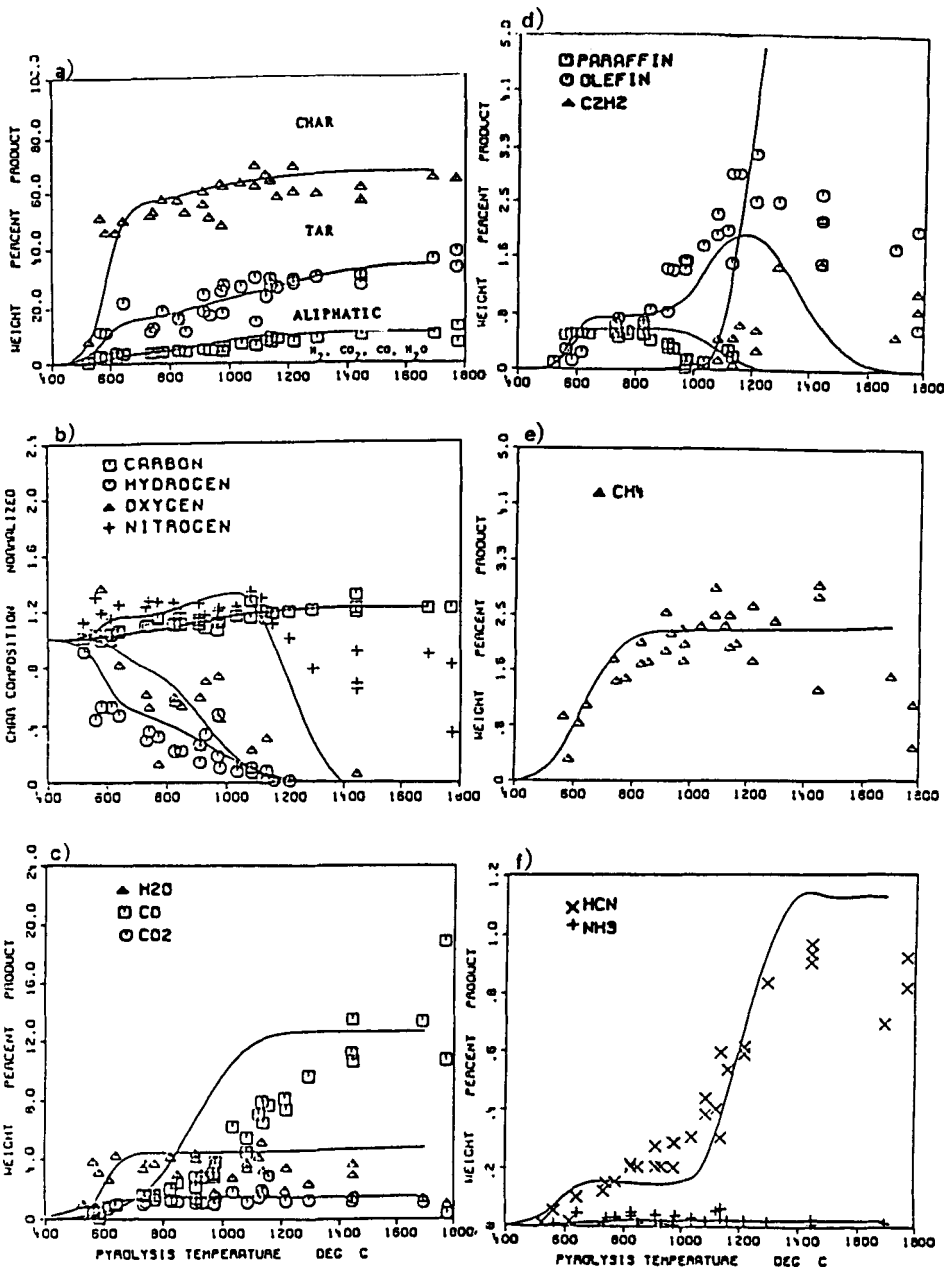

Figure 3-10. Pyrolysis Product Distribution for Pittsburgh Seam Bituminous Coal in Vacuum for 10 Seconds in a Heated Grid. (30).

TABLE 3-1

Kinetic Rate Coefficients and Functional Group Compositions

Composition Parameters		PSOC 170 Pittsburgh Seam Coal (WT% DAF)	Beulah Lignite (WT% DAF)	Kinetic Rate Coefficients (sec^{-1})		
	C	.819	.703			
	H	.054	.049			
	N	.014	.011			
	S(organic)	.019	.011			
	O	.094	.226			
		1.000	1.000			
Y^o_1	CO_2 - Loose	.006	.052	k_1	$= 1.0 \times 10^{21}$	$\exp((-38,376 \pm 4000)/T)$
Y^o_2	CO_2 - Tight	.002	.013	k_2	$= 2.4 \times 10^{11}$	$\exp((-28,800 \pm 1000)/T)$
Y^o_3	H_2O	.029	.101	k_3	$= 1.7 \times 10^{14}$	$\exp((-30,000 \pm 1500)/T)$
Y^o_4	CO - Ether Loose	.006	.020	k_4	$= 1.7 \times 10^{11}$	$\exp((-25,000 \pm 2500)/T)$
Y^o_5	CO - Ether Tight	.103	.136	k_5	$= 2.5 \times 10^{7}$	$\exp((-23,000 \pm 2300)/T)$
Y^o_6	HCN - Loose	.003	.008	k_6	= 5400	exp(-8850/T)*
Y^o_7	HCN - Tight	.024	.012	k_7	$= 7.0 \times 10^{7}$	exp(-32,000/T)*
Y^o_8	NH_3	.0004	.001	k_8	$= 1.2 \times 10^{12}$	$\exp((-27,300 \pm 3000)/T)$
Y^o_9	CH_x - Aliphatic	.196	.169	k_9	$= 1.7 \times 10^{14}$	$\exp((-30,000 \pm 1500)/T)$
Y^o_{10}	Methane	.033	.021	k_{10}	$= 1.2 \times 10^{12}$	$\exp((-27,300 \pm 3000)/T)$
Y^o_{11}	H-Aromatic	.017	.015	k_{11}	$= 1.6 \times 10^{7}$	$\exp((-23,000 \pm 2300)/T)$
Y^o_{12}	C-Non Volatile	.562	.441	k_{12}	= 0	
Y^o_{13}	S-Organic	.019	.011			
	Total	1.000	1.000			
X^o	Tar	.43	.16	K_T	$= 4.5 \times 10^{12}$	$\exp((-26,400 \pm 1500)/T)$
Cracking Rates:						
	Paraffins - Olefins			k_{OL}	$= 1.5 \times 10^{11}_{7}$	exp((-27,600/T)
	Olefin - Acetylene			k_{AC}	$= 2.1 \times 10^{7}$	exp (-22,000/T)

*Distributed rates have not yet been determined.

but the amplitude is low. This may be due to the conversion of hydroaromatic to aromatic hydrogen accompanying the stabilization of tar and aliphatic free radicals. This effect has now been incorporated into the mathematical model.

The evolution of paraffins, olefins and acetylene are considered in Figs 3-8d and 3-10d. Both data sets show the cracking of paraffins to form olefins and the cracking of olefins to form acetylene. The data are reasonably well predicted by the model except for acetylene for which the prediction is too high. This is probably due to soot formation from the acetylene. Determination of the kinetics for paraffin and olefin cracking were obtained by injecting ethane into the furnace. These data are illustrated in Fig. 3-9a along with the data on ethane and ethylene from coal pyrolysis in Fig. 3-9b. Acetylene yields for the pure ethane case were in agreement with theory indicating that there is less soot formation in the pure case than with coal present. The incorporation of soot production into the model will be the subject of future work.

The predictions for methane formation (Figs. 3-8e and 3-10e) need additional work. Cracking of methane which is evident for the bituminous coal from the low concentrations of methane at high temperatures has not been modeled. Additional methane formed from methyl groups created during the stabilization of radicals and from cracking of other species has also been neglected. This may be the reason for the low prediction for the lignite.

Results for HCN and NH_3 are presented in Figs. 3-8f and 3-10f. HCN production is the dominant nitrogen gas species. The model prediction is in good agreement with the data. The high prediction for HCN from the bituminous coal is in agreement with the low prediction for nitrogen in the char, Fig. 3-10b.

The oxygen containing species are considered in Figs. 3-9d-f and Fig. 3-10c. The data for the heated grid case (Fig. 3-10c) where secondary reactions are minimized are reasonably predicted except for CO for which the rate seems too high. The predictions for the entrained flow reactor (Figs. 3-9d-f), where secondary reactions occur, are very inaccurate. Incorporation of these reactions into the model will be the subject of future work.

Section 4

PYROLYSIS RESULTS

Pyrolysis measurements were performed on 6 coals with variations in temperature, ambient gas composition and coal type. This section presents the data obtained with four coals (Pittsburgh #8 and Illinois #6 bituminous coals, a Wyoming subbituminous coal and a Montana lignite) pyrolyzed in helium at furnace temperatures from 700°C to 1200°C, during initial testing of the reactor. The initial test suggested a number of improvements in the reactor configuration to improve product collection. These improvements were made under DOE contract #DE-AC21-81FE05122. Using the improved reactor, additional data were obtained for a second Illinois #6 and a Utah bituminous in Nitrogen at 1100°C at 1 atmosphere. Compositions for the six coals are given in Table 4-1.

INITIAL RESULTS WITH FOUR COALS

During the initial testing of the reactor, pyrolyses were performed in helium at temperatures from 700°C to 1200°C. The run conditions are presented in Table 4-2. During this period of operation, weights of the coal fed and products collected were not determined. Instead, the gas was sampled during a period when the coal feed rate was held constant. Measurements were made of the volume feed rate of coal in cc/min in the coal feeder and of the density of the coal powder in grams/cc to determine the coal feed rate in grams/min. The volume percent of pyrolysis gases were determined in the external FT-IR cell. The gases were determined as a weight % of coal from the molecular weight of the gas and the known input gas feed rate in liter/min.

Char samples were collected for analysis. Average coal and char particle weights were determined by counting and weighing groups of particles. An example is shown in Table 4-3. The table shows the results for Jacob's Ranch chars obtained at increasing distance in the reactor at a temperature of 1000°C. The determinations for a given char show good reproducibility and the averages for the five chars show a continuous weight loss with reactor distance.

Elemental analyses for the chars were obtained at Galbraith Laboratory. Under the DOE contract #DE-AC21-81FE05122, FT-IR spectra were obtained for all the chars

TABLE 4-1

Ultimate Analyses for Six Coals
Used in the Entrained Flow Reactor Study

COAL	TYPE	WT% (DAF)					
		C	H	N	S	O	ASH (Dry)
Savage	Montana Lignite	71.2	4.6	1.1	1.3	21.8	10.6
Jacob's Ranch	Wyom. Subbituminous	74.3	5.2	1.1	.6	18.8	7.8
Illinois #6	Bituminous (C.E.)	73.9	5.1	1.4	4.2	15.4	11.0
Pittsburgh #8	Bituminous	83.5	5.5	1.6	3.3	6.1	9.2
Utah	Bituminous (Texaco)	75.9	5.4	1.3	.5	16.9	8.5
Illinois #6	Bituminous (Texaco)	75.9	5.5	1.5	4.1	12.4	13.2

TABLE 4-2

Experimental Conditions

Run #	Coal	Wall Temp (°C)	Ambient Gas	Coal Feed Rate (g/min)	Carrier and Sheath Gas Feed (l/min)	Secondary Gas Feed Rate (l/min)	Average Hot Gas Velocity (m/sec)
1.	Ill. #6 (CE)	800	Helium	2.4	1.0	46.5	1.5
2.	Pitts. #8	800	Helium	2.4	1.0	46.5	1.5
3.	Savage Lignite	800	Helium	2.4	1.0	46.5	1.5
4.	Jacob's Ranch	700	Helium	2.4	1.0	50.4	1.5
5.	Jacob's Ranch	800	Helium	2.4	1.0	46.5	1.5
6.	Jacob's Ranch	900	Helium	2.4	1.0	42.0	1.5
7.	Jacob's Ranch	1000	Helium	2.4	1.0	39.2	1.5
8.	Jacob's Ranch	1200	Helium	2.4	1.0	33.6	1.5
9.	Ill. #6 (Tex)	1100	Nitrogen	1.5	1.0	26.6	1.1
10.	Utah	1100	Nitrogen	1.7	1.0	26.6	1.1

TABLE 4-3

Determination of Average Particle Weights

Injector Distance	Sample Weight (micrograms)	#of Particles in Sample	Average Weight/Particle (micrograms)
66 cm	4.1	60	$6.83X10^{-2}$
	7.2	105	$6.86X10^{-2}$
	3.0	43	$6.98X10^{-2}$
	6.2	92	$6.74X10^{-2}$
	4.8	69	$6.96X10^{-2}$
			Average $6.87X10^{-2}$
56 cm	7.6	105	$7.24X10^{-2}$
	5.5	69	$7.97X10^{-2}$
	4.0	52	$7.69X10^{-2}$
	7.8	107	$7.29X10^{-2}$
	5.9	78	$7.56X10^{-2}$
			Average $7.55X10^{-2}$
46 cm	9.8	122	$8.03X10^{-2}$
	7.4	94	$7.87X10^{-2}$
	8.6	108	$7.96X10^{-2}$
	9.6	119	$8.07X10^{-2}$
	4.4	55	$8.00X10^{-2}$
			Average $7.99X10^{-2}$
36 cm	9.0	97	$9.28X10^{-2}$
	3.2	36	$8.89X10^{-2}$
	4.6	50	$9.20X10^{-2}$
	9.2	102	$9.02X10^{-2}$
	6.6	75	$8.80X10^{-2}$
			Average $9.04X10^{-2}$
21 cm	5.2	49	$10.6X10^{-2}$
	8.0	83	$9.64X10^{-2}$
	12.0	116	$10.3X10^{-2}$
	5.4	52	$10.4X10^{-2}$
	6.5	67	$9.70X10^{-2}$
			Average $10.1X10^{-2}$
6 cm	3.4	27	$12.6X10^{-2}$
	11.0	98	$11.2X10^{-2}$
	8.5	67	$12.7X10^{-2}$
	11.8	91	$13.0X10^{-2}$
	18.2	141	$12.9X10^{-2}$
			Average $12.5X10^{-2}$

produced in the reactor using the techniques described in Section 2.

Spectra for the chars produced at 800°C are illustrated in Figs. 4-1 to 4-8. Spectra in Figs. 4-1 to 4-4 are for dry KBr pellets. The slope is due to scattering by the char particles which increases with carbon concentration. A scattering correction has removed the slope in Figs. 4-5 to 4-8. The spectra show rapid removal of aliphatic (peaks near 2900 cm-1), and about 1/2 the hydroxyls (broad hill peaked at 3400 wavenumbers). The spectra show retention of aromatic hydrogen (peaks near 800 and 3100 wavenumbers) and of C-O bonds (broad peak near 1200 wavenumbers). The peak at 1600 is also retained. This peak is believed to be due to strongly hydrogen bonded hydroxyls (perhaps to ring nitrogens) (37). Mineral peaks increase as volatiles are removed from the char. The results for Illinois #6, Pittsburgh #8, Montana Lignite, and the Wyoming subbituminous are all similar indicating that the functional group chemistry in the chars is insensitive to coal rank. Evidence such as this suggests that a pyrolysis model can be created using kinetic rate coefficients which are independent of coal.

Spectra for Jacob's Ranch chars produced at 700, 900, 1000°C and 1200°C are presented in Figs. 4-9 to 4-16. Spectra for 1000°C and above show aromatic hydrogen (peaks near 800 and 3100 wavenumbers) reaching a maximum and then dropping at long residence distances. The C-O bond concentration also appears to be reduced at long residence distances. The 1600 peak is also drastically reduced. The slopes increase with increasing carbon concentration in the char.

Normalized functional group concentrations presented in Figs. 4-17c to 4-24c, have been obtained by dividing the respective peak heights by the corresponding peak heights in the parent coal.

The pyrolysis data for Runs 1-8 are compared to the theoretical predictions in Figs. 4-17 to 4-24. The kinetic rate coefficients and coal composition parameters are presented in Tables 4-4 and 4-5. Note that all coals are fitted using the same kinetic rate coefficients.

Figures 4-17a to 4-24a present the particle temperature calculated for each run. A complete time-temperature history is calculated for each injector position and temperature. Swelling effects which would influence the radiation absorption have not been included.

Figures 4-17b to 4-24b present the elemental compositions normalized by their

respective values in the parent coal (i.e. C (char) /C (coal)). Predicted values for C and H are in good agreement with the data. The trends for O+S are predicted but, there are substantial differences in magnitude. Since O+S are determined by differences, this is not surprising. Predictions for nitrogen are too high. The problem with nitrogen is discussed in the next section.

Figures 4-17c to 4-24c present the hydrogen functional group concentrations normalized to their respective values in the parent coal. In general, the trends and magnitudes have been predicted with good accuracy. The predicted aromatic hydrogen in the lignite is too low, an effect also seen in Fig. 3-8c. There appears to be some chemical effect not modeled which is most important for lignites.

Figures 4-17d to 4-24d present the char and volatiles. The weight percent char has been determined by weighing groups of char particle as discussed above. The results are in reasonable agreement with the predictions except for the Pittsburgh coal, Fig. 4-18. This was the only swelling coal studied and the effects of swelling and sticking may cause a sytematic increase in the char weight.

Results for methane, CO and CO_2 are presented in Figs. 4-17 to 4-24 e and f. The trends and orders of magnitude are correct but there is substantial scatter in the gas data. The modifications to the reactor made subsequent to these runs have reduced the scatter for Runs 9 and 10 presented below.

In general there is reasonable agreement between the data and the prediction of the model.

RESULTS FOR ILLINOIS #6 AND UTAH BITUMINOUS COALS

After reactor modifications which resulted in the final configuration described in Section 2, pyrolyses were performed in nitrogen for Illinois #6 and Utah bituminous coal samples (received from Texaco) at a furnace temperature of 1100°C (Runs 9 and 10).

FT-IR spectra for chars and tars are presented in Figs. 4-25 to 4-28. The Utah and Illinois #6 chars show almost identical behavior. The scattering slope variations with injector position are similar. They are intermediate between those for the Jacob's Ranch chars at 1000°C and 1200°C. In agreement with the observations for Runs 1-8, the functional groups react at different rates. Aliphatics are fastest, methyl groups and hydroxyls are slower, aromatic hydrogen increases and then

decreases, and C-O bonds appear to be the least volatile. Mineral peaks increase proportionately as the volatile species are removed.

The theoretical results were obtained using the most recent version of the pyrolysis theory (56). The kinetic rate coefficients and coal composition parameters are presented in Table 4-4 and 4-5.

The comparisons of theory and experiment are presented in Figs. 4-29 to 4-39. It has been possible to obtain accurate simulations of most species for both coals. The analysis has suggested changes for kinetic rate coefficients presented previously (21) for CO-tight and tar. It also is apparent that cracking of heavy hydrocarbons to produce lighter species, which has not been modeled, prevents accurate modeling of the split between hydrocarbon species. It also appears that the evolution of HCN must be tied to the evolution of aromatic hydrogen as the formation of HCN requires hydrogen.

The char yields are presented in Fig. 4-29. There is good agreement between theory and experiment. Weight loss appears to occur slightly faster than predicted. This may result from more rapid particle temperature increases than are predicted. This would be expected if there were mixing of the particles and gas which removed them from the center line of the reactor.

The elemental compositions for the chars are presented in Fig. 4-30. The elemental composition of the char is normalized by the composition of the parent coal. The agreement between theory and experiment is good except for nitrogen at high temperature which is lower than predicted. Problems in modeling the nitrogen evolution occur because HCN evolution must be tied to the availability of hydrogen in the char. This modification is presently being addressed. As expected, there is scattering in the oxygen data which are done by difference.

The hydrogen functional group compositions for the chars are presented in Fig. 4-31. The functional group composition is normalized by the composition of the parent coal. There is good agreement between theory and experiment except for the high aromatic concentrations for the Utah Bituminous coal. This is the same problem that occurred for the lingite. A possible explanation is the formation of an aromatic hydrogen when a hydroxyl abstracts a hydrogen from the hydroaromatic or aliphatic to form water. Such chemistry would be expected for hydroxyl groups originally attached to hydroaromatics or aliphatics.

Figure 4-32 present data for the yields of tar and "dry gas" (gas minus water). The predicted gas values are good but the tar yields are too low. It is clear experimentally that tar is accumulating on the walls of the water cooled collector and in the cyclone. Comparing the predicted tar values with "tar plus missing" in Fig. 4-33 shows much closer agreement between theory and experiment.

Figure 4-34 presents the comparison for paraffins, olefins and acetylene. The results show the progressive cracking of compounds to form less saturated compounds as time or temtemperature increases. The general trends are predicted. While the start of the acetylene production occurs at the right place, the predicted values are much too high. This is believed to be due to soot formation which will be modeled in the future. The predicted values of olefin and paraffin are good for the Utah Bituminous coal and are in agreement with results for several other coals. For the Illinois #6 coal, the olefins are lower than predicted. The ratio of maximum olefin to paraffin for this coal is different from all other coals studied in this reactor.

Results for methane are presented in Fig. 4-35. Agreement between theory and experiment is excellent. In the present version of the theory, the tar gets enriched in methyl groups (the source for the methane) when it abstracts hydrogen to stabilize free radical sites. The subsequent cracking of the tar produces higher methane values than observed for the same coal in heated grid experiments where the tars cool quickly after formation.

Ethane and ethylene are presented in Fig. 4-36. Predictions for ethane are in agreement with the data. Predictions for ethylene are too low. This is most likely due to the cracking of higher molecular weight species to form ethylene which has not been modeled.

CO and CO_2 are presented in Fig. 4-37. Predictions for CO_2 are in good agreement with the data. Predictions for CO are not good for the Illinois #6. The predicted CO ultimate yield is determined from the oxygen which remains after CO_2 and H_2O evolution. Any errors in the coal's oxygen determination shows up in CO. The high sulfur values which include mineral sulfur is likely to result in an anomalously low oxygen value.

The results for water are presented in Fig. 4-38. There is good agreement between theory and experiment.

HCN and NH_3 are presented in Fig. 4-39. The predictions of NH_3 are good. The predictions of HCN need work and as discussed above, must be coupled to the hydrogen evolution.

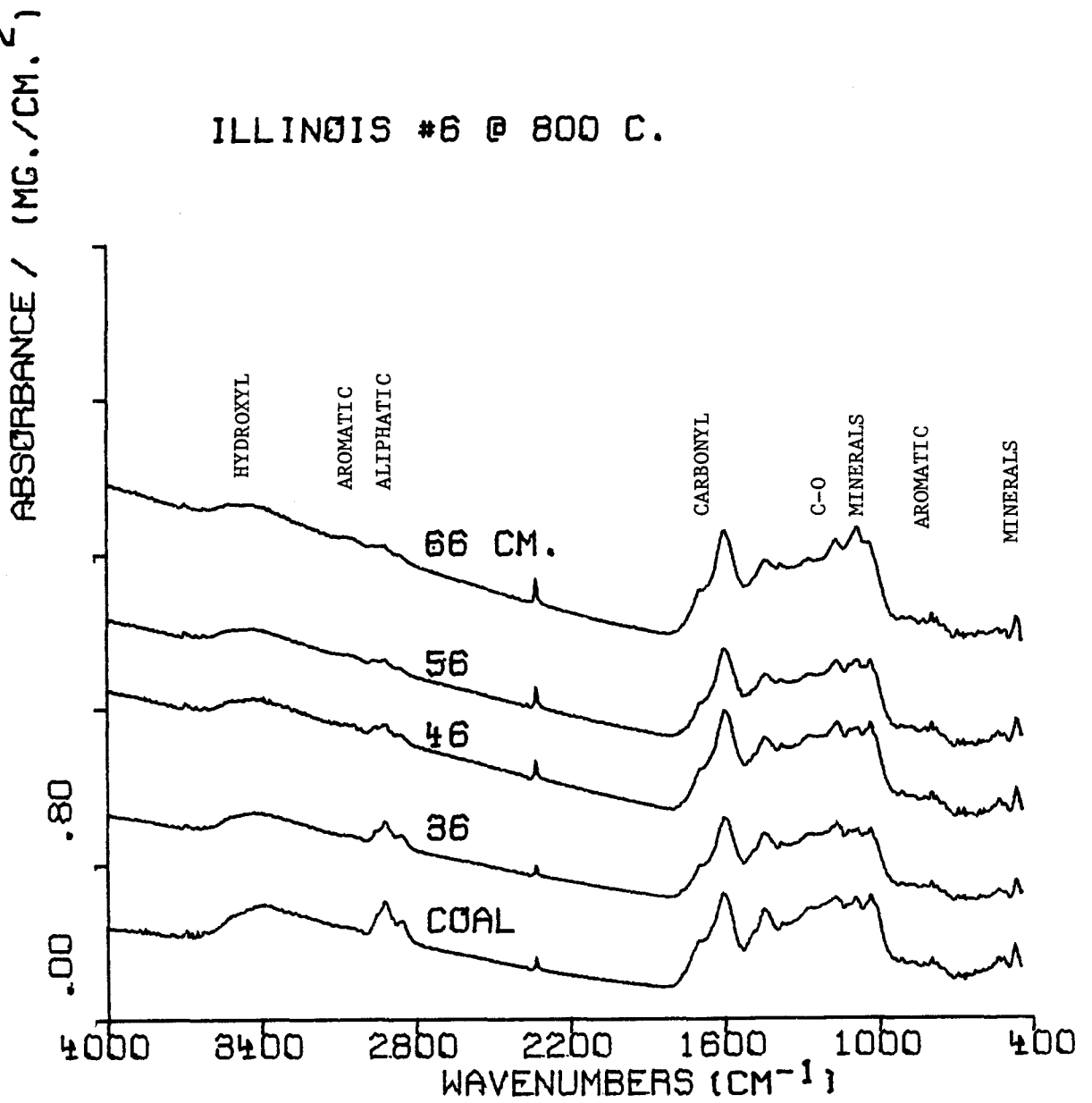

Figure 4-1. FT-IR Spectra of Chars from Illinois #6 Bituminous Coal Pyrolyzed at 800°C in Helium (Run #1). The spectra are for dried KBr pellets.

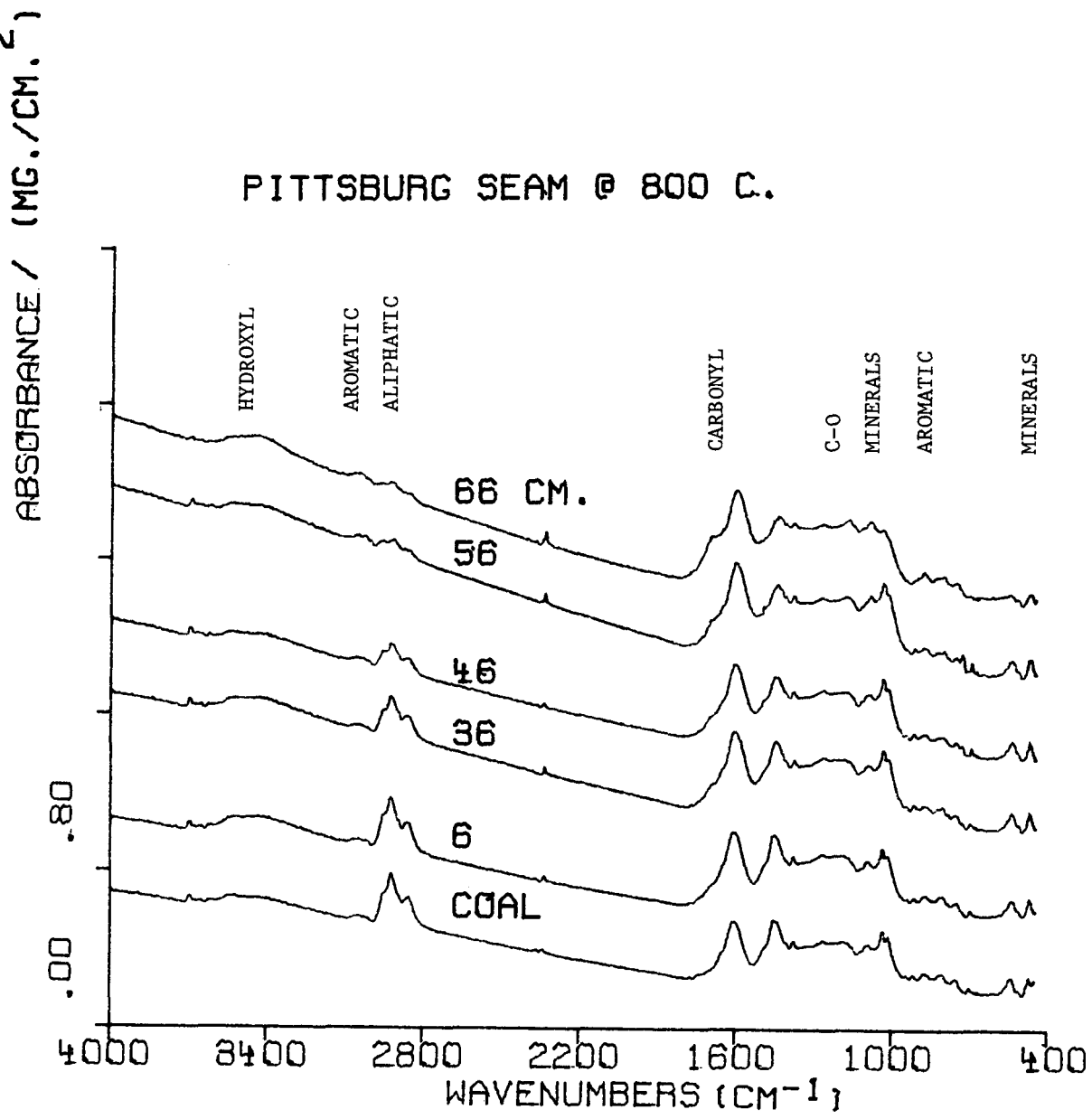

Figure 4-2. FT-IR Spectra of Chars from Pittsburgh Seam Bituminous Coal Pyrolyzed at 800°C in Helium (Run #2). The spectra are for dried KBr pellets.

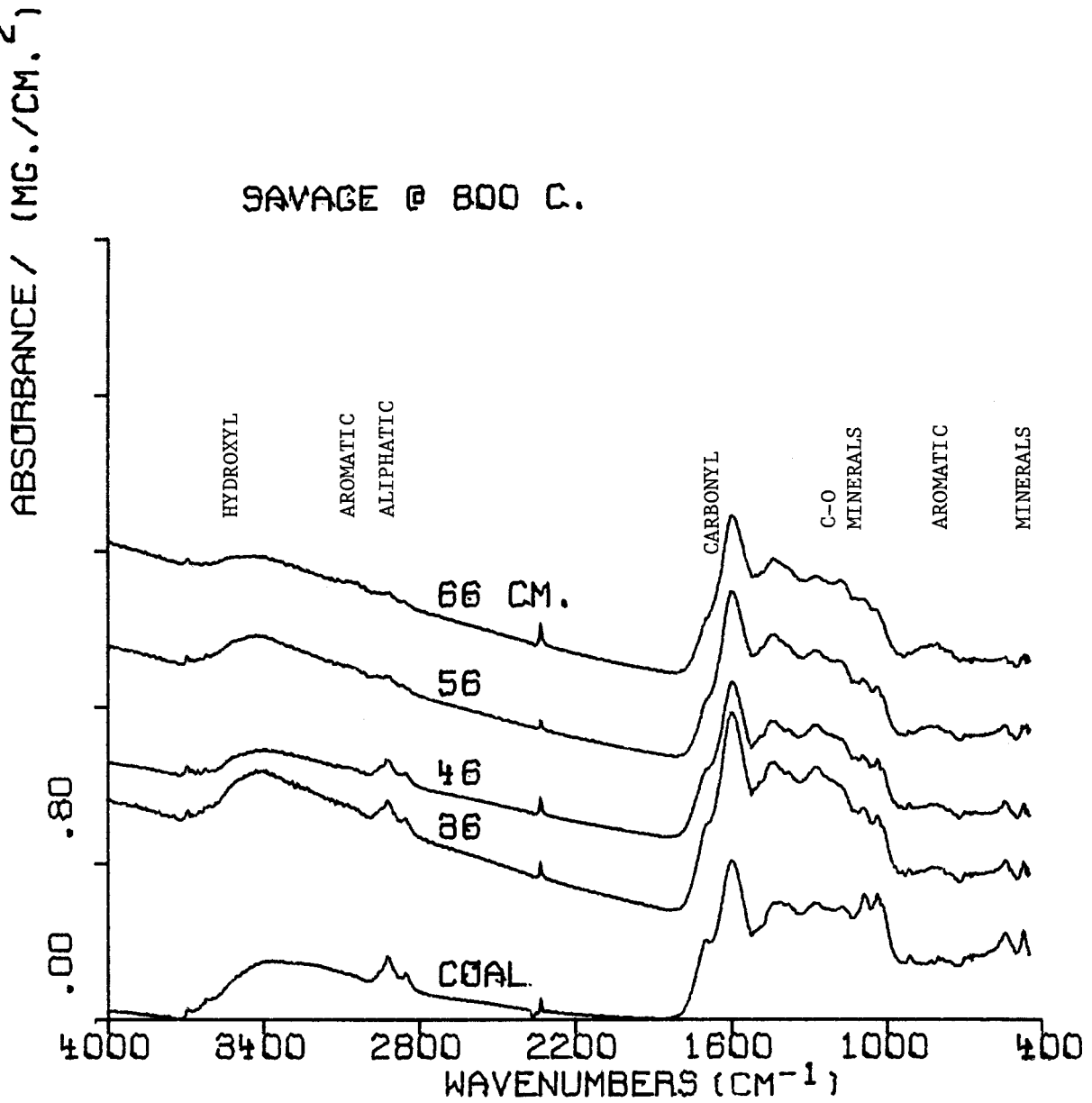

Figure 4-3. FT-IR Spectra of Chars from Savage, Montana Lignite Pyrolyzed at 800°C in Helium (Run #3). The spectra are for dried KBr pellets.

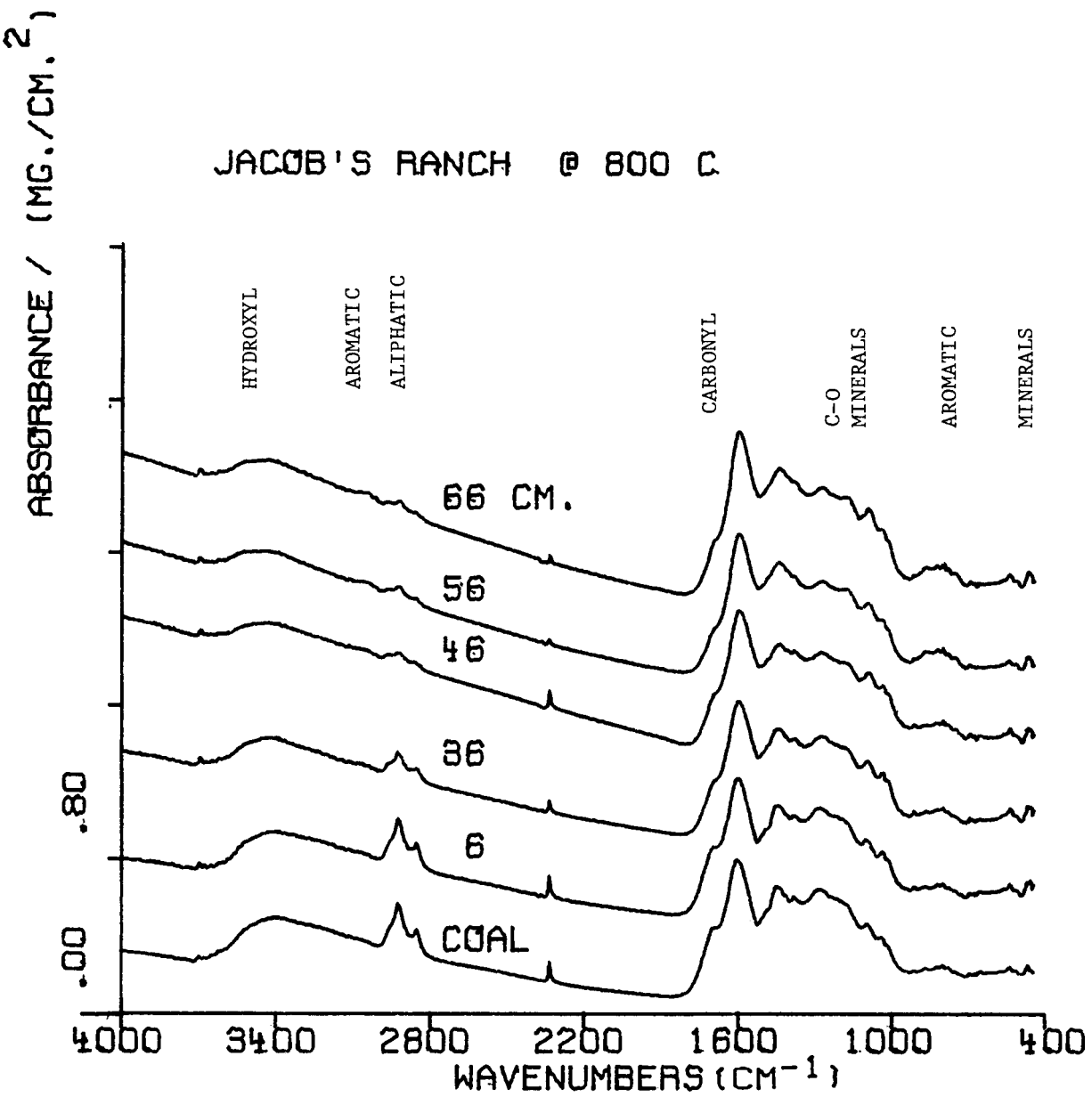

Figure 4-4. FT-IR Spectra of Chars from Jacob's Ranch Subbituminous Coal Pyrolyzed at 800°C in Helium (Run #5). The spectra are for dried KBr pellets.

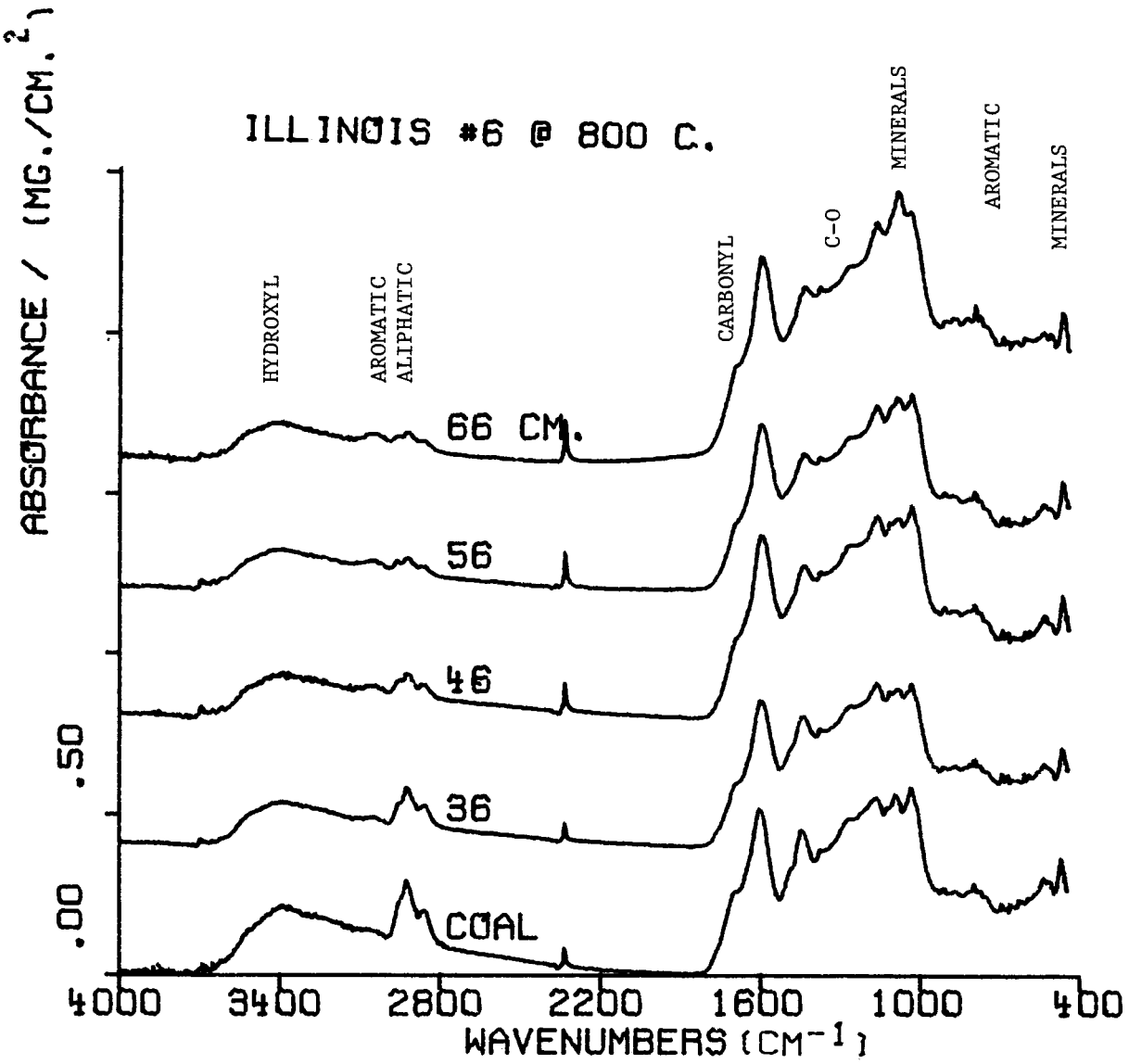

Figure 4-5. FT-IR Spectra of Chars from Illinois #6 Bituminous Coal Pyrolyzed at 800°C in Helium (Run #1). A scattering base line correction has been applied and the spectra have been scaled to 1 mg/cm^2 DRY.Coal.

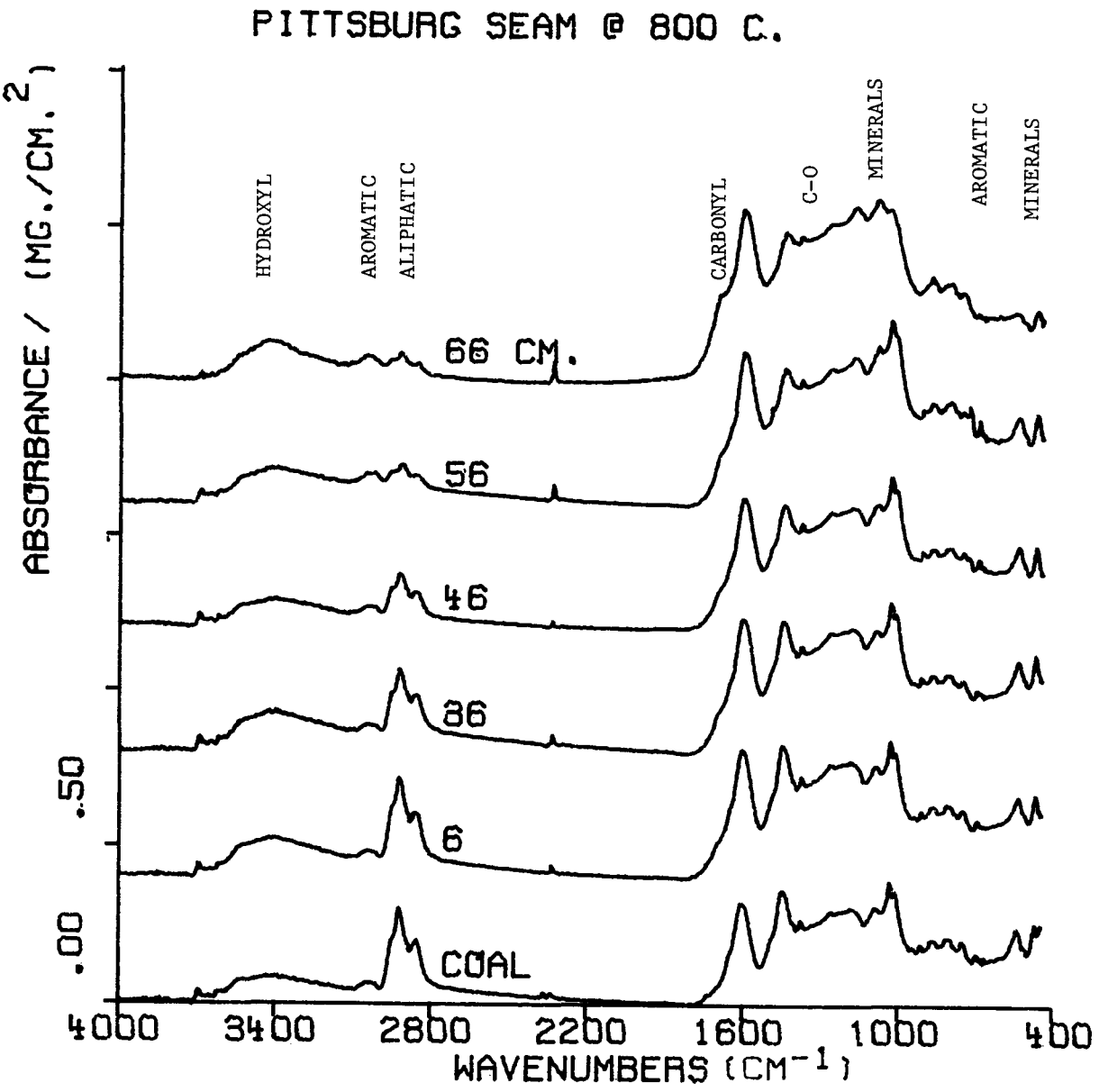

Figure 4-6. FT-IR Spectra of Chars from Pittsburgh Seam Bituminous Coal Pyrolyzed at 800°C in Helium (Run #2). A scattering base line correction has been applied and the spectra have been scaled to 1 mg/cm^2 DRY Coal.

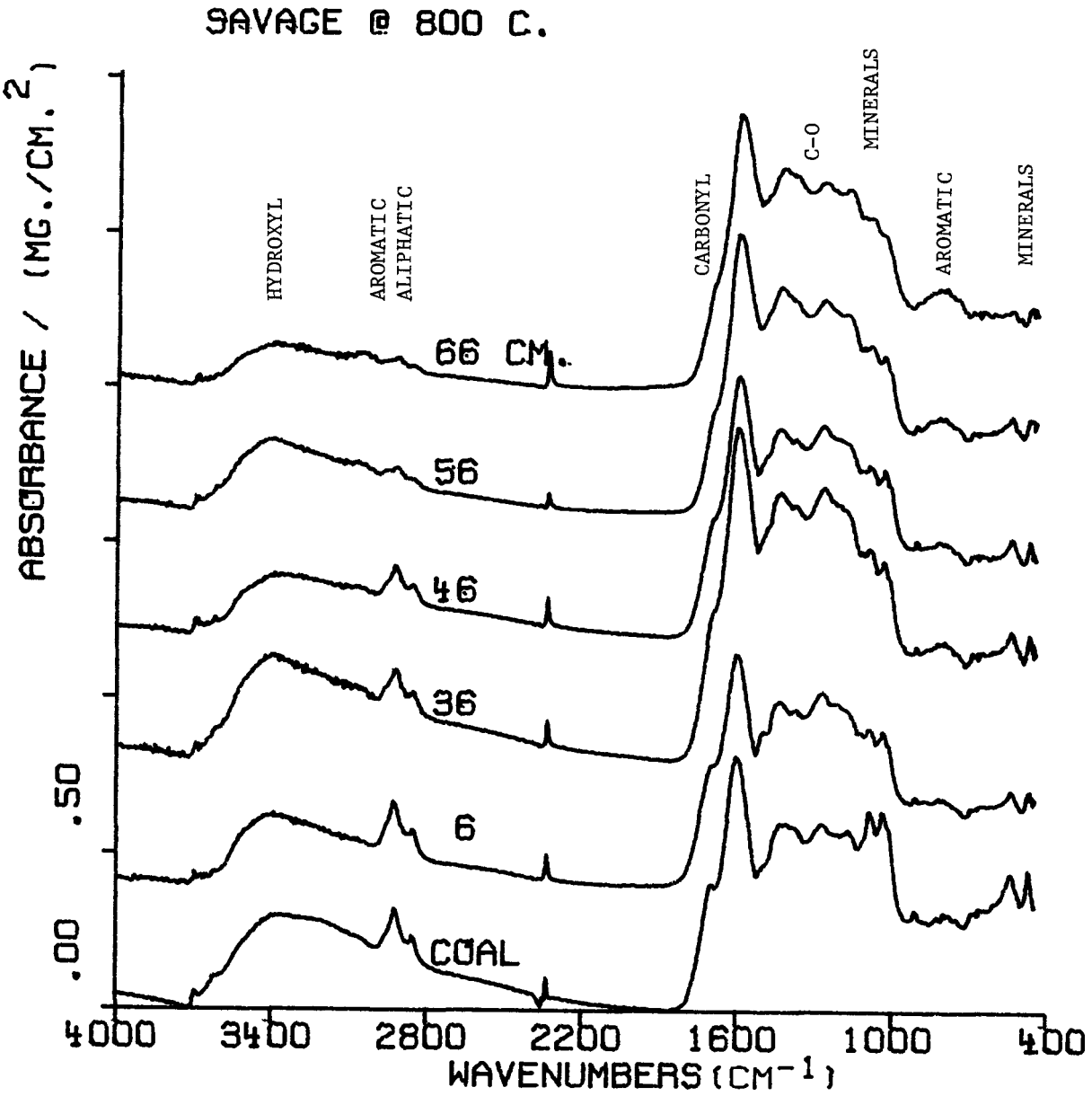

Figure 4-7. FT-IR Spectra of Chars from Savage, Montana Lignite Pyrolyzed at 800°C in Helium (Run #3). A scattering base line correction has been applied and the spectra have been scaled to 1 mg/cm^2 DRY Coal.

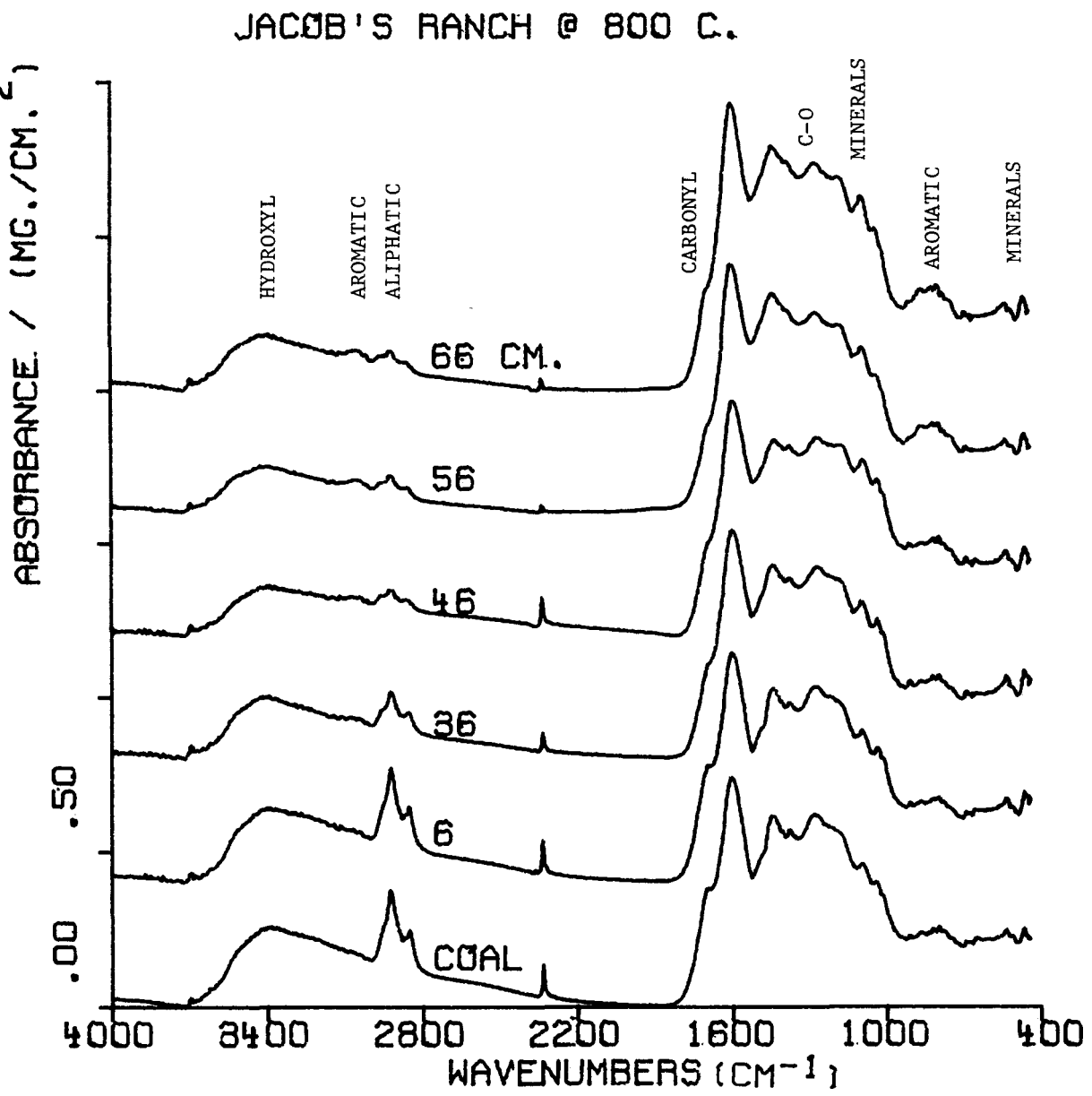

Figure 4-8. FT-IR Spectra of Chars from Jacob's Ranch Subbituminous Coal Pyrolyzed at 800°C in Helium (Run #5). A scattering base line correction has been applied and the spectra have been scaled to 1 mg/cm^2 DRY Coal.

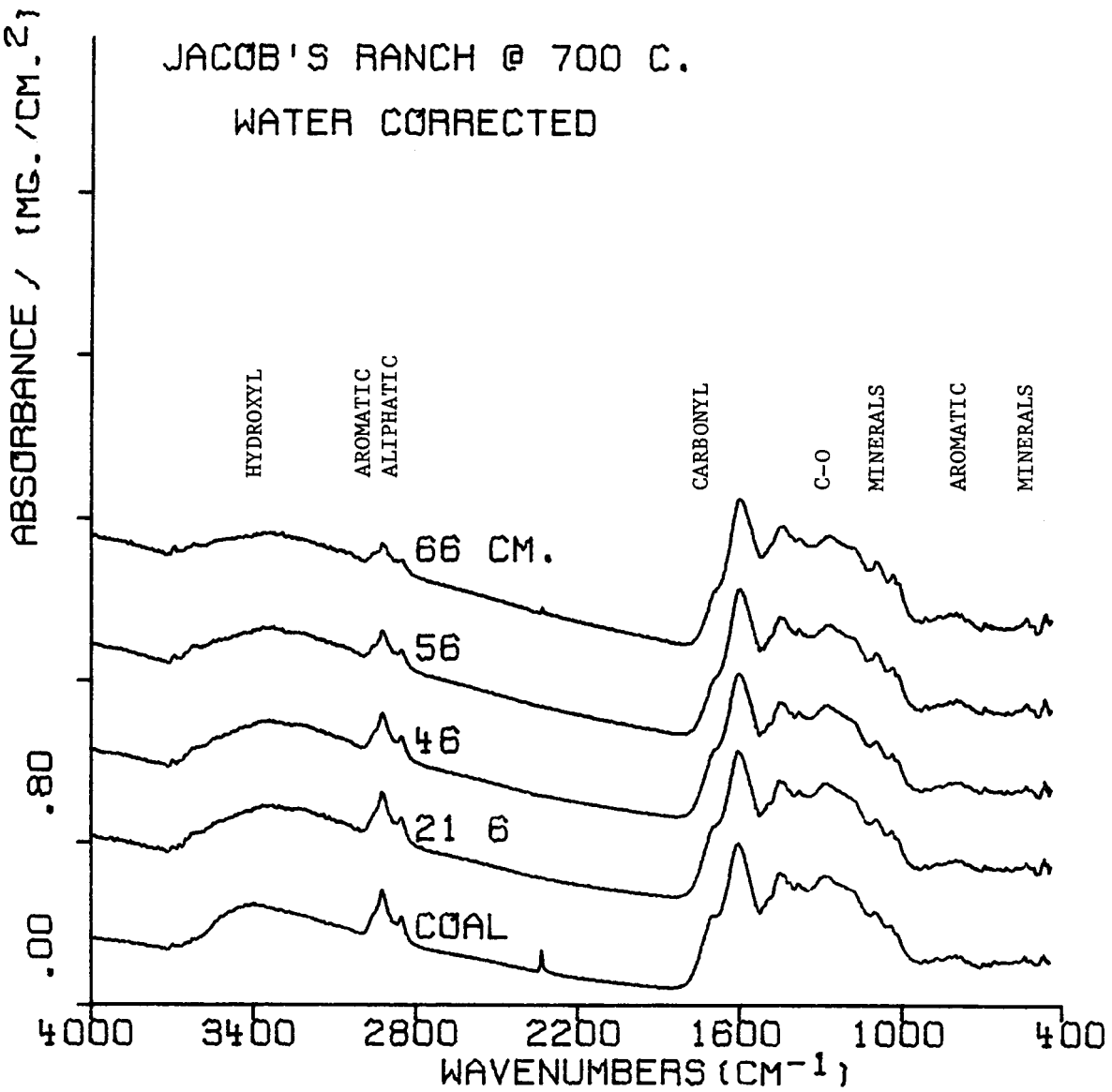

Figure 4-9. FT-IR Spectra of Chars from Jacob's Ranch Subbituminous Coal in Helium at 700°C (Run #4). The spectra are for dried KBr pellets.

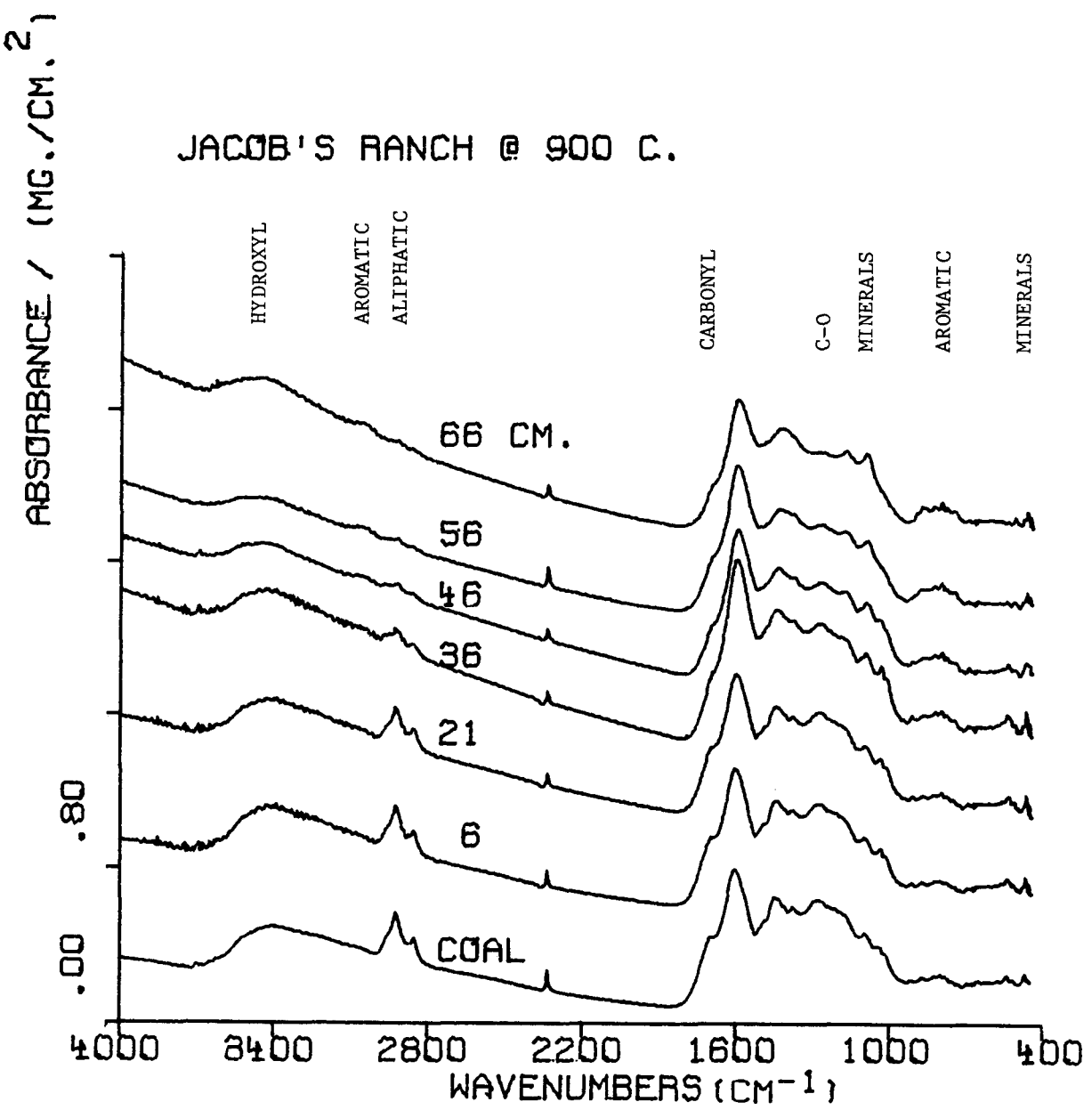

Figure 4-10. FT-IR Spectra of Chars from Jacob's Ranch Subbituminous Coal in Helium at 900°C (Run #6). The spectra are for dried KBr pellets.

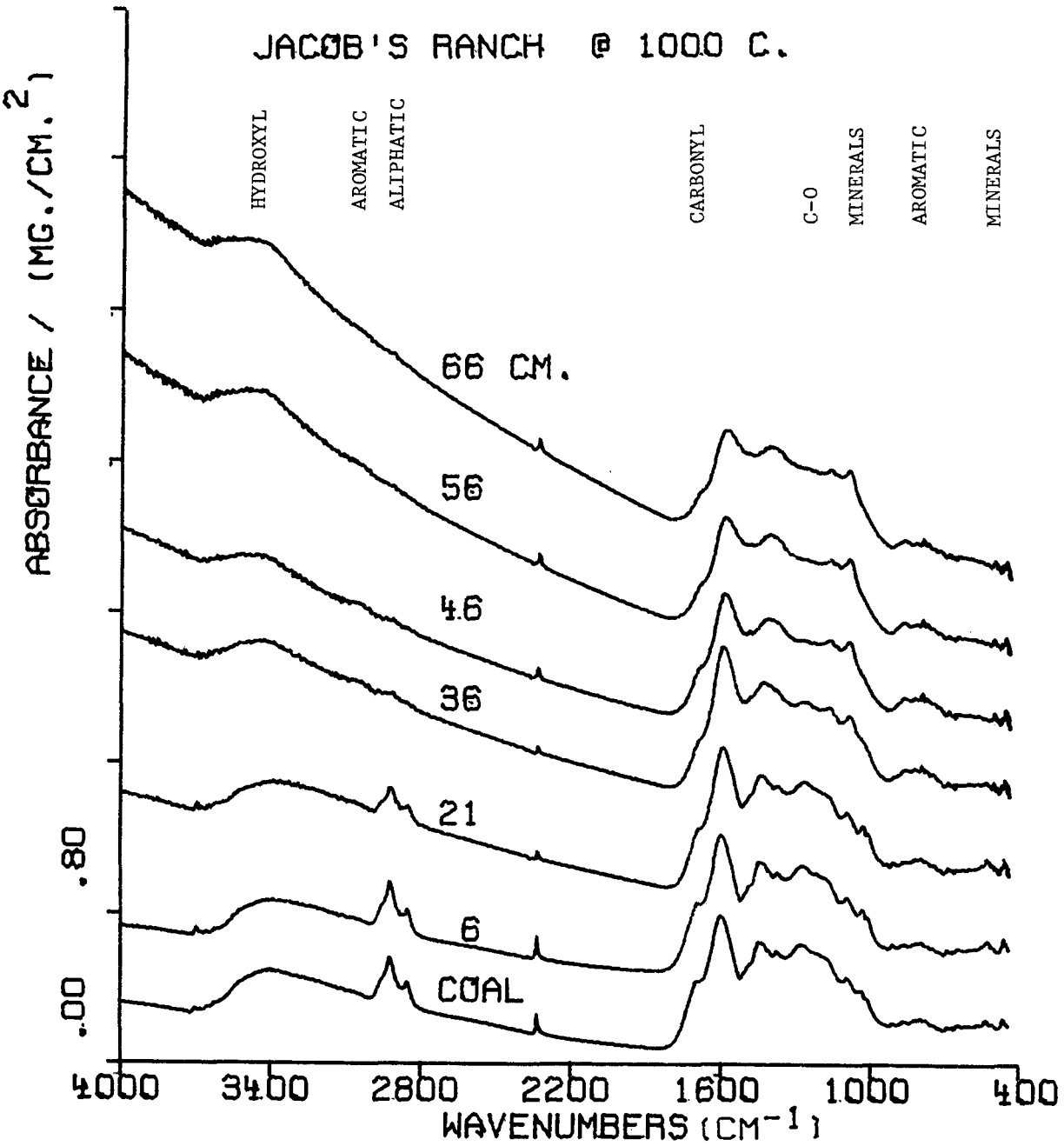

Figure 4-11. FT-IR Spectra of Chars from Jacob's Ranch Subbituminous Coal in Helium at 1000°C (Run #7). The spectra are for dried KBr pellets.

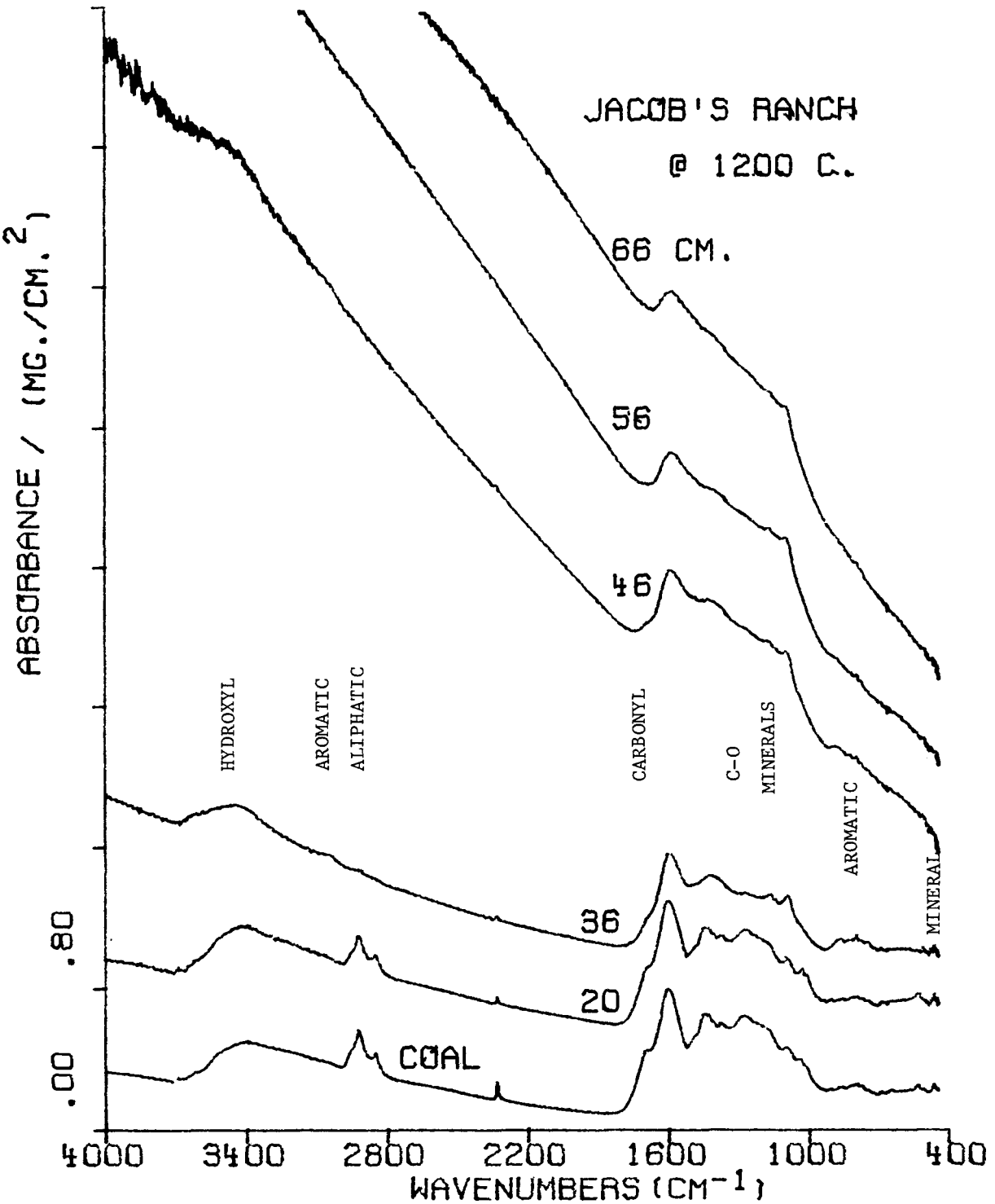

Figure 4-12. FT-IR Spectra of Chars from Jacob's Ranch Subbituminous Coal in Helium at 1200°C (Run #8). The spectra are for dried KBr pellets.

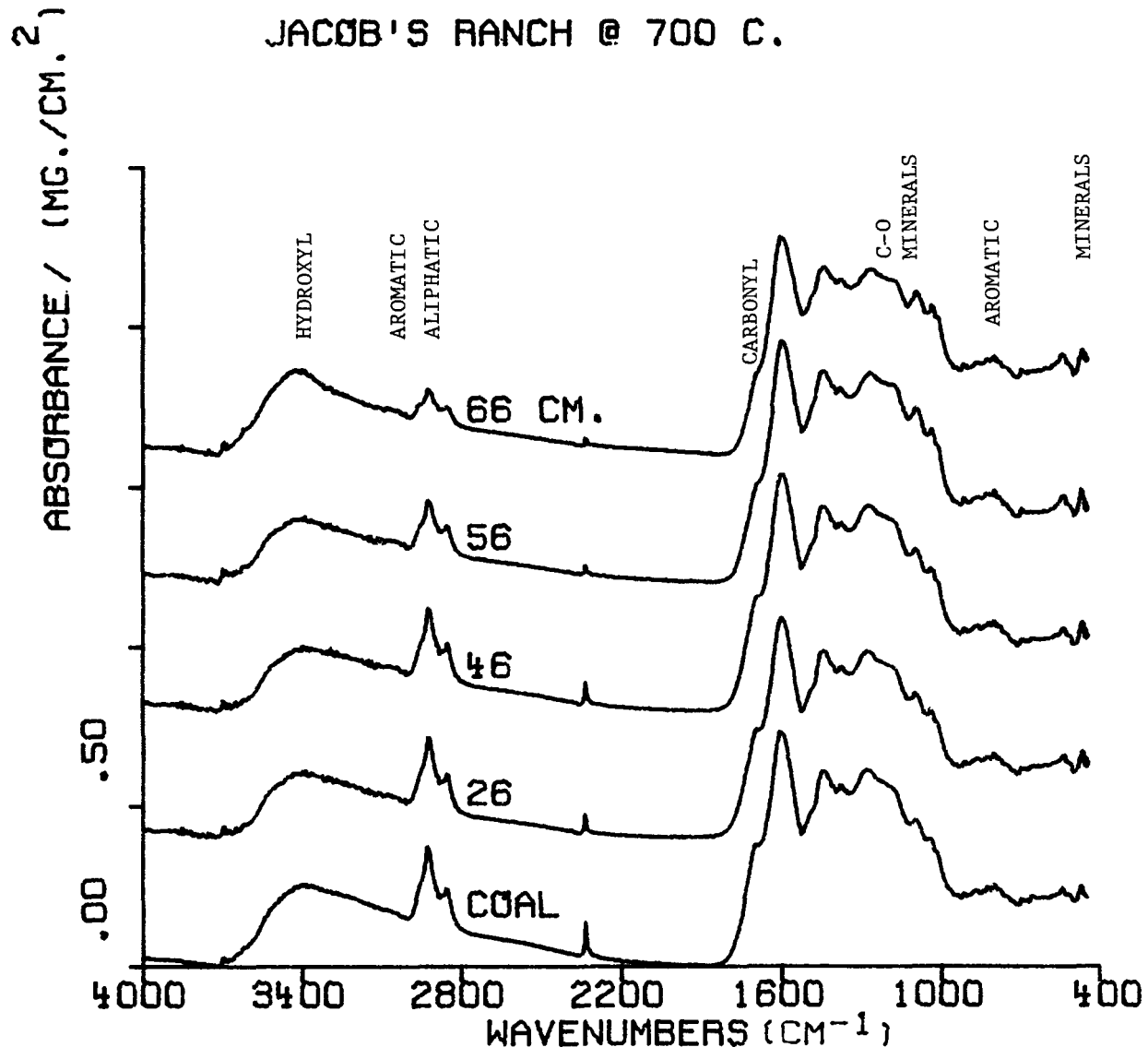

Figure 4-13. FT-IR Spectra of Chars from Jacob's Ranch Subbituminous in Helium at 700°C (Run #4). A scattering base line correction has been applied and the spectra have been scaled to 1 mg/cm^2 DRY Coal.

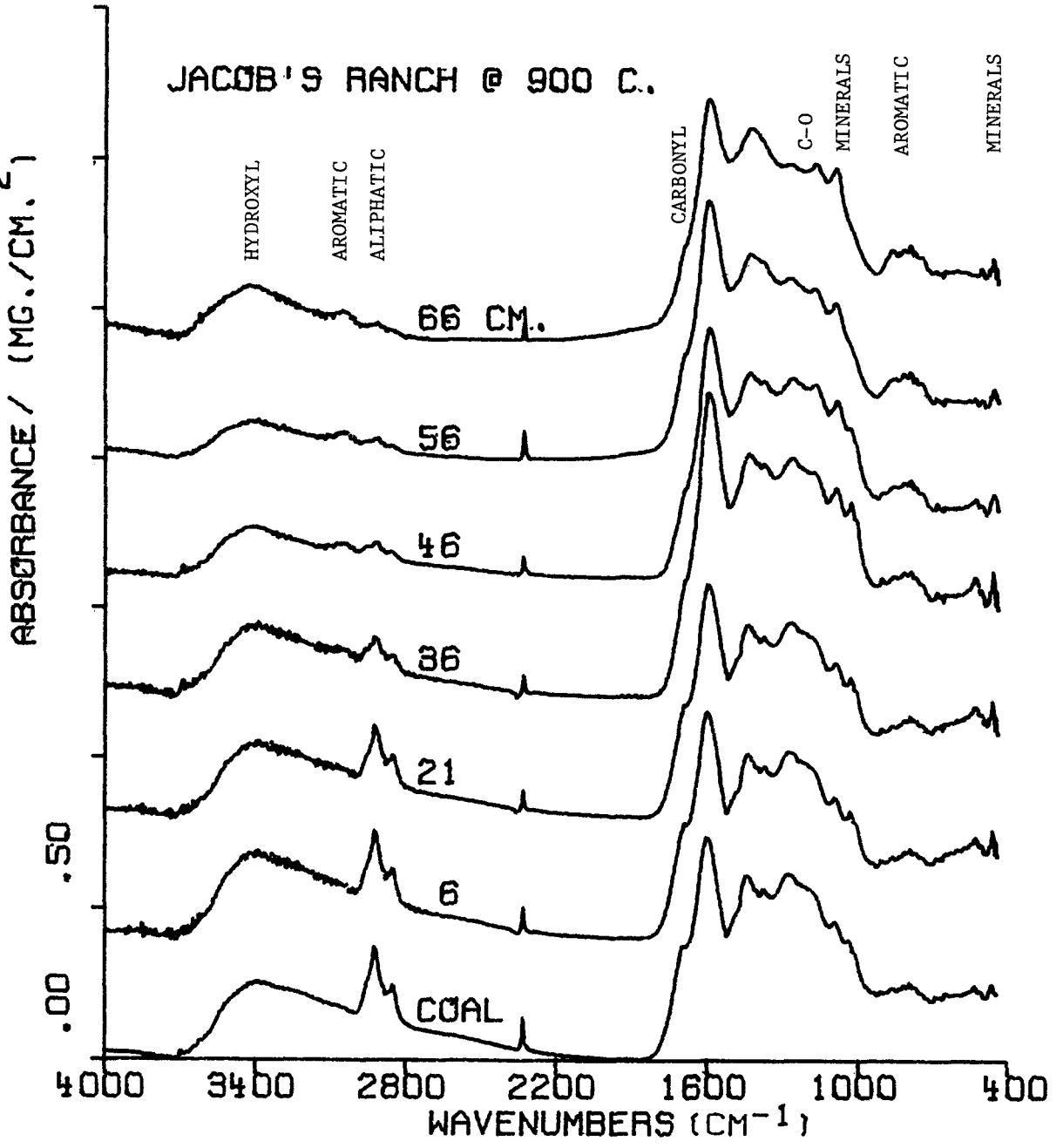

Figure 4-14. FT-IR Spectra of Chars from Jacob's Ranch Subbituminous in Helium at 900°C (Run #6). A scattering base line correction has been applied and the spectra have been scaled to 1 mg/cm^2 DRY Coal.

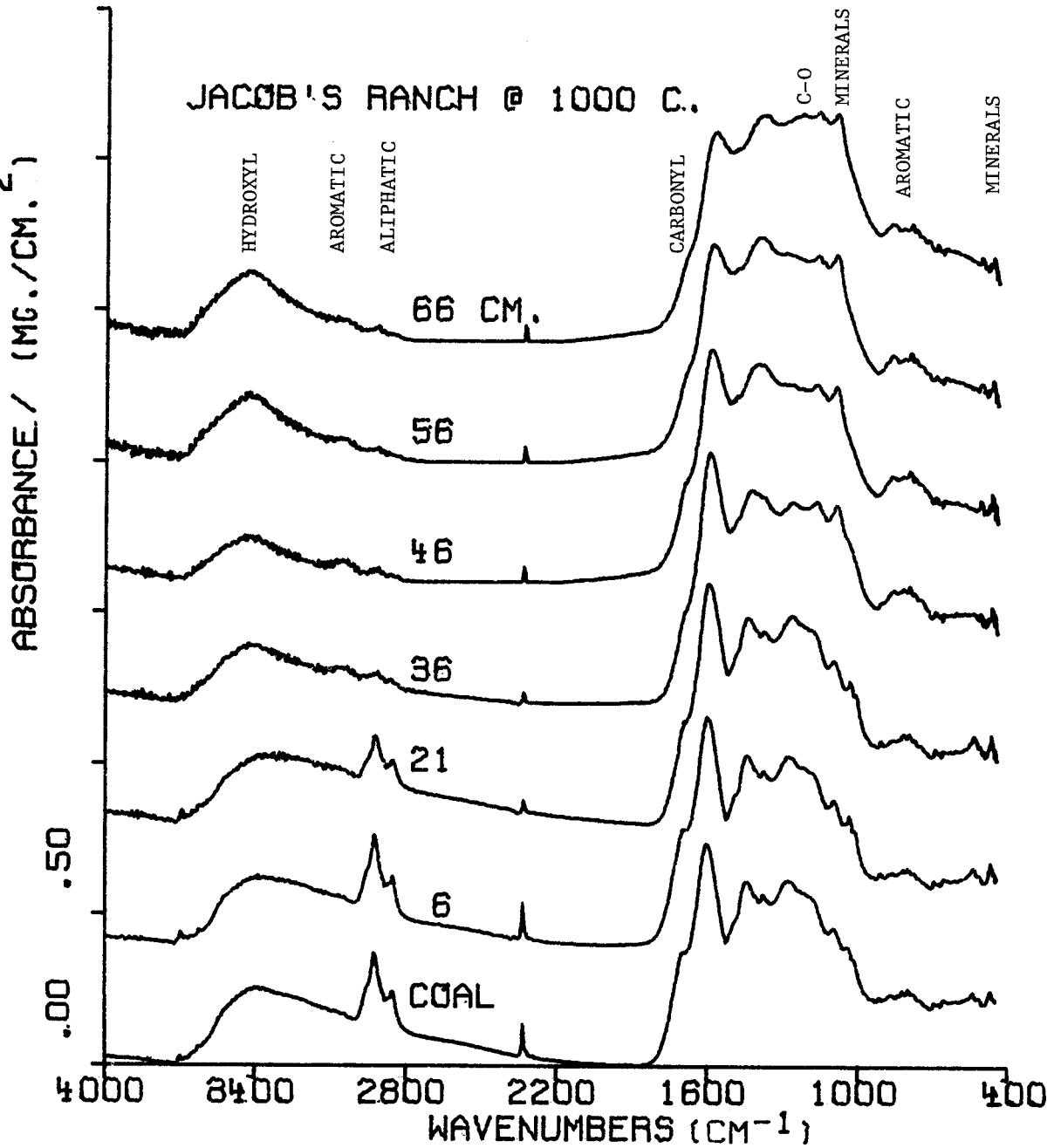

Figure 4-15. FT-IR Spectra of Chars from Jacob's Ranch Subbituminous in Helium at 1000°C (Run #7). A scattering base line correction has been applied and the spectra have been scaled to 1 mg/cm^2 DRY Coal.

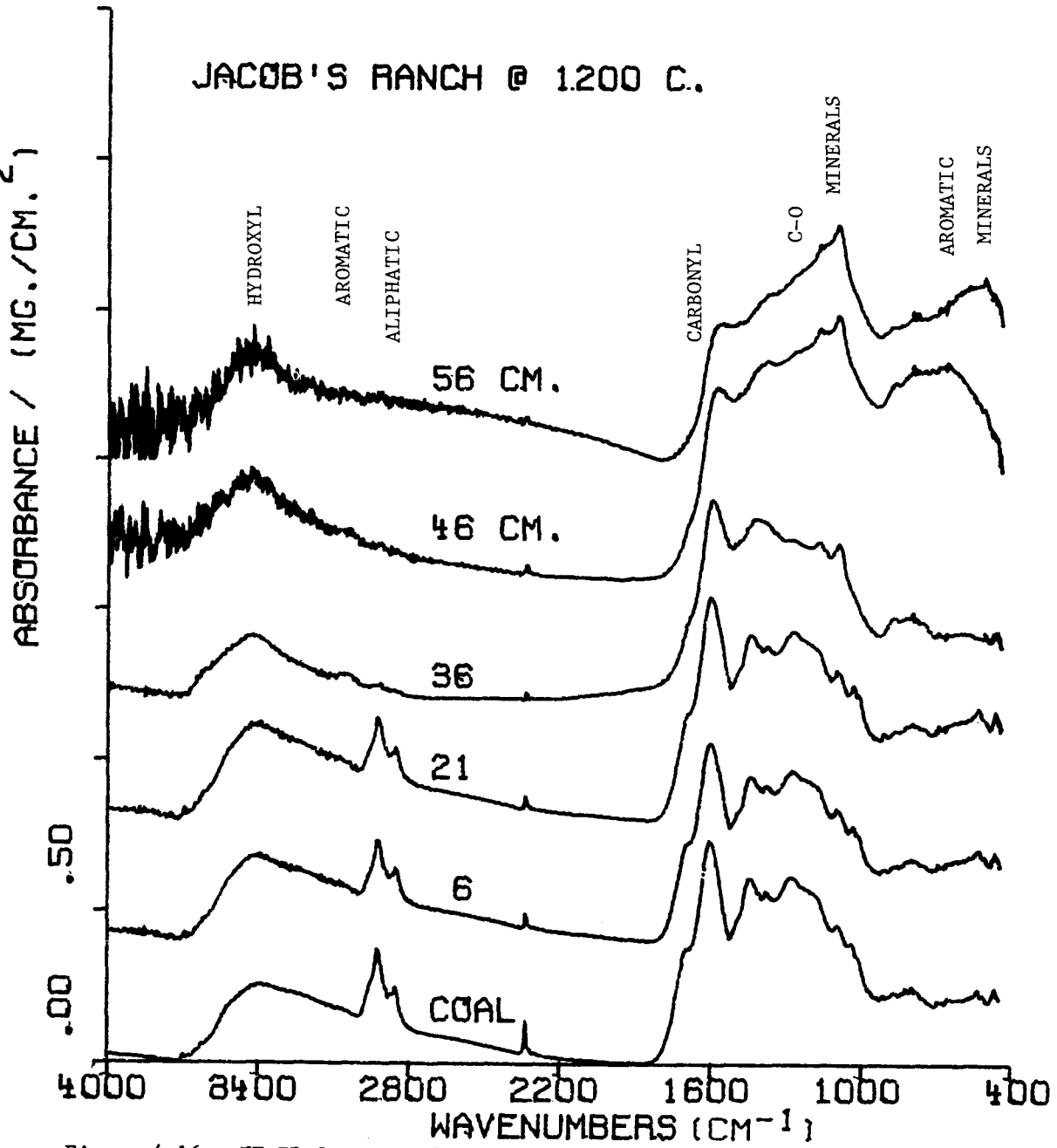

Figure 4-16. FT-IR Spectra of Chars from Jacob's Ranch Subbituminous in Helium at 1200°C (Run #8). A scattering base line correction has been applied and the spectra have been scaled to 1 mg/cm^2 DRY Coal.

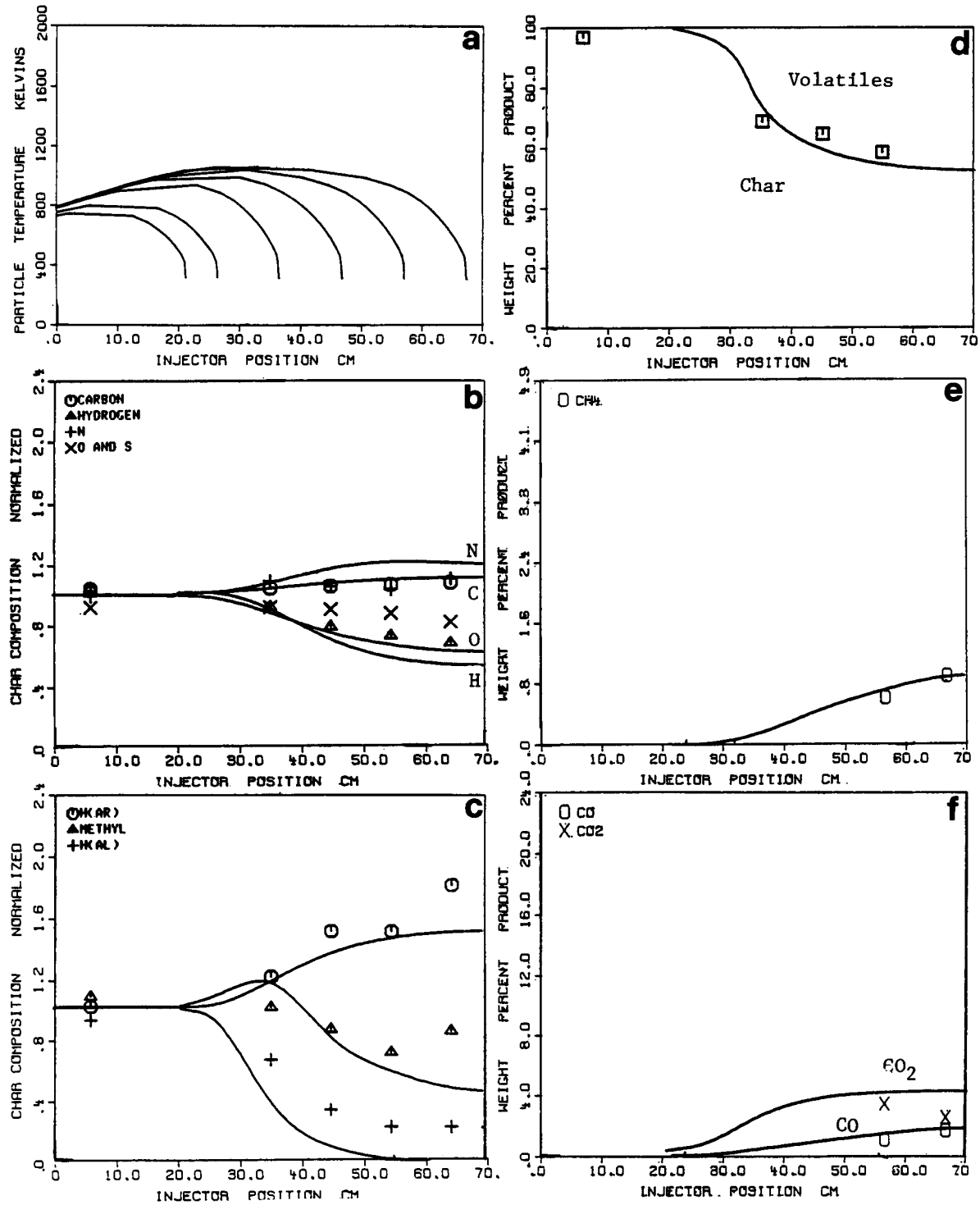

Figure 4-17. Comparison of Theory and Experiment for Illinois #6 Bituminous Coal Pyrolyzed in Helium with a 800°C Wall Temperature (Run #1). Symbols are experimental data, lines are theory. a) Coal particle temperature, b) Char elemental composition normalized to parent coal, c) Char hydrogen functional group composition normalized to parent coal, d) Product Distribution as weight percent of DAF coal, e) Methane as weight percent of DAF coal and f) CO and CO_2 as weight percent of DAF coal.

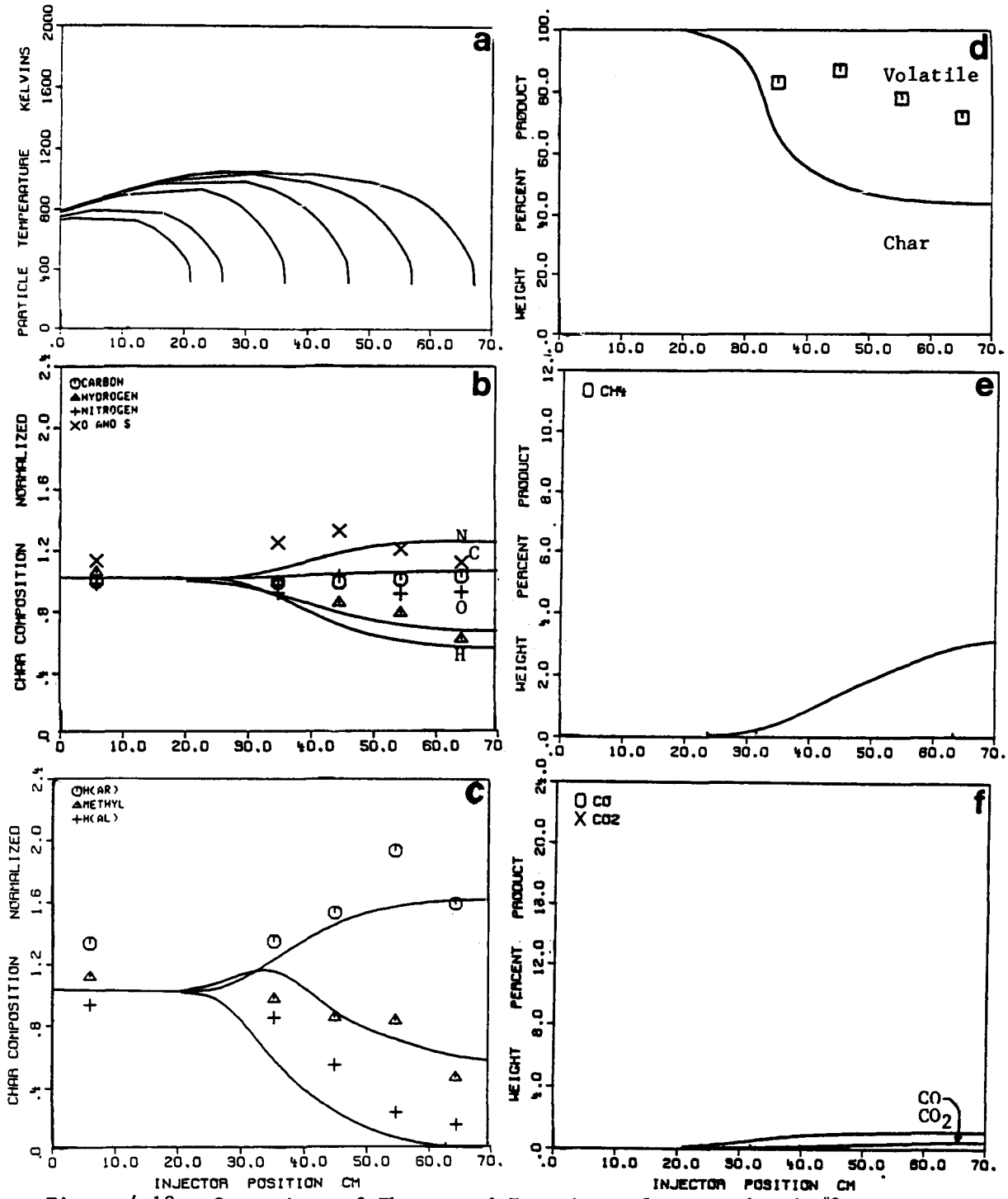

Figure 4-18. Comparison of Theory and Experiment for Pittsburgh #8 Bituminous Coal Pyrolyzed in Helium with a 800°C Wall Temperature (Run #2). Symbols are Experimental Data, Lines are Theory. a) Coal Particle Temperature, b) Char Elemental Composition Normalized to Parent Coal, c) Char hydrogen functional Group Composition Normalized to Parent Coal, d) Product Distribution as Weight Percent of DAF Coal, e) Methane as Weight Percent of DAF Coal and f) CO and CO_2 as Weight Percent of DAF Coal. (Note that the aromatic hydrogen H(ar) values were obtained by difference due to interference from the mineral peaks in the region of the FT-IR spectra near 800 wavenumbers).

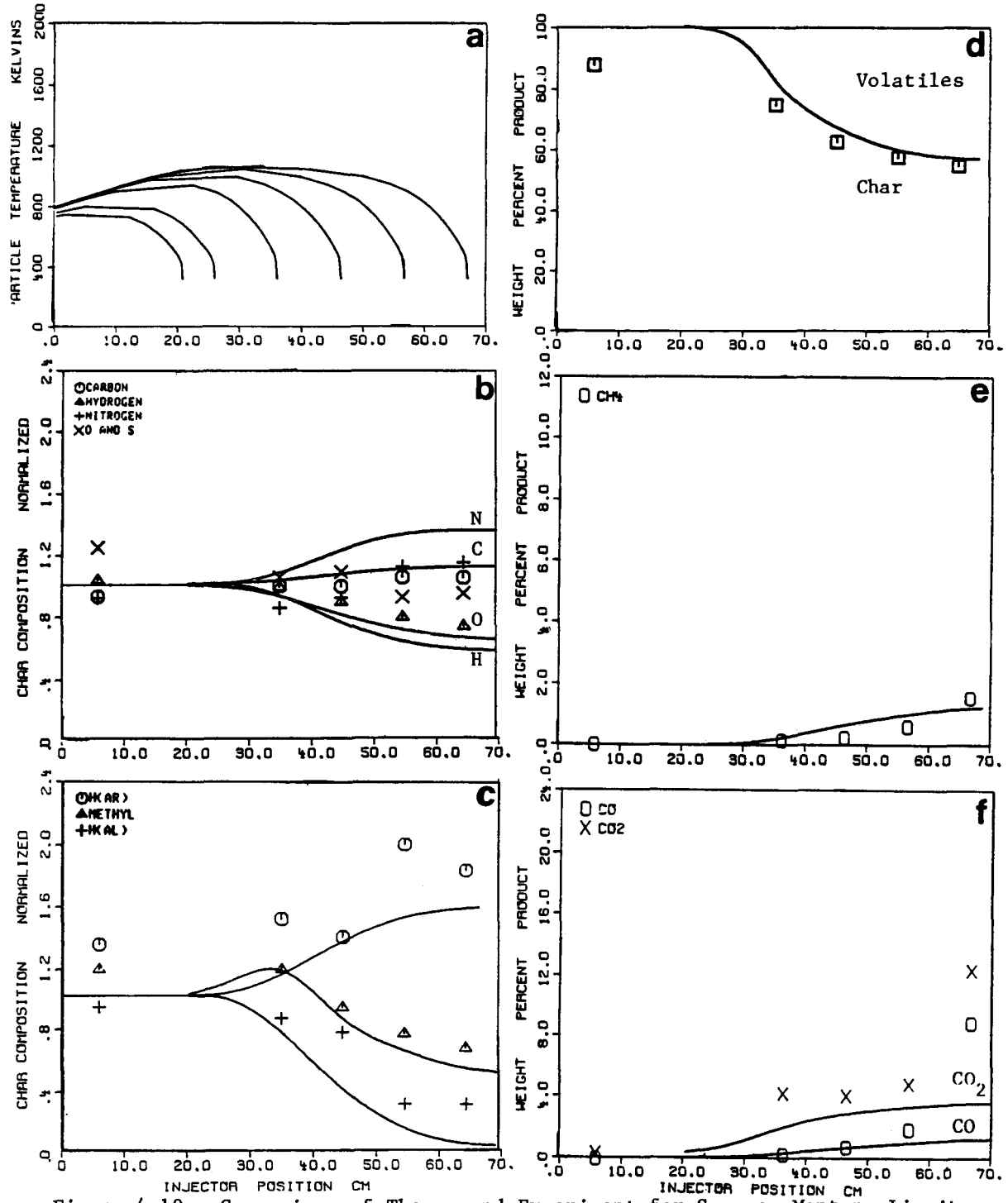

Figure 4-19. Comparison of Theory and Experiment for Savage, Montana Lignite Pyrolyzed in Helium at 800°C Wall Temperature (Run #3). Symbols are Experimental Data, Lines are Theory. a) Coal Particle Temperature, b) Char Elemental Composition Normalized to Parent Coal, c) Char Hydrogen Functional Group Composition Normalized to Parent Coal, d) Product Distribution as Weight Percent of DAF Coal, e) Methane as Weight Percent of DAF Coal and f) CO and CO_2 as Weight Percent of DAF Coal. (Note that the aromatic hydrogen H(ar) values were obtained by difference due to interference from the mineral peaks in the region of the FT-IR spectra near 800 wavenumbers).

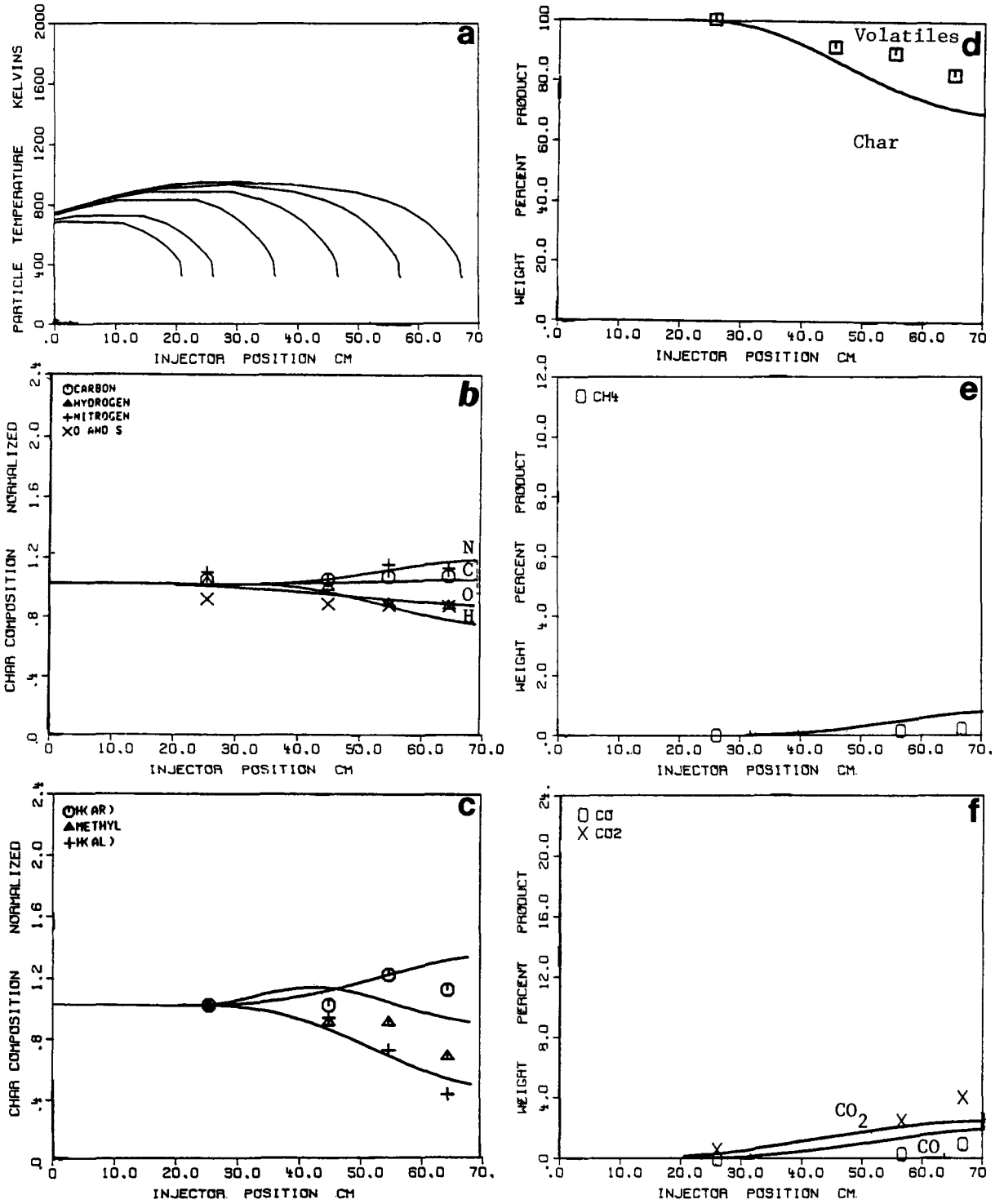

Figure 4-20. Comparison of Theory and Experiment for Jacob's Ranch Subbituminous Coal Pyrolyzed in Helium at 700°C Wall Temperature (Run #4). Symbols are experimental data, lines are theory. a) Coal particle temperature, b) Char elemental composition normalized to parent coal, c) Char hydrogen functional group composition normalized to parent coal, d) Product Distribution as weight percent of DAF coal, e) Methane as weight percent of DAF coal and f) CO and CO_2 as weight percent of DAF coal.

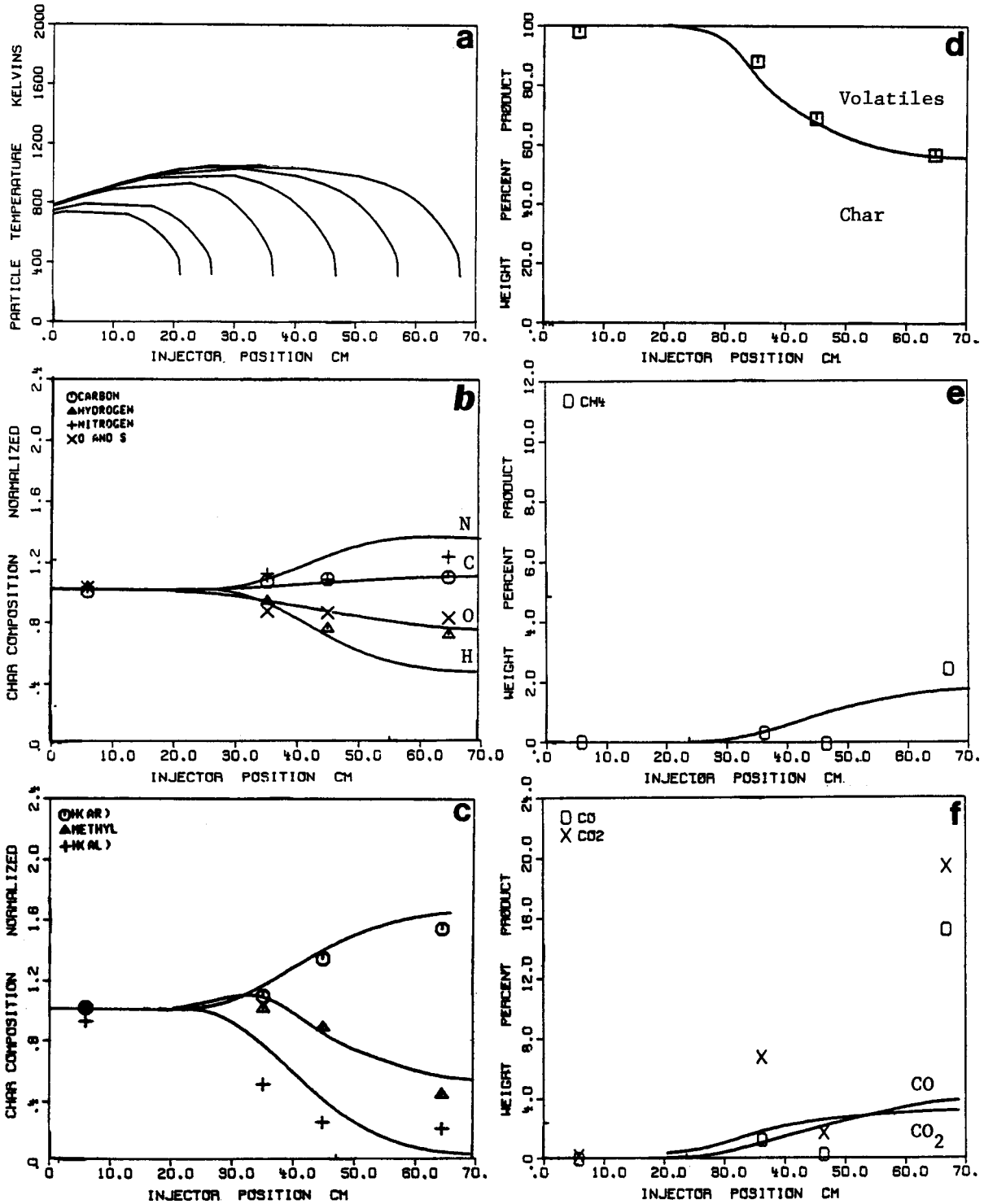

Figure 4-21. Comparison of Theory and Experiment for Jacob's Ranch Subbituminous Coal Pyrolyzed in Helium at a 800°C Wall Temperature (Run #5). Symbols are experimental data, lines are theory. a) Coal particle temperature, b) Char elemental composition normalized to parent coal, c) Char hydrogen functional group composition normalized to parent coal, d) Product Distribution as weight percent of DAF coal, e) Methane as weight percent of DAF coal and f) CO and CO_2 as weight percent of DAF coal.

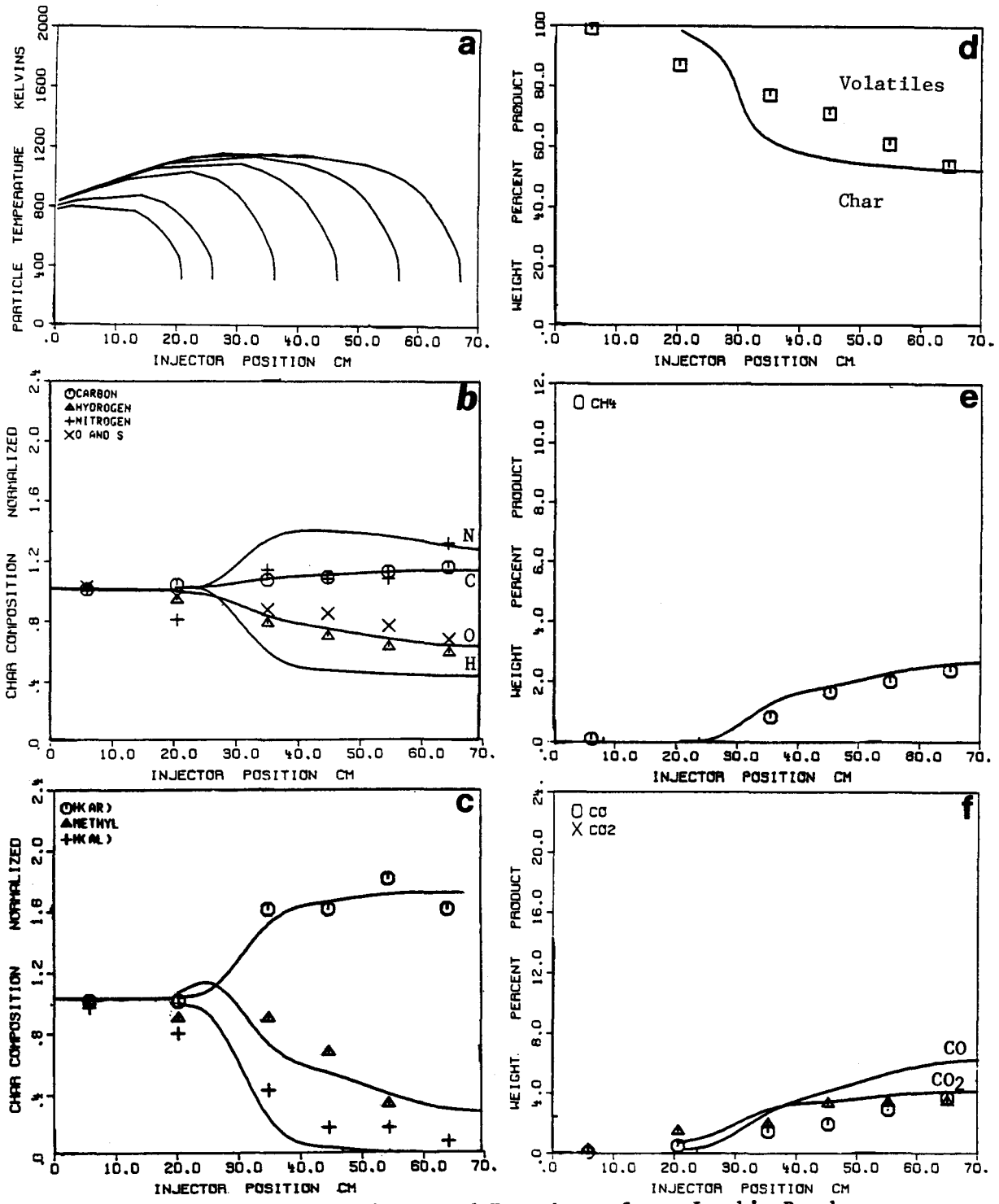

Figure 4-22. Comparison of Theory and Experiment for a Jacob's Ranch Subbituminous Coal Pyrolyzed in Helium at a 900°C and Wall Temperature (Run #6). Symbols are experimental data, lines are theory. a) Coal particle temperature, b) Char elemental composition normalized to parent coal, c) Char hydrogen functional group composition normalized to parent coal, d) Product Distribution as weight percent of DAF coal, e) Methane as weight percent of DAF coal and f) CO and CO_2 as weight percent of DAF coal.

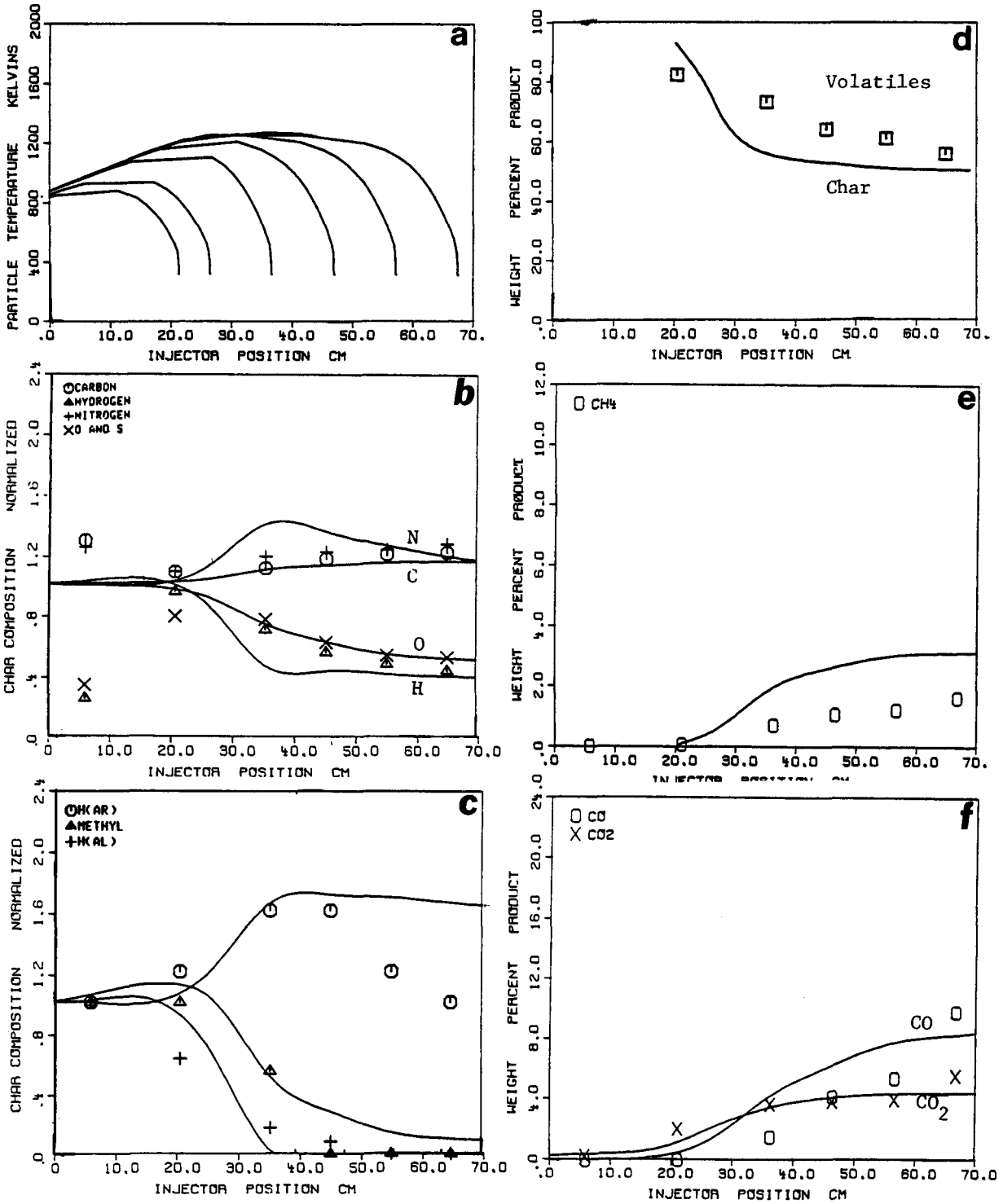

Figure 4-23. Comparison of Theory and Experiment for a Jacob's Ranch Subbituminous Coal Pyrolyzed in Helium at a 1000°C Wall Temperature (Run #7). Symbols are experimental data, lines are theory. a) Coal particle temperature, b) Char elemental composition normalized to parent coal, c) Char hydrogen functional group composition normalized to parent coal, d) Product Distribution as weight percent of DAF coal, e) Methane as weight percent of DAF coal and f) CO and CO_2 as weight percent of DAF coal.

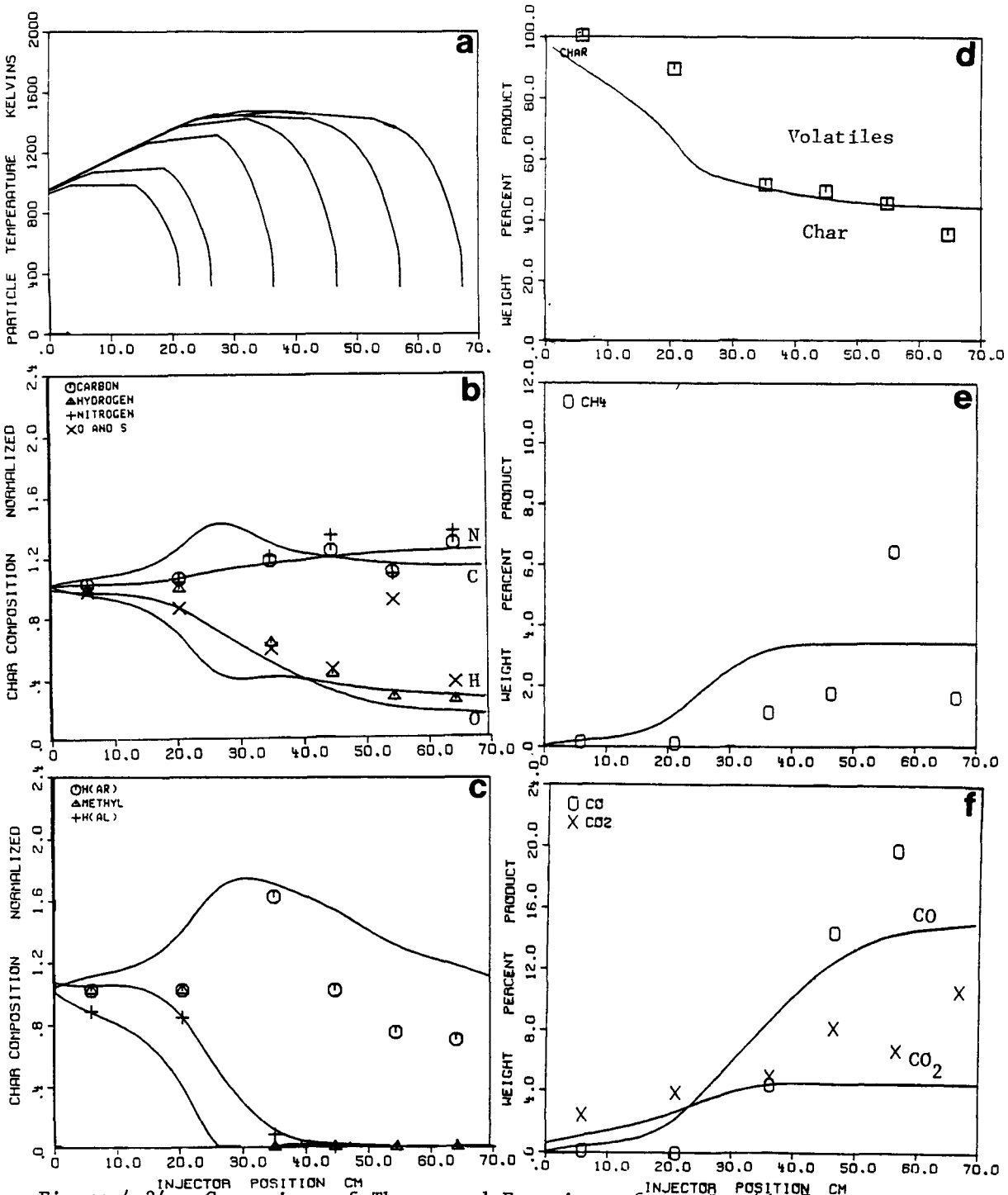

Figure 4-24. Comparison of Theory and Experiment for a Jacob's Ranch Subbituminous Coal Pyrolyzed in Helium at 1200°C Wall Temperature (Run #8). Symbols are Experimental Data, Lines are Theory. a) Coal Particle Temperature, b) Char Elemental Composition Normalized to Parent Coal, c) Char Hydrogen Functional Group Composition Normalized to Parent Coal, d) Product Distribution as Weight Percent of DAF Coal, e) Methane as Weight Percent of DAF Coal and f) CO and CO_2 as Weight Percent of DAF Coal. (Note that the aromatic hydrogen H(ar) for injector position of 56 and 66 cm were obtained by difference due to a high level of noise in the FT-IR spectra of these chars).

TABLE 4-4

Kinetic Rate Coefficients

Y^o_1	CO_2 - Extra-loose	k_1	= 0.10E+15 exp((23900. ± 2500.)/T)
Y^o_2	CO_2 - Loose	k_2	= 0.10E+15 exp((27900. ± 1400.)/T)
Y^o_3	CO_2 - Tight	k_3	= 0.10E+15 exp((32900. ± 3300.)/T)
Y^o_4	H_2O	k_4	= 0.17E+15 exp((30000. ± 1500.)/T)
Y^o_5	CO - Ether Loose	k_5	= 0.17E+12 exp((25000. ± 2500.)/T)
Y^o_6	CO - Ether Tight	k_6	= 0.10E+19 exp((54900. ± 5000.)/T)
Y^o_7	HCN - Loose	$*k_7$	= 0.54E+04 exp((8850. ± 0.)/T)
Y^o_8	HCN - Tight	$*k_8$	= 0.70E+08 exp((32000. ± 0.)/T)
Y^o_9	NH_3	k_9	= 0.12E+13 exp((27300. ± 3000.)/T)
Y^o_{10}	CH_x-Aliphatic	k_{10}	= 0.17E+15 exp((30000. ± 1500.)/T)
Y^o_{11}	Methane-loose	k_{11}	= 0.17E+15 exp((30000. ± 1500.)/T)
Y^o_{12}	Methane-tight	k_{12}	= 0.17E+13 exp((30000. ± 3000.)/T)
Y^o_{13}	H-Aromatic	k_{13}	= 0.16E+08 exp((23000. ± 2300.)/T)
Y^o_{14}	C-Non Volatile	k_{14}	= 0
Y^o_{15}	S-Organic		
X^o	Total Tar	k_T	= 0.45E+14 exp((26400. ± 1500.)/T)

Cracking Rates:

Paraffins - Olefins	k_{OL}	= 0.15E+12 exp((27600.)/T)
Olefin - Acetylene	k_{AC}	= 0.21E+08 exp((22000.)/T)

*Distributed rates have not yet been determined.

TABLE 4-5

Coal Functional Group Composition for Six Coals

Composition Parameter		Savage Montana Lignite (WT% DAF)	Jacob's Ranch Subbituminous (WT% DAF)	Illinois #6 Bituminous Coal (C.E.) (WT% DAF)	Pittsburgh #8 Bituminous Coal (WT% DAF)	Utah Bituminous Coal (Texaco) (WT% DAF)	Illinois #6 Bituminous Coal (Texaco) (WT% DAF)
C		0.712	0.754	0.739	0.835	0.759	0.759
H		0.046	0.053	0.051	0.055	0.054	0.055
N		0.011	0.012	0.014	0.016	0.013	0.015
S(organic)		0.013	0.005	0.042	0.033	0.005	0.047
O		0.218	0.176	0.154	0.061	0.169	0.124
		1.000	1.000	1.000	1.000	1.000	1.000
Y^o_1	CO_2 - Extra-loose	0.0100	0.0090	0.0100	0.0036	0.0110	0.0100
Y^o_2	CO_2 - Loose	0.0150	0.0135	0.0300	0.0060	0.0165	0.0300
Y^o_3	CO_2 - Tight	0.0250	0.0225	0.0100	0.0024	0.0275	0.0100
Y^o_4	H_2O	0.1006	0.0503	0.0450	0.0238	0.0344	0.0450
Y^o_5	CO - Ether Loose	0.0200	0.0600	0.0300	0.0060	0.0300	0.0300
Y^o_6	CO - Ether Tight	0.1414	0.1125	0.1059	0.0484	0.1422	0.0534
Y^o_7	HCN - Loose	0.0036	0.0101	0.0100	0.0071	0.0073	0.0121
Y^o_8	HCN - Tight	0.0160	0.0130	0.0170	0.0237	0.0170	0.0170
Y^o_9	NH_3	0.0010	0.0000	0.0000	0.0000	0.0000	0.0000
Y^o_{10}	CH_x-Aliphatic	0.1864	0.2251	0.1491	0.2319	0.1810	0.1946
Y^o_{11}	Methane-loose	0.0065	0.0110	0.0110	0.0126	0.0110	0.0110
Y^o_{12}	Methane-tight	0.0065	0.0110	0.0110	0.0224	0.0110	0.0110
Y^o_{13}	H-Aromatic	0.0150	0.0120	0.0160	0.0170	0.0160	0.0160
Y^o_{14}	C-Non Volatile	0.4400	0.4450	0.5130	0.5620	0.4900	0.5130
Y^o_{15}	S-Organic	0.0130	0.0050	0.0420	0.0330	0.0051	0.0469
	Total	1.0000	1.0000	1.0000	1.0000	1.0000	1.0000
X^o	Tar	0.1600	0.1500	0.3100	0.4300	0.3600	0.3100

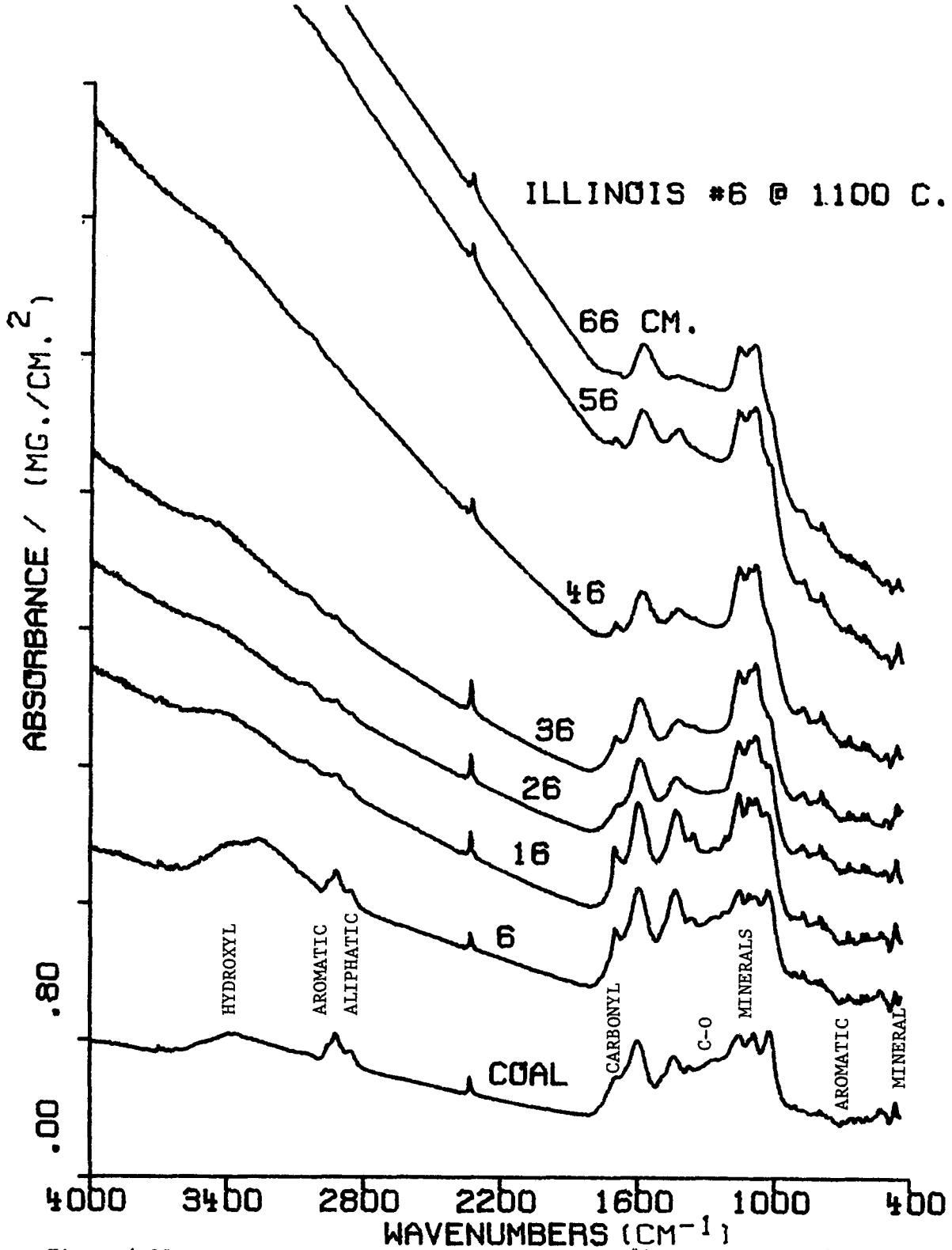

Figure 4-25. FT-IR Spectra of Chars from Illinois #6 Bituminous Coal Pyrolyzed at 1100°C in Nitrogen (Run #9). The spectra are for dried KBr pellets.

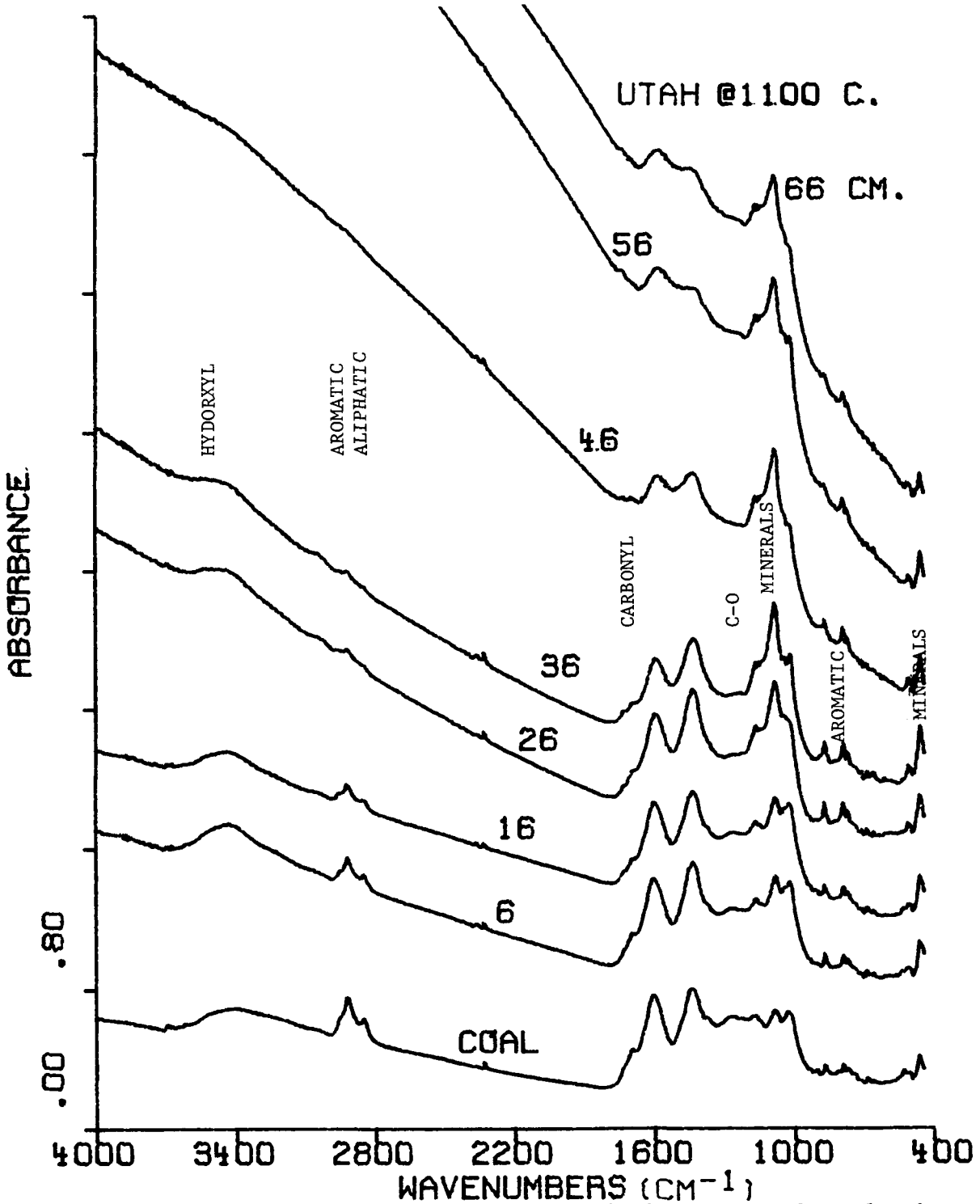

Figure 4-26. FT-IR Spectra of Chars from Utah Bituminous Coal Pyrolyzed at 1100°C in Nitrogen (Run #10). The spectra are for dried KBr pellets.

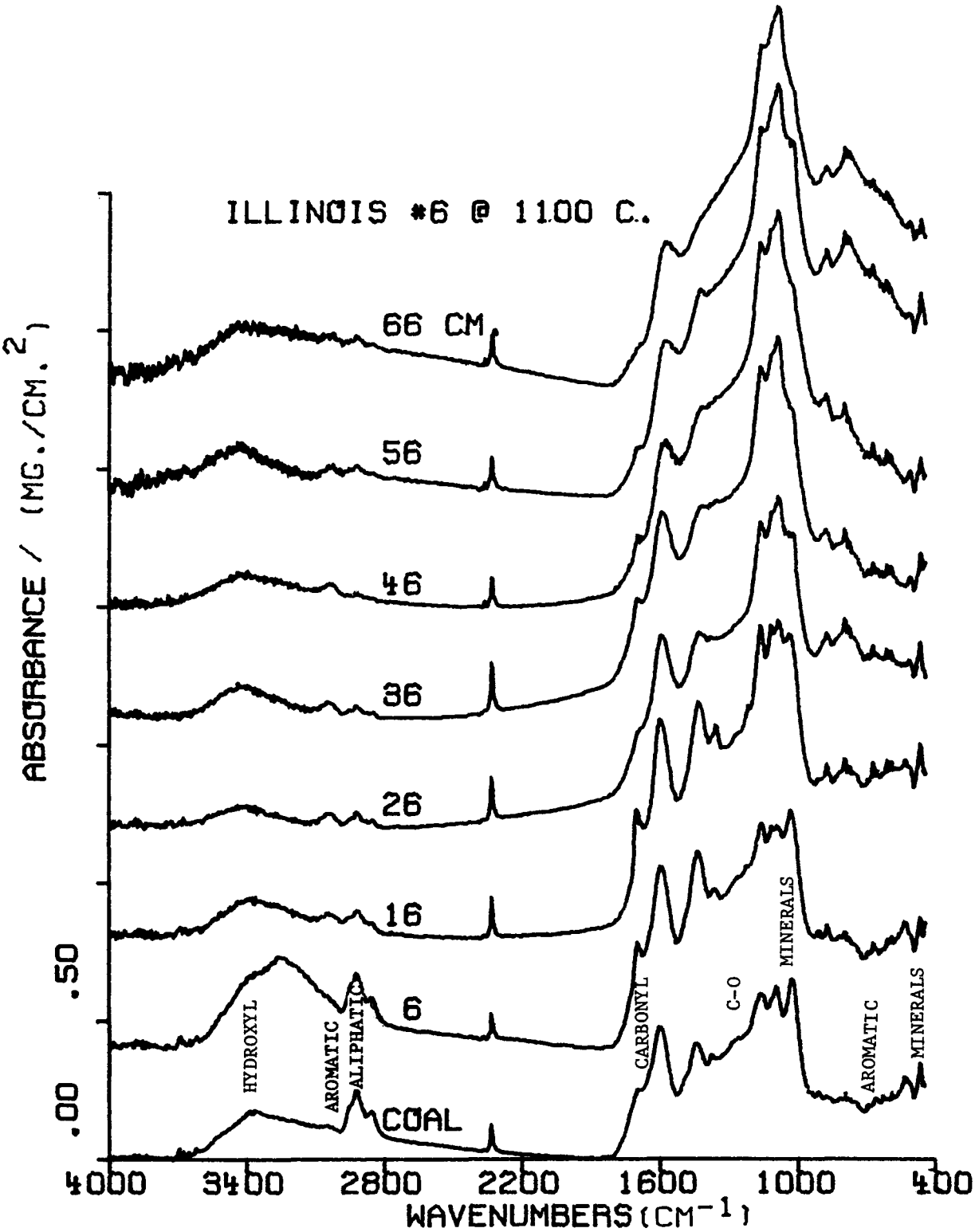

Figure 4-27. FT-IR Spectra of Chars from Illinois #6 Bituminous Coal Pyrolyzed at 1100°C in Nitrogen (Run #9). A scattering base line correction has been applied and the spectra have been scaled to 1 mg/cm^2 DRY Coal.

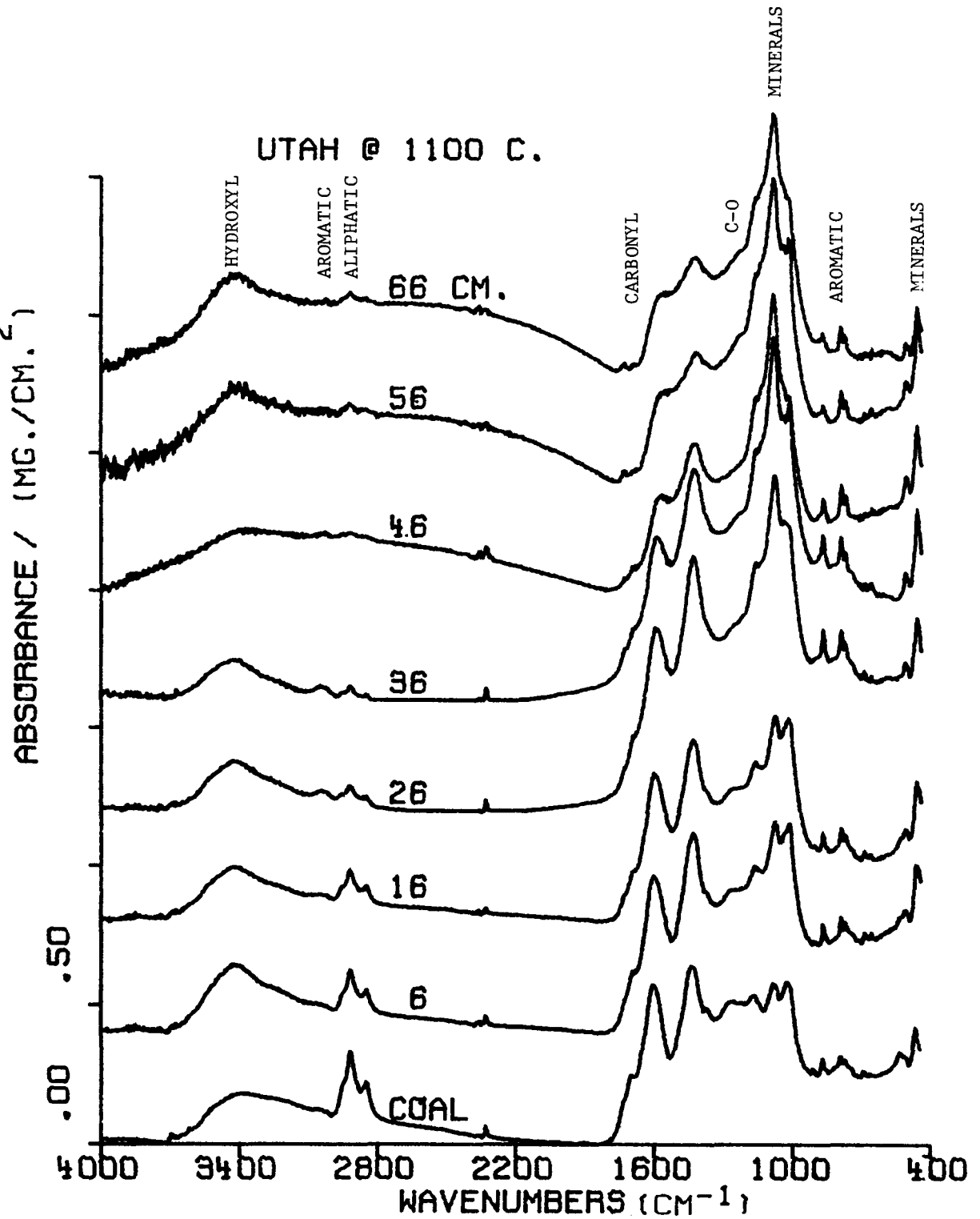

Figure 4-28. FT-IR Spectra of Chars from Utah Bituminous Coal Pyrolyzed at 1100°C in Nitrogen (Run #10). A scattering base line correction has been applied and the spectra have been scaled to 1 mg/cm^2 DRY.

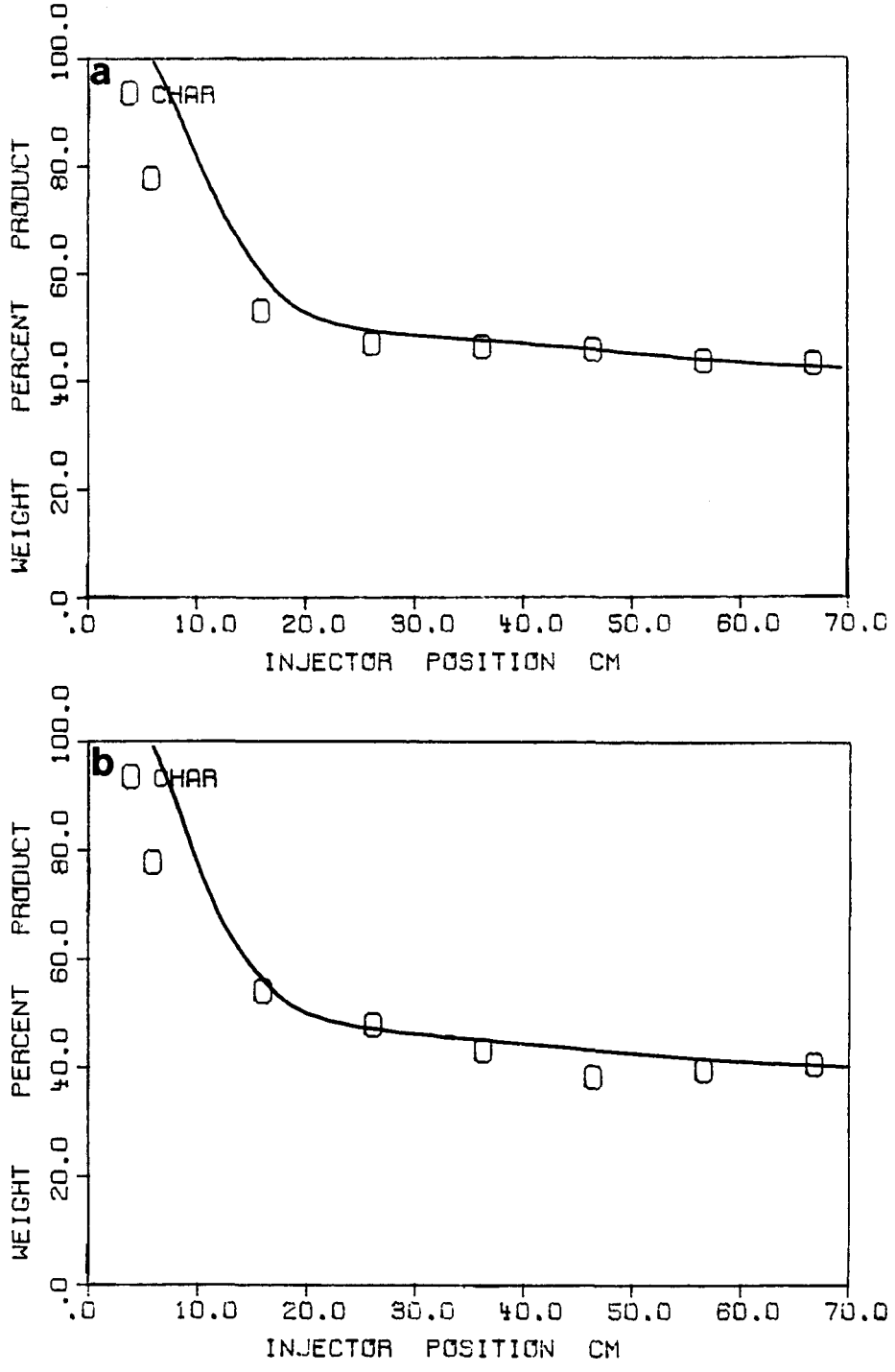

Figure 4-29. Char Yield as Weight Percent of DAF Coal for Coal Pyrolyzed in Nitrogen with a Furnace Temperature of 1100°C. a) Illinois #6 Bituminous Coal (Run #9) and b) Utah Bituminous Coal (Run #10).

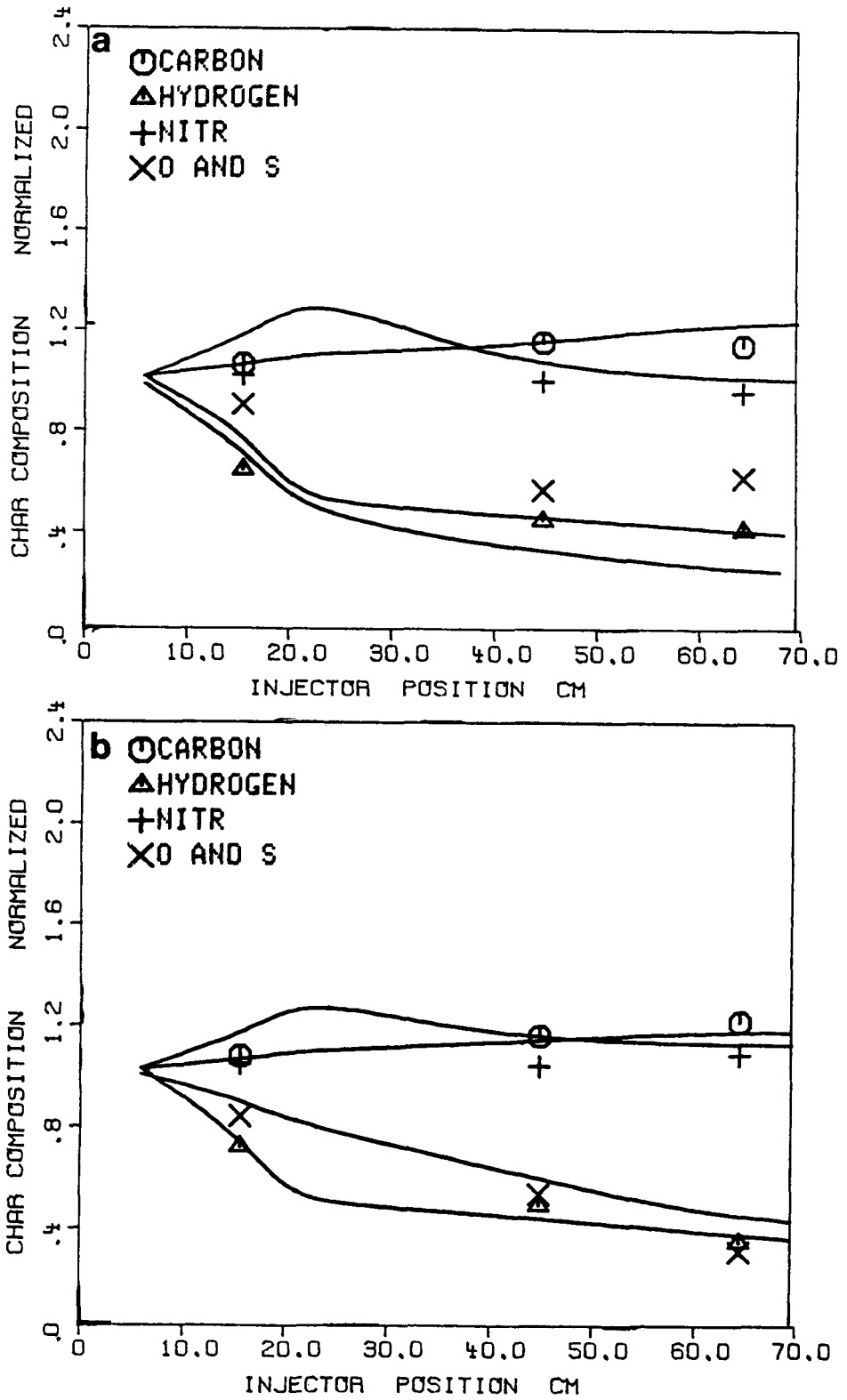

Figure 4-30. Char Elemental Composition (DAF) Normalized to Parent Coal Elemental Composition (DAF) for Pyrolysis in Nitrogen with a Furnace Temperature of 1100°C. a) Illinous #6 Bituminous Coal (Run #9) and b) Utah Bituminous Coal (Run #10).

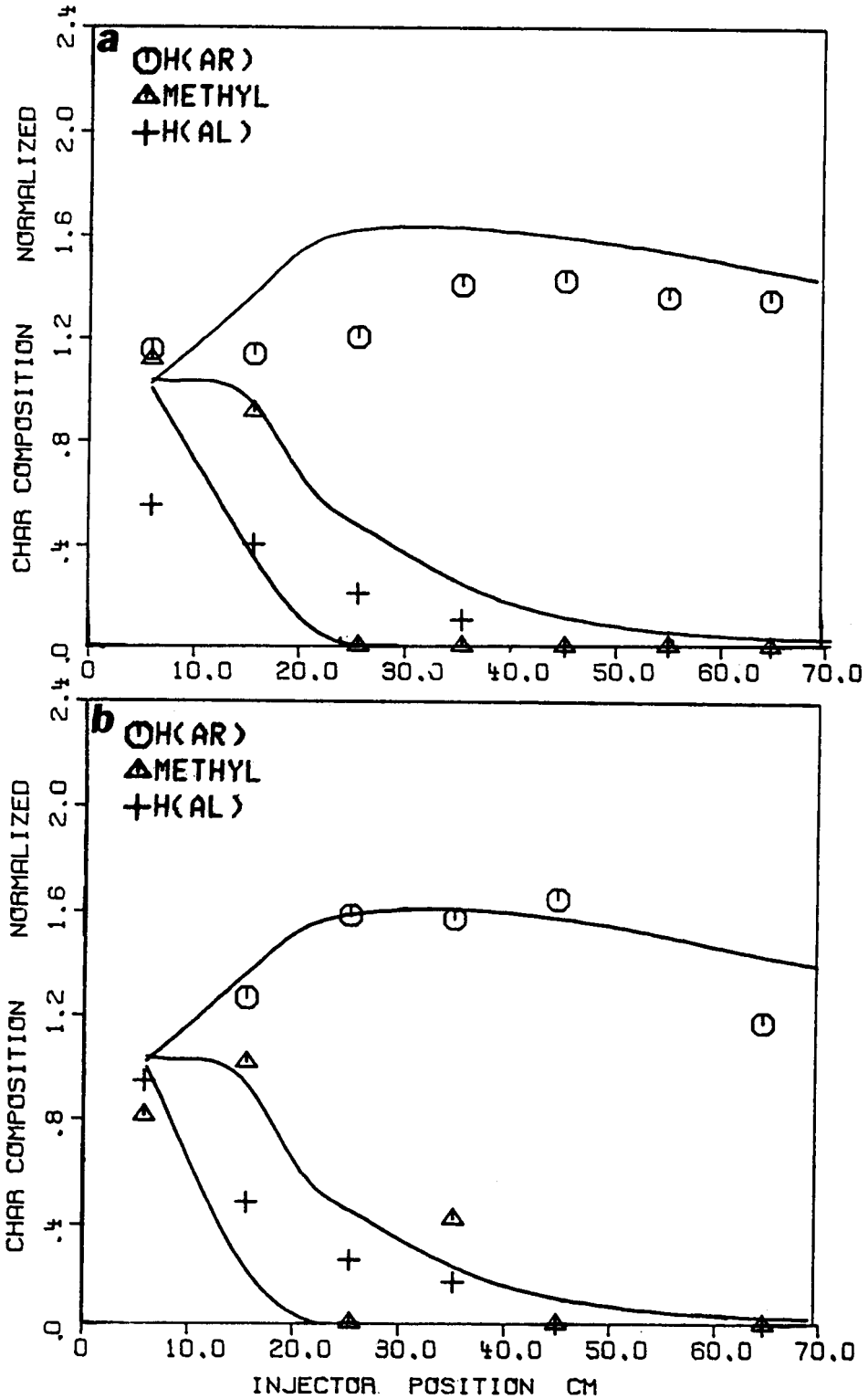

Figure 4-31. Char Functional Group Composition (DAF) Normalized to Parent Coal Functional Group Composition (DAF) for Pyrolysis in Nitrogen with a Furnace Temperature of 1100°C. a) Illinois #6 Bituminous Coal (Run #9), b) Utah Bituminous Coal (Run #10). (Note that the aromatic hydrogen is determined by difference because of interference of large mineral peaks in the FT-IR spectra).

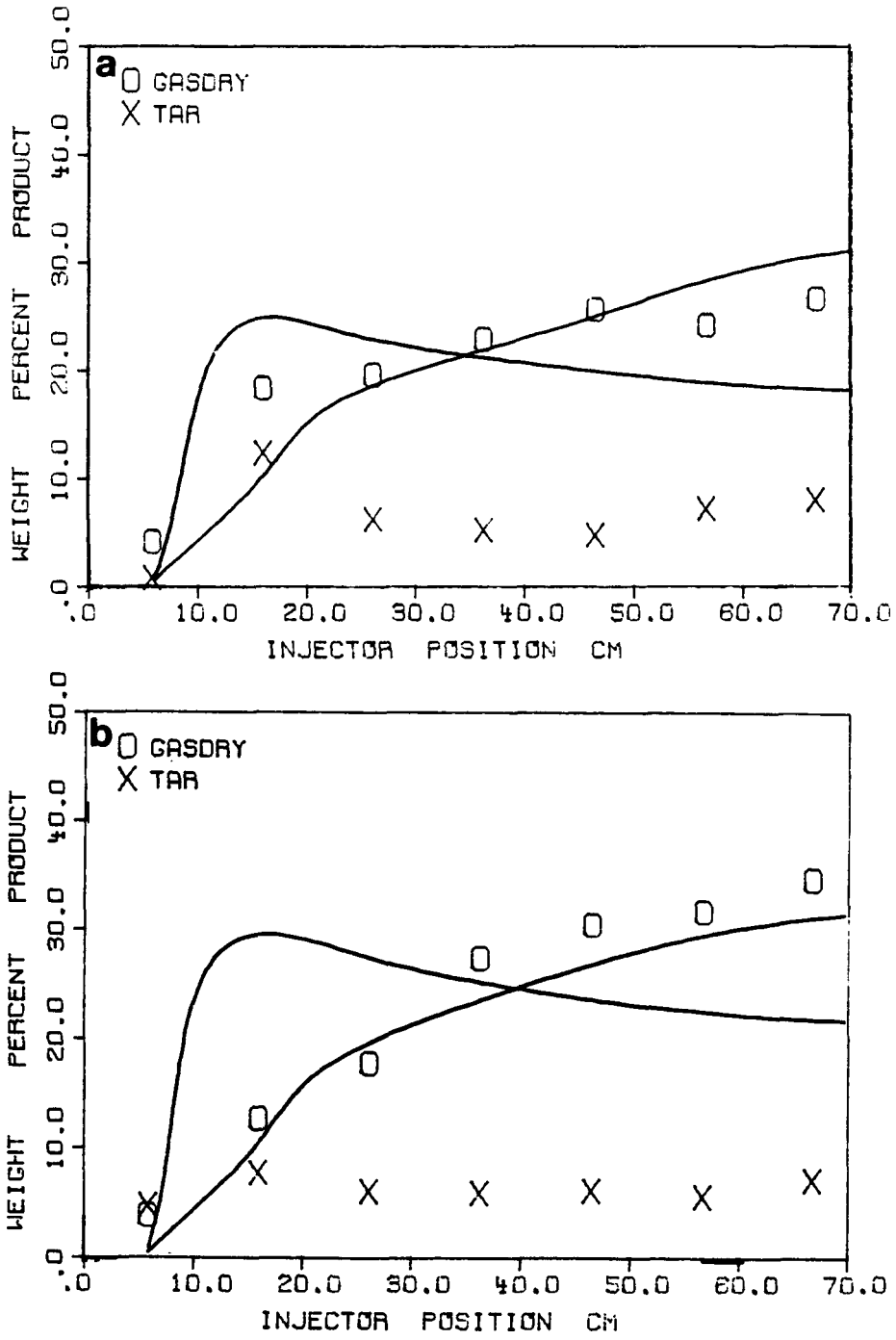

Figure 4-32. Dry Gas (Gas Minus Water) and Tar as Weight Percent of DAF Coal for Pyrolysis in Nitrogen with a Furnace Temperature of 1100°C. a) Illinois #6 Bituminous Coal (Run #9), b) Utah Bituminous Coal (Run #10).

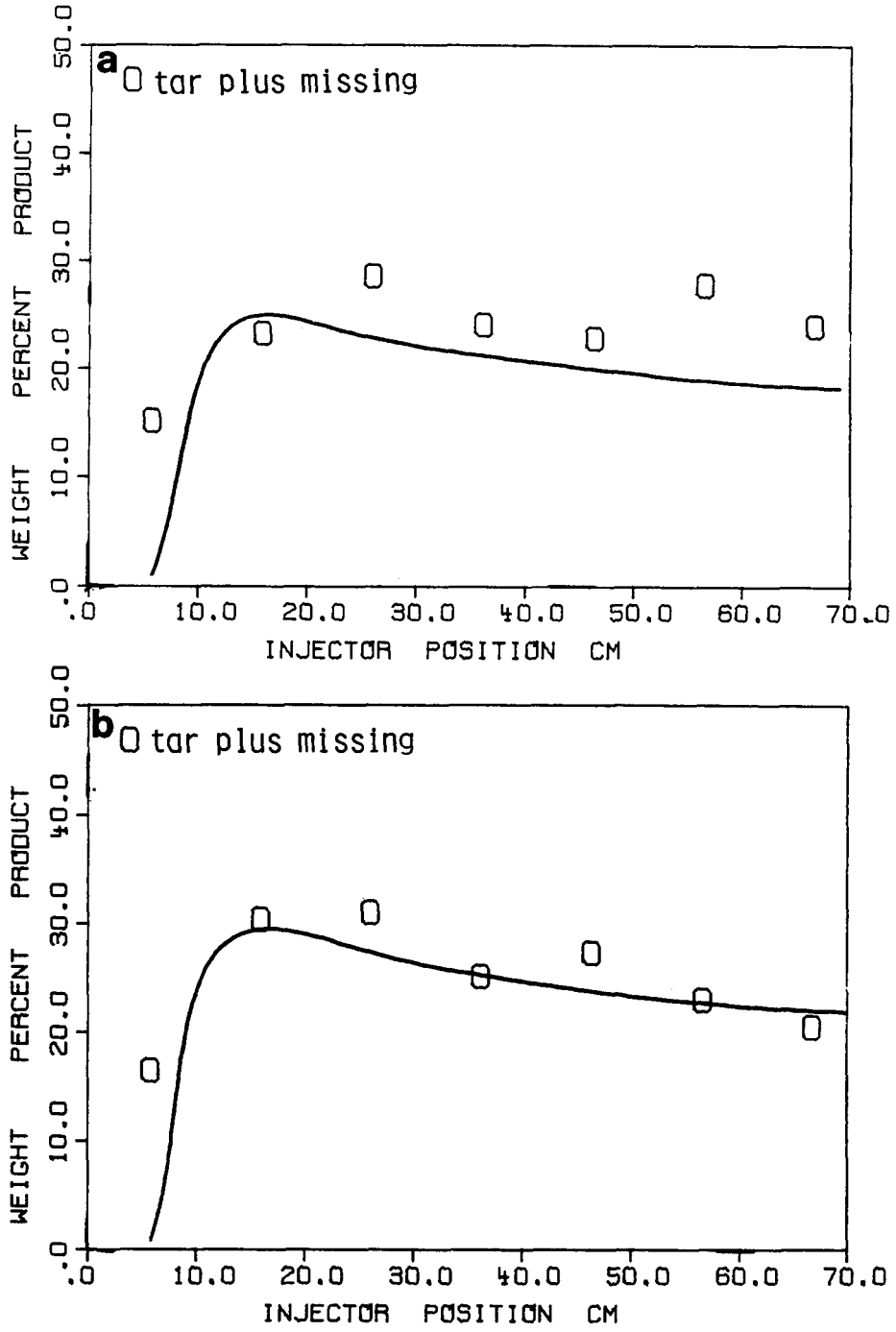

Figure 4-33. Tar plus Missing Gas as Weight Percent of DAF Coal for Pyrolysis in Nitrogen with a Furnace Temperature of 1100°C. a) Illinois #6 Bituminous Coal (Run #9), b) Utah Bituminous Coal (Run #10).

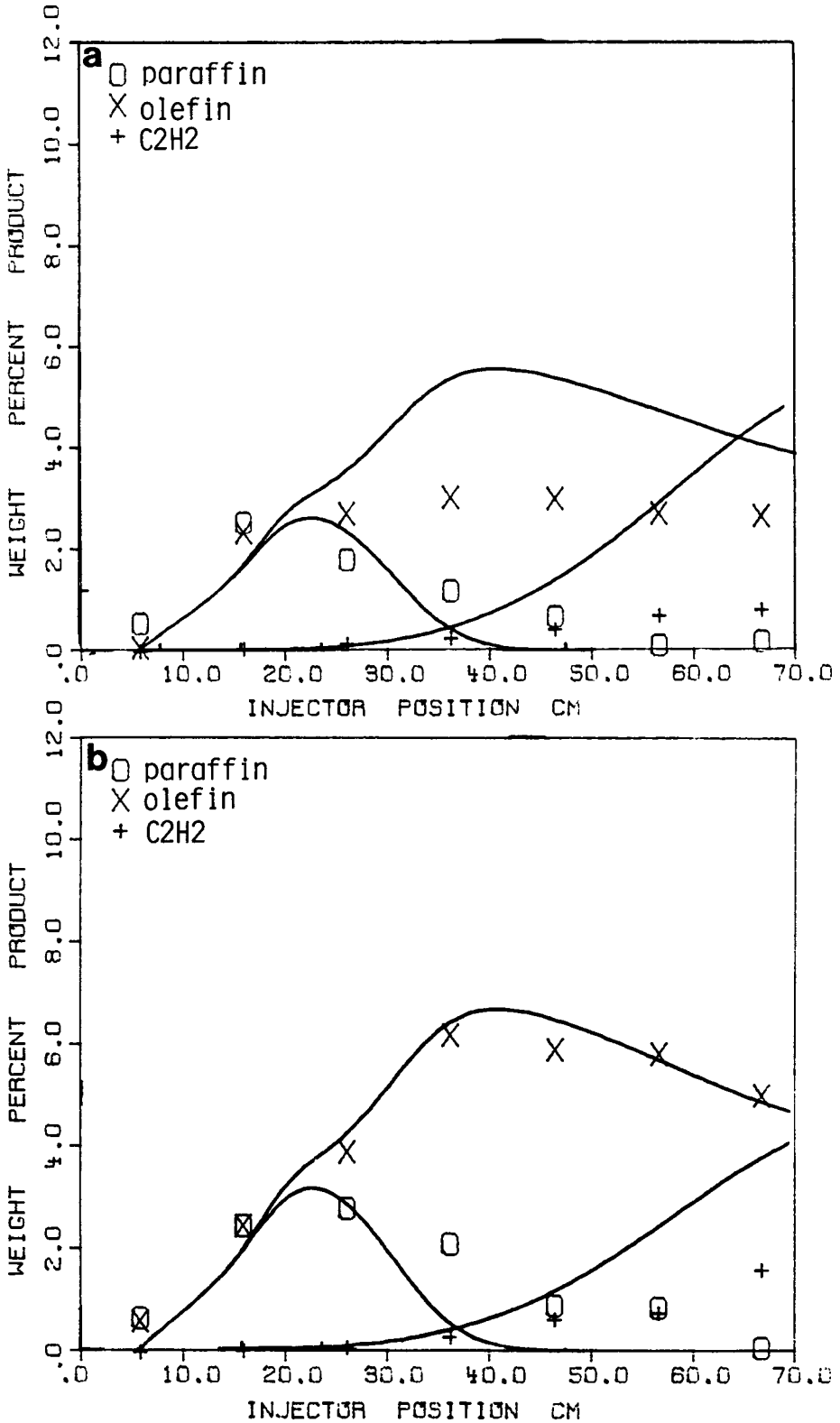

Figure 4-34. Paraffins, Olefins and Acetylene as Weight Percent of DAF Coal for Pyrolysis in Nitrogen with a Furnace Temperature of 1100°C. a) Illinois #6 Bituminous Coal (Run #9), b) Utah Bituminous Coal (Run #10).

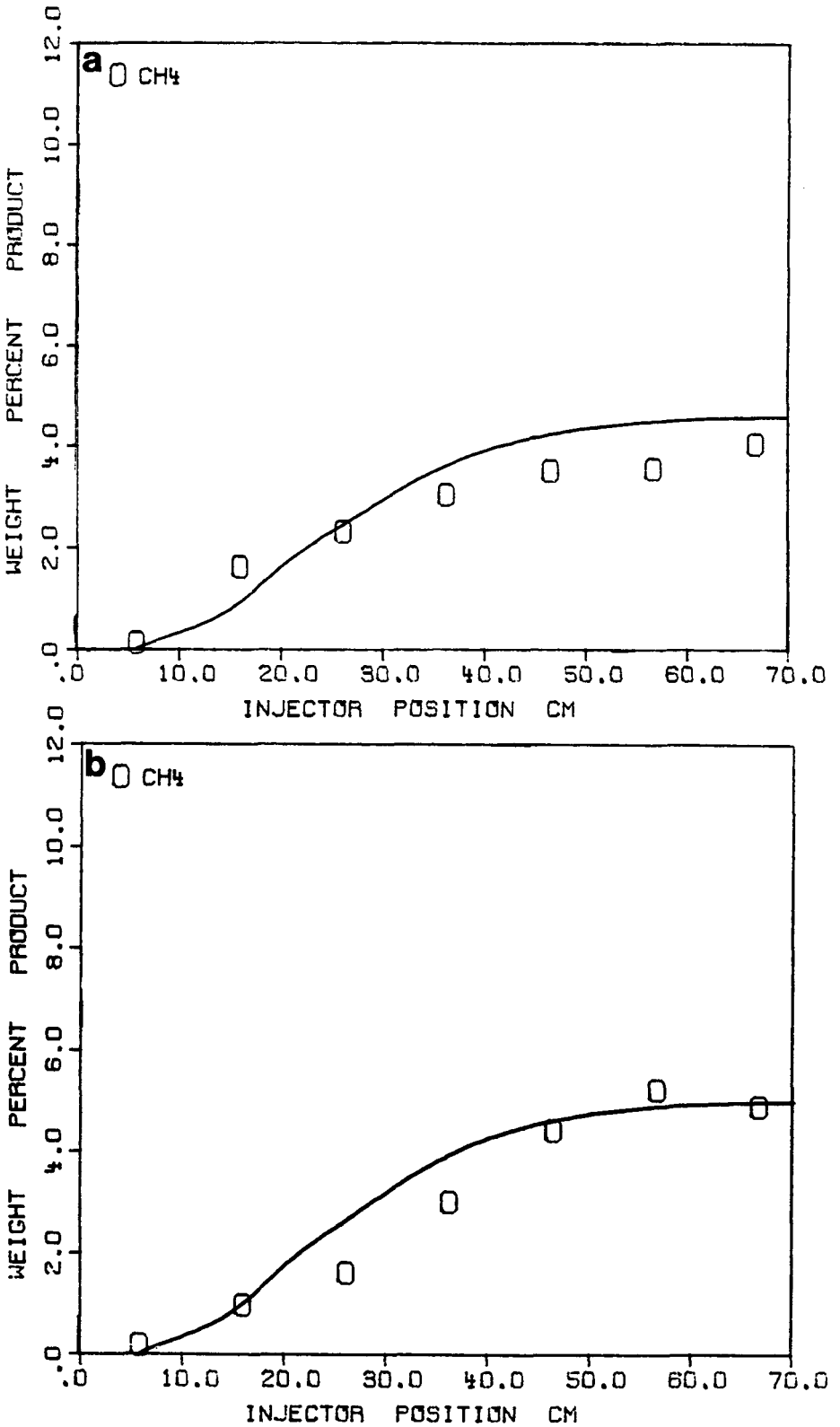

Figure 4-35. Methane as Weight Percent of DAF Coal for Pyrolysis in Nitrogen with a Furnace Temperature of 1100°C. a) Illinois #6 Bituminous Coal (Run #9), b) Utah Bituminous Coal (Run #10).

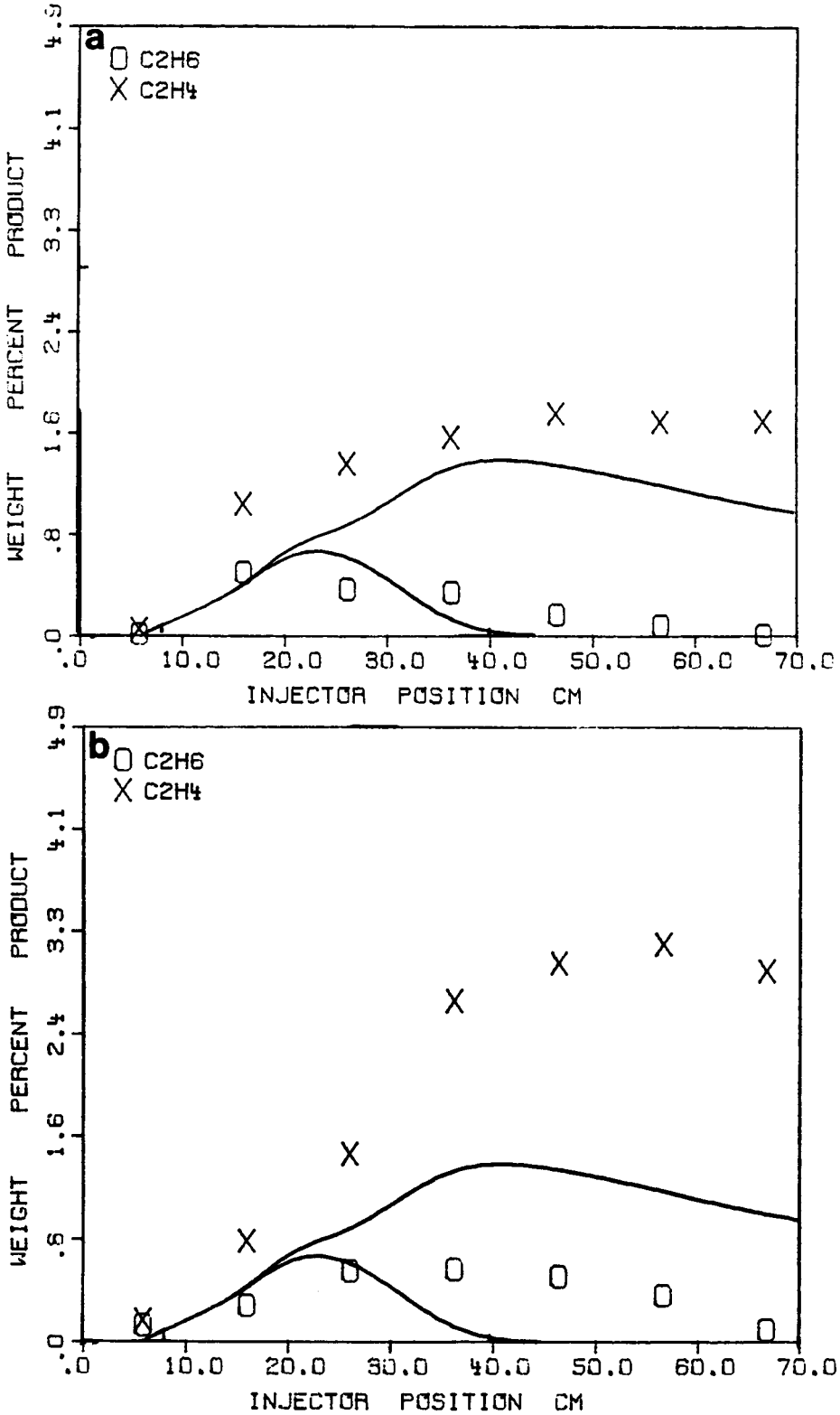

Figure 4-36. Ethane and Ethylene as Weight Percent of DAF Coal for Pyrolysis in Nitrogen with a Furnace Temperature of 1100°C. a) Illinois #6 Bituminous Coal (Run #9), b) Utah Bituminous Coal (Run #10).

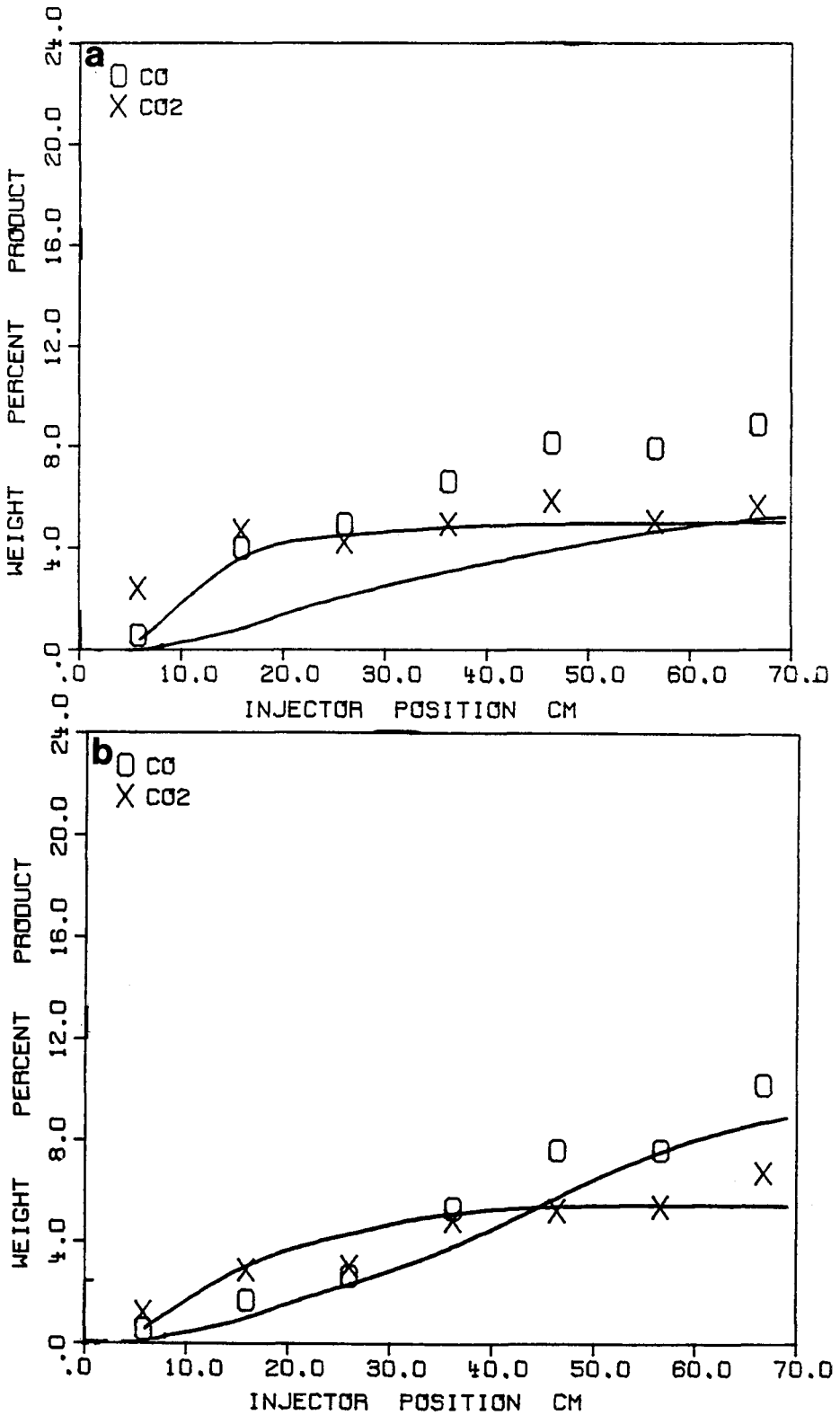

Figure 4-37. CO and CO_2 as Weight Percent of DAF Coal for Pyrolysis in Nitrogen with a Furnace Temperature of 1100°C. a) Illinois #6 Bituminous Coal (Run #9), b) Utah Bituminous Coal (Run #10).

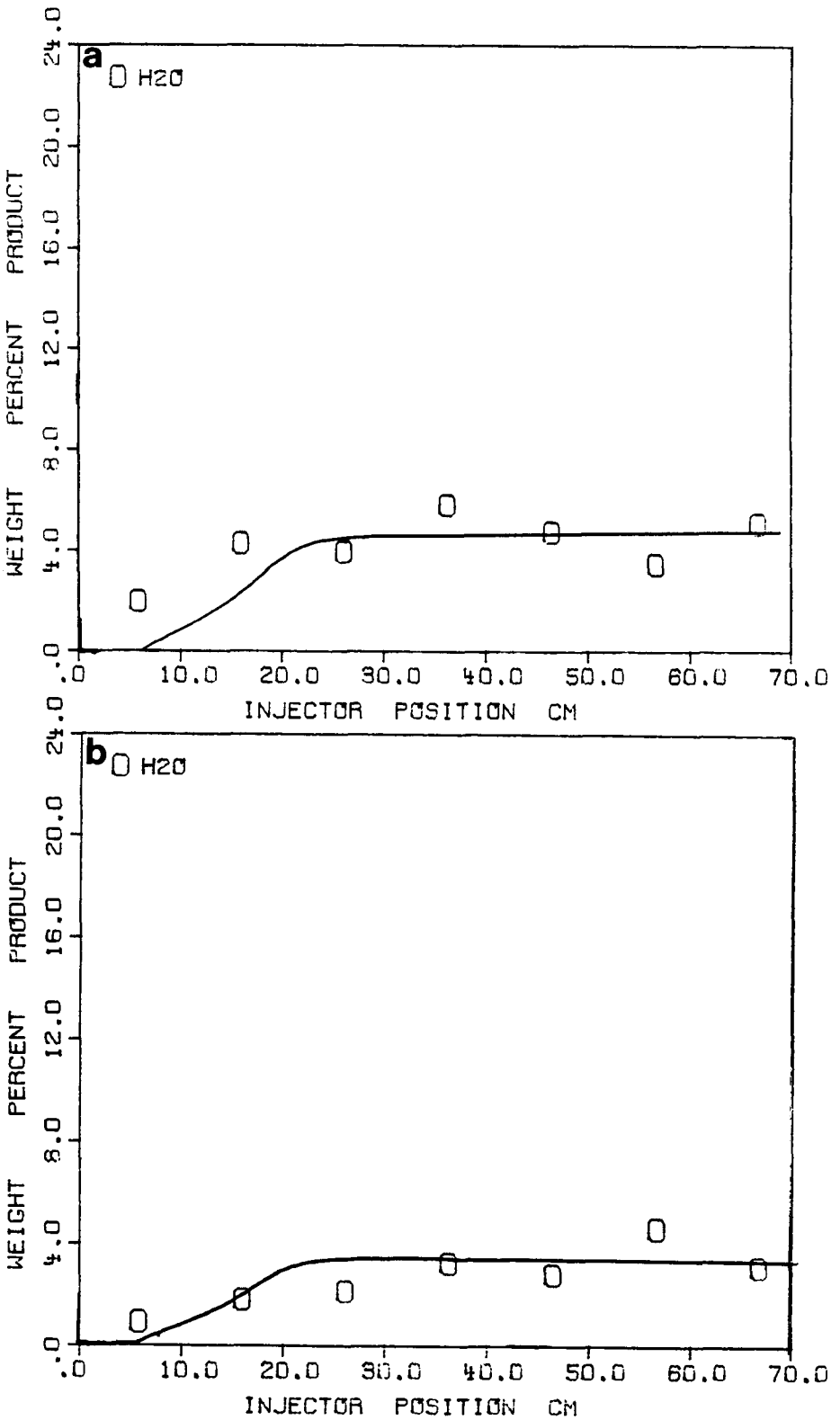

Figure 4-38. Water as Weight Percent of DAF Coal for Pyrolysis in Nitrogen with a Furnace Temperature of 1100°C. a) Illinois #6 Bituminous Coal (Run #9), b) Utah Bituminous Coal (Run #10).

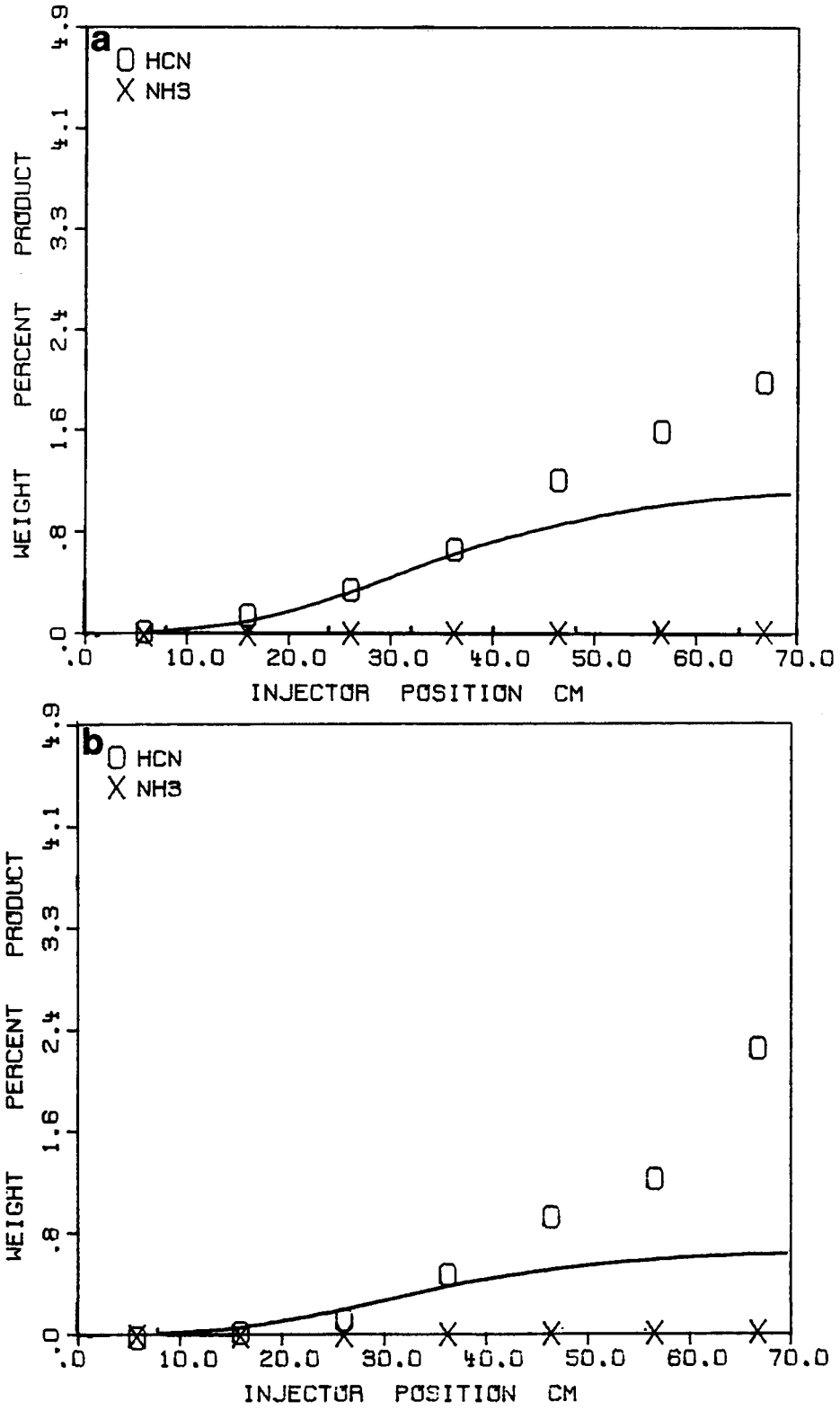

Figure 4-39. HCN and NH_3 as Weight Percent of DAF Coal for Pyrolysis in Nitrogen with a Furnace Temperature of 1100°C. a) Illinois #6 Bituminous Coal (Run #9), b) Utah Bituminous Coal (Run #10).

Section 5

ASSESSMENT OF EXPERIMENT AND THEORY APPLICATIONS TO LARGE SCALE GASIFIERS

The objective of this program is the development of correlations between the products of pyrolysis and the time-temperature history experienced by coal in a reactor. Under task 7 of the program, an assessment was made of the application of these correlations to large scale entrained flow gasifiers.

There are two immediate applications of the correlations: 1) given samples of char, tar and gas extracted from test points in a large-scale gasifier, information can be obtained about the time-temperature history of the coal and pyrolysis products (this assumes that the composition of the char is essentially determined by pyrolysis at the gasifier temperature with gasification reactions primarily reducing the char mass at constant functional group compositions); 2) given the approximate conditions of the gasifier and a choice of feed coal, predictions can be made for volatile yield and composition. It is intended that future expansion of the model will allow predictions of char reactivity, swelling, tar molecular weight distribution and reactivity, plus soot yield and reactivity.

With additional work, an accurate predictive model for thermal decomposition effects in an entrained gasifier may be obtained by coupling the pyrolysis model (generalized to include the additional properties discussed above) with comprehensive computer codes simulating heat transfer, fluid mechanics and chemical reactions. Such detailed codes have been developed (see EPRI Report AP2470) (57) and currently require experimental data on coal devolatilization. The pyrolysis correlations presented herein may substitute for such data allowing variations of coal properties, (e.g. volatile yield and char reactivity) with gasifier conditions.

USING GASIFIER SAMPLES TO INFER GASIFIER CONDITIONS

On the basis of the pyrolysis experiments and pyrolysis theory, it is possible to estimate the conditions inside a gasifier from char samples taken from the different functional groups disappear from the char at rates which can vary substantially. For example, with reference to Figs. 4-1 to 4-16, if reaction times are on the order of a second, temperatures above 700°C must be reached by the coal particle to cause

any pyrolysis; and a temperature above 1100°C is required to remove aromatic hydrogen and ether oxygen. Analysis of tar provides additional information. At 1100°C, aliphatic hydrogen functional groups are very volatile while aromatic hydrogen is reasonably stable. The swelling behavior of a swelling coal provides information on the particle heating rate as discussed below.

The availability of a data base characterizing thermal decomposition for the coals of interest with the pyrolysis model for interpretation should allow a determination of the time-temperature history of the particle.

USING GASIFIER SAMPLES TO PREDICT REACTION PRODUCTS

In designing and operating a coal gasifier it is important to know a number of parameters which affect gasification behavior of a coal, and the effect on these parameters of changing the coal feedstock or operating conditions. The parameters are: volatile yield, volatile production rate, volatile composition, char reactivity, volatile reactivity, swelling and sticking behavior, soot production and reactivity, and pollutant formation potential. The pyrolysis theory tested under this contract and being generalized under DOE contracts #DE-AC01-81-FE05122 (56) and DE-AC-82-PC50254 (58) will provide the tools necessary to make such predictions, given the gasifier operating conditions. The theory is presently capable of providing good volatile yield predictions and recent developments in the model are addressing the additional properties.

Volatile Yield and Composition

The pyrolysis theory allows the prediction of the products of pyrolysis from: 1) a set of kinetic rate coefficients independent of the coal, 2) the structural composition of the coal, and 3) the time-temperature history of the coal. Application to entrained flow reactors and heated grid pyrolysis are discussed in this report and in References 30,38,56, and 58. Good predictions of volatile yield and composition are obtained.

Char Reactivity

Of the reactions occurring in coal gasification, char gasification has been shown to be significantly slower relative to gasification of volatiles (16), so it dominates the overall reaction time. But, char reactivity may be controlled by the initial pyrolysis conditions, which are in turn controlled by the volatile combustion. It

is therfore important to understand the effect of char formation conditions on its reactivity.

Under DOE Contract #DE-AC22-82PC50254, the effect of molecular alignment on reactivity (58) is being studied. The fact that the reactivity of graphite is a strong function of the molecular alignment suggests that increasing the molecular alignment in coal will reduce reactivity. An extreme example of molecular alignment may occur with cenosphere formation. In cases of swelling, a volume of liquid coal is subjected to bilateral extension. If the stress is sufficiently large, the aromatic molecules of the coal will align so their planes lie parallel to the surface of the cenosphere.

The effect of such alignment on reactivity under combustion conditions may be seen in Fig. 5-1. The figure shows a char particle (from pyrolysis of a Pittsburgh Seam coal) which is being attacked at holes in the surface while, large regions of the surface appear impervious to oxygen attack. Such holes have been observed for pyrolysis under non-reacting conditions and are caused by evolution of volatile gases (56). These holes presumably provide access to the reactive edge carbons which are not available in the molecularly aligned surface. The density of such holes and the degree of alignment are controlled by the coal plasticity and particle heating rate. So, the control of heating rate is an important factor in char reactivity. The heating rate is in turn controlled by the volatile yield, rate and composition and the reaction conditions. To predict the heating rate will require coupling the pyrolysis theory to a model for the gas concentration in the reactor and gas phase chemistry.

While the above effect is most prevalent for swelling coals, molecular alignment may be important for non-swelling coals as well. Figures 5-2 and 5-3 present chars for Illinois #6 and Utah bituminous coals which don't exhibit swelling. The chars do, however, show evidence of melting with holes blown to release gases. The particle in Fig. 5-3b shows no melting, therefore it may be fusinite. Additional work is required to develop a correlation between the reactivity and time temperature history of the coal.

Tar Evolution

At present, the pyrolysis model treats tar as a single product with an elemental and functional group distribution based on the parent coal. The tar yield is treated as a parameter of the model. A more detailed understanding of tar formation is

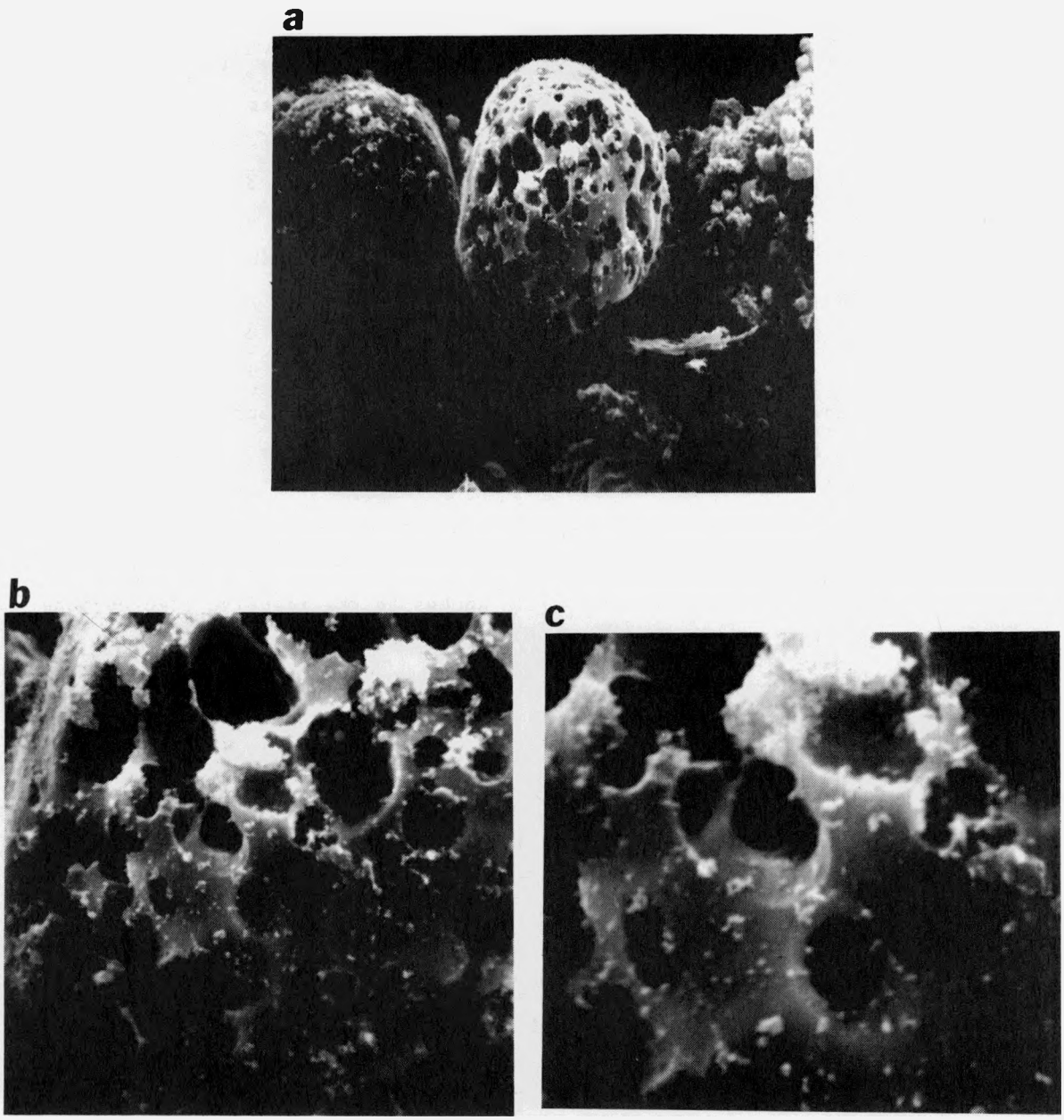

Figure 5-1. Electronmicrographs of Char Produced from Pittsburgh Seam Coal in a 13% Oxygen/87% Nitrogen Ambient at 1100°C. The Chars Show Attack of Oxygen at Holes (Believed to be Produced by Volatile Release) with Little Attack on the Surface.

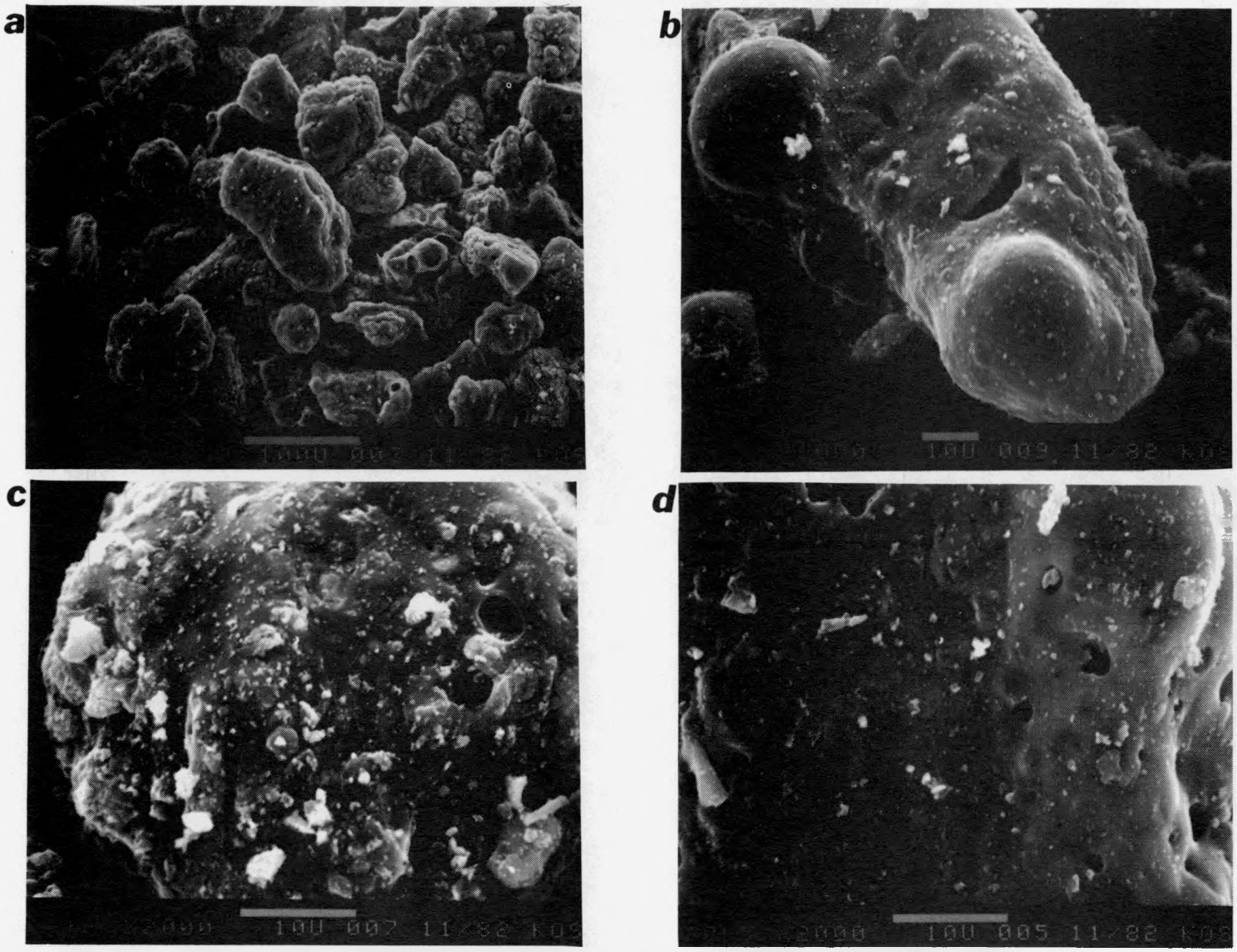

Figure 5-2. Electronmicrographs of Char from Illinois #6 Bituminous Coal Pyrolyzed in Nitrogen at 1100°C with the Injector at 66 cm.

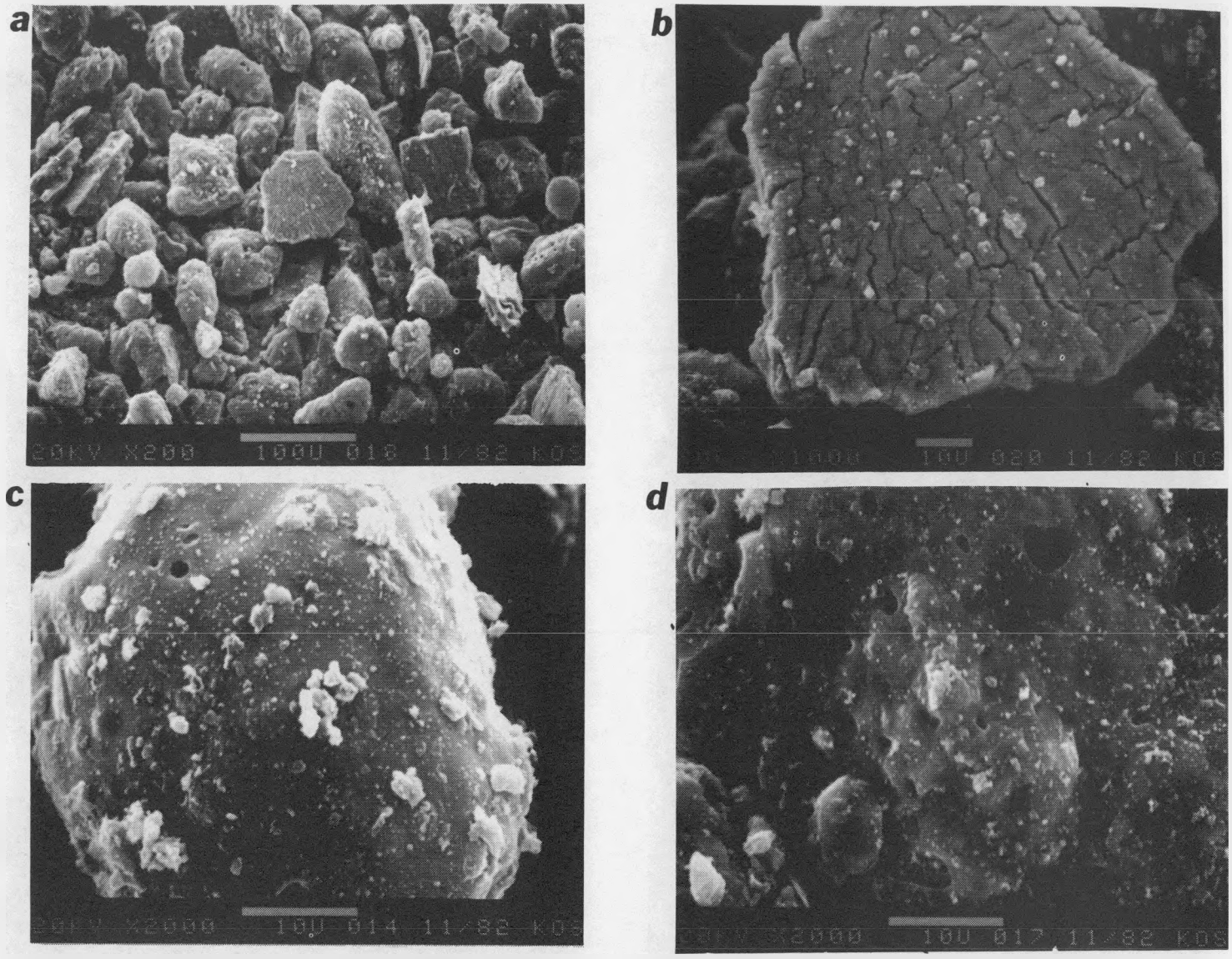

Figure 5-3. Electronmicrographs of Char from Utah Bituminous Coal Pyrolyzed in Nitrogen at 1100°C with the Injector at 66 cm.

required to predict the effects of pressure and bed geometry on tar yield, the gasification and soot formation properties of the tar and the viscosity of the coal melt as the tar evolves. As a foundation for a better tar evolution model a successful theory for polymer depolymerization recently developed under sponsorship of the Gas Research Institute (51) is being incorporated into the pyrolysis model (56). The theory combines statistical depolymerization with vaporization and diffusion to predict product yield and composition.

The theory was validated with experiments on poly(1,4-dimethylenenaphthalene) which we have synthesized to model certain aspects of coal chemistry. It predicts many features observed for coal and provides new insight into the role of donatable hydrogen in controlling product yields. It also provides predictions of the product distribution in pyrolysis experiments under various conditions which affect the transport of the molecules. Such distributions have been measured with field ionization mass spectrometry (FIMS). As presented in Fig. 5-4, higher external pressure retards the evaporation of heavier products and leads to a narrower product distribution. The experimental intensities (see numbers on figure) are in good agreement with the prediction (numbers in parenthesis). Because the average product size decreases as pressure increases, the demand of hydrogen donor per unit mass of product increases. If the amount of donatable hydrogen is limited, the increased demand results in lower tar production. The prediction of the pressure effect on tar yield for the model polymer is presented in Fig. 5-5 along with the pressure effect on tar yield for coal. Our experimental results show that the char yield in polymer pyrolysis increases from 5% to 19% when the pressure increases from 2 torr to 5 atm in agreement with the prediction (51).

To apply the depolymerization theory for coal, experiments are being performed to determine the molecular weight distribution of coal tar and its variation with process conditions (56). The field ionization mass spectra (FIMS) for the Pittsburgh coal tars produced in the FIMS itself are shown in Fig. 5-6. The spectra indicate that the average molecular weight of tar increase as reaction temperature increases. The prediction for the polymer shows a similar trend.

Work is proceeding to incorporate the depolymerization model into the coal pyrolysis model and compare the predictions with the results of the above experiments and others to be performed.

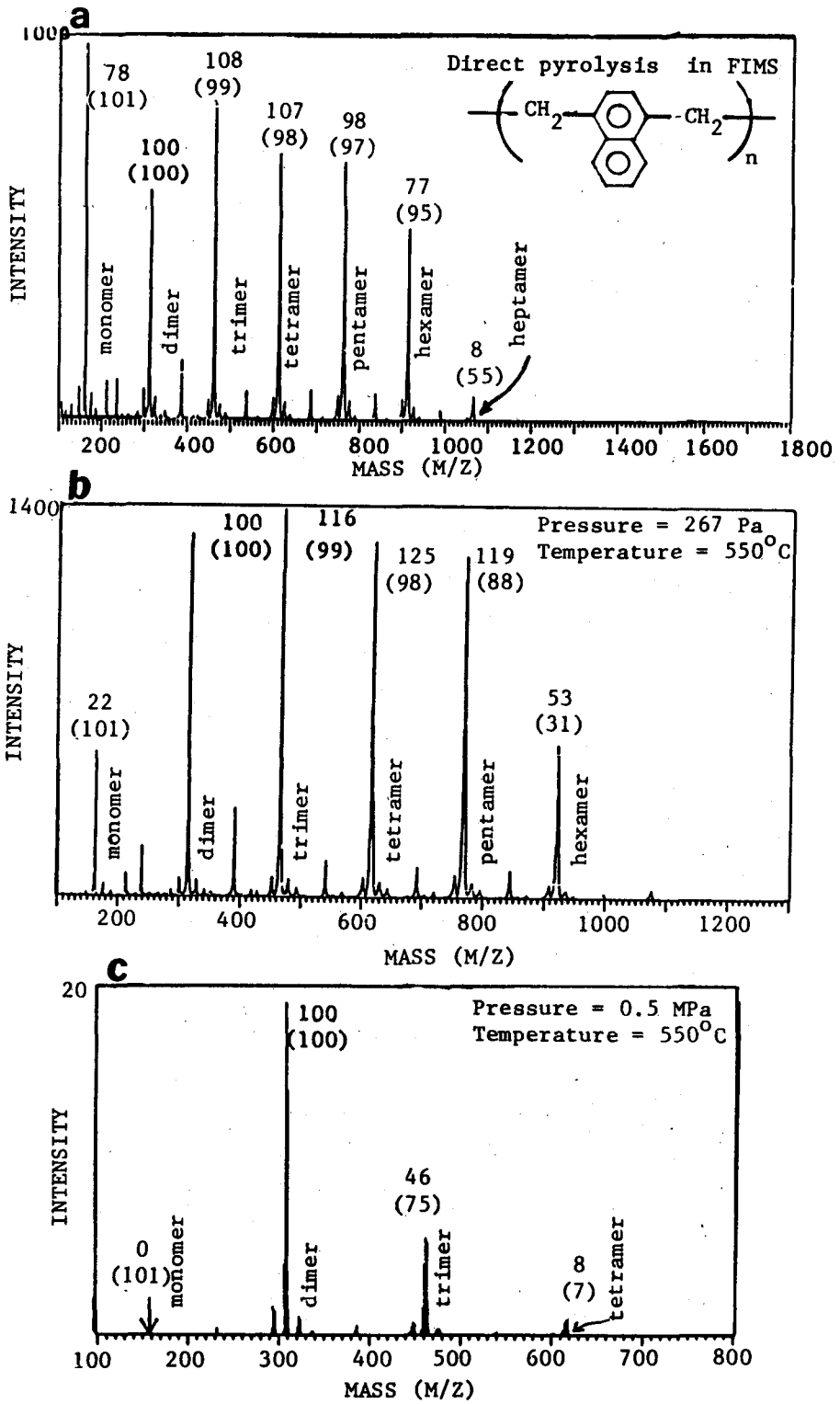

Figure 5-4. Field Ionization Mass Spectrometry of Tars Produces from Poly(1,4-Dimethylenenaphthalene). The Top Numbers are the Sum of Intensities for each Oligomer Group. The Numbers in Parentheses are the Predicted Distributions. All Numbers are Normalized with the Intensities of Dimer being 100.

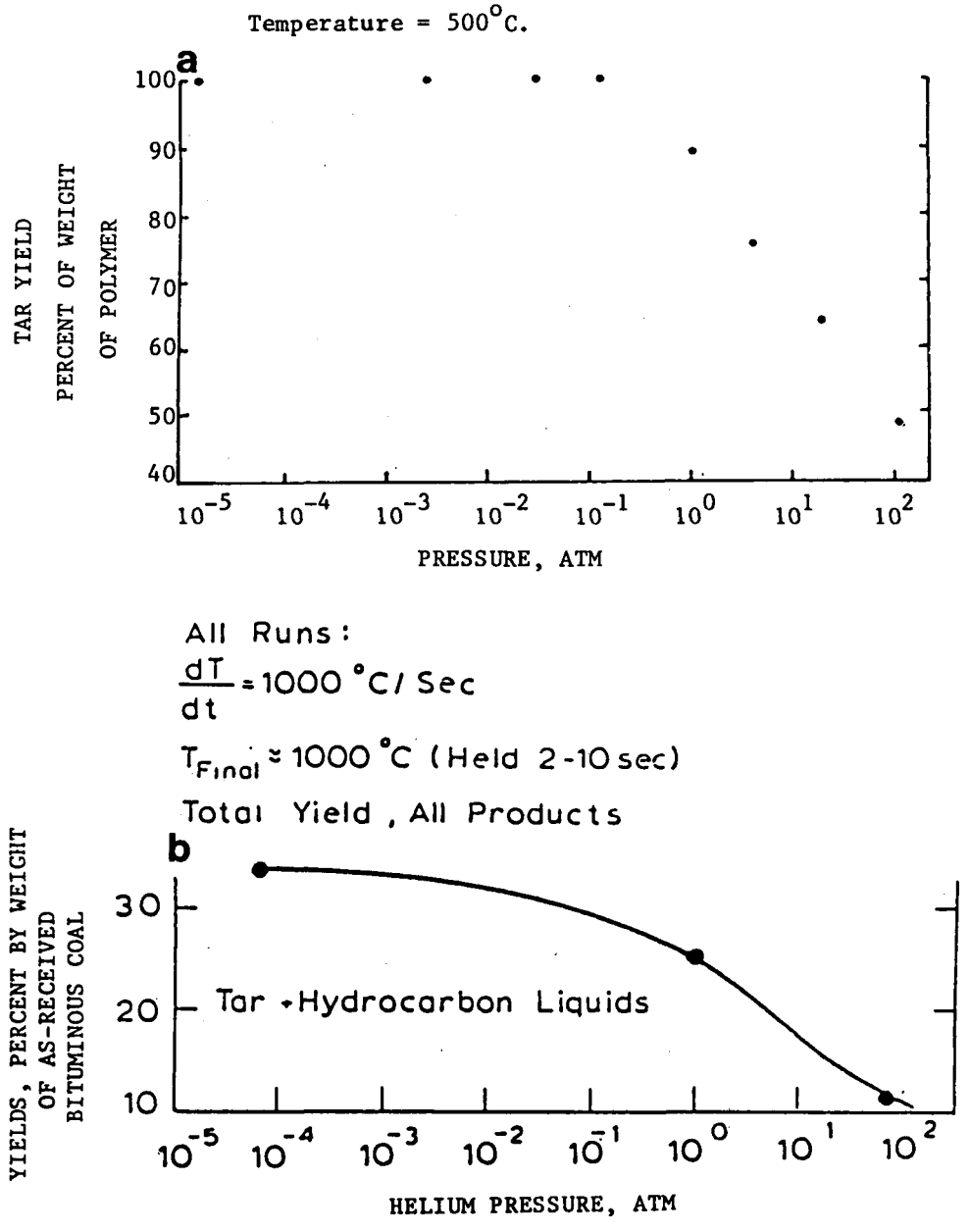

Figure 5-5. Pyrolysis Yields as a Function of Pressure.
a) Prediction for Poly(1,4-dimethylenenaphthalene).
b) From Suuberg, E. M., (1977), Ph.D. Thesis, MIT. (55).

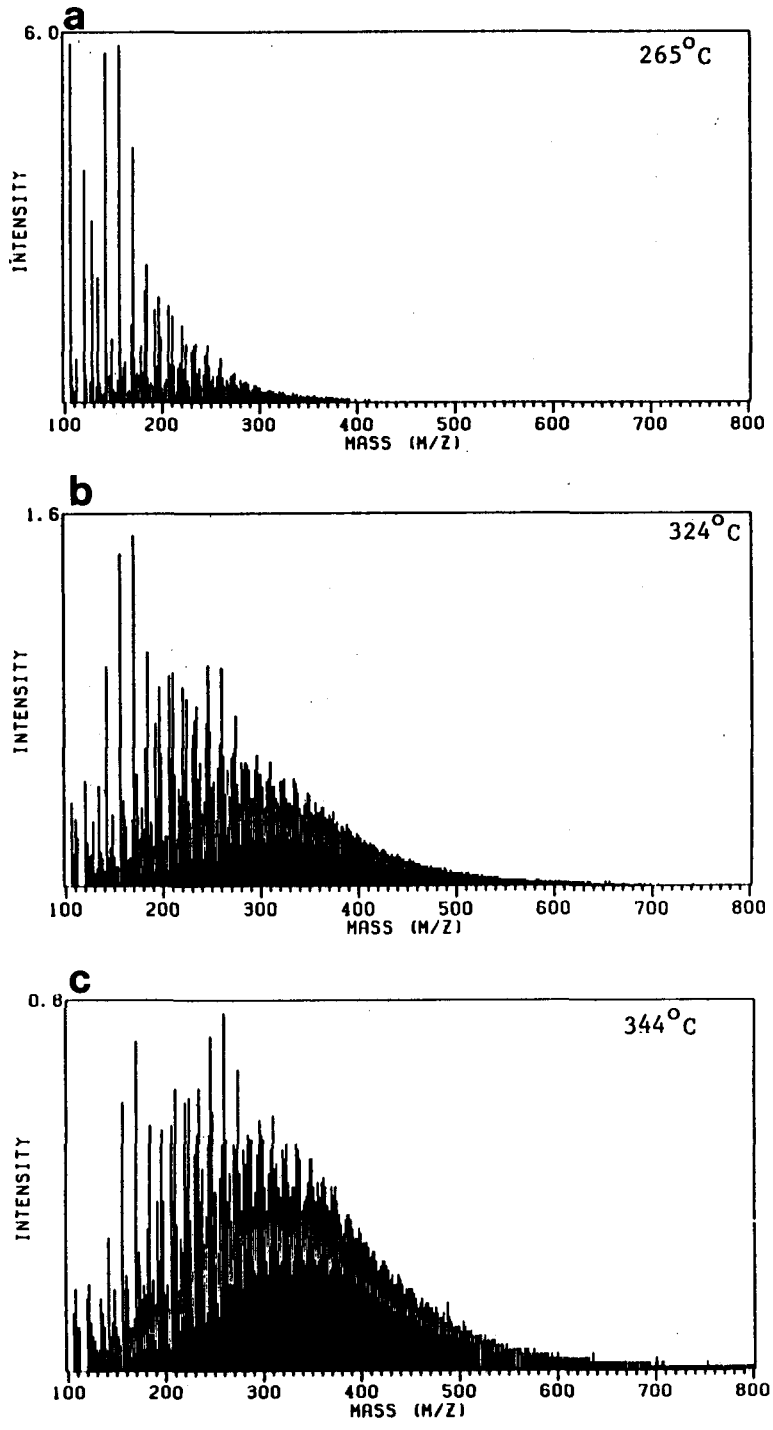

Figure 5-6. Field Ionization Mass Spectrometry of Selected Tars Produced in FIMS at Indicated Temperatures.

Volatile Reactivity

The heat released by the volatiles during gasification or combustion will control the particle heating rate (and hence the char reactivity). There is almost no data available on the combustion kinetics of volatiles. Such information is essential for predicting ignition. Data on combustion of volatile species have been obtained as a function of oxygen in the entrained flow reactor under DOE Contract #DE-AC22-82PC50254.

Figure 5-7 presents data for a Pittsburgh #8 bituminous coal. Figure 5-7a shows that for up to 6% oxygen there is little attack on the char. A surprising result was that under the same conditions there was little attack on the tar. At 13% oxygen, both tar and char react with oxygen. Figure 5-7b shows the effect of oxygen on the hydrocarbon gases. Paraffins are initially small, olefins dissapear quickly and acetylene increases initially (due to higher temperature pyrolysis) before being oxidized.

Additional data obtained with variations in oxygen, steam, CO, temperature and time are needed for a complete gasification model.

Swelling

For swelling coals, formation of cenospheres in a gasifier will drastically affect the fluid mechanical properties and the reactivity of the char. A model is being developed for predicting the swelling behavior of coal, especially cenosphere formation, in an entrained flow reactor (56). Although a number of attempts have been made to model this behavior, none of them have been directly related to the chemical structure, i.e. functional group distribution, of coal.

Two equations have been derived which predict the swelling behavior of coal. The first equation describes the growth of single cell spheres. It is based on the work of Chiou and Levine (59) and relates the swelling due to the pressure of the evolving gases against only the viscous forces in the coal melt. The equation relates the velocity of the outer wall to the pressure drop across the cell wall, and the viscosity. The pressure inside the cell is calculated using AFR's pyrolysis model to determine the rate of gas evolution, and is corrected for the loss by diffusion through the cell wall.

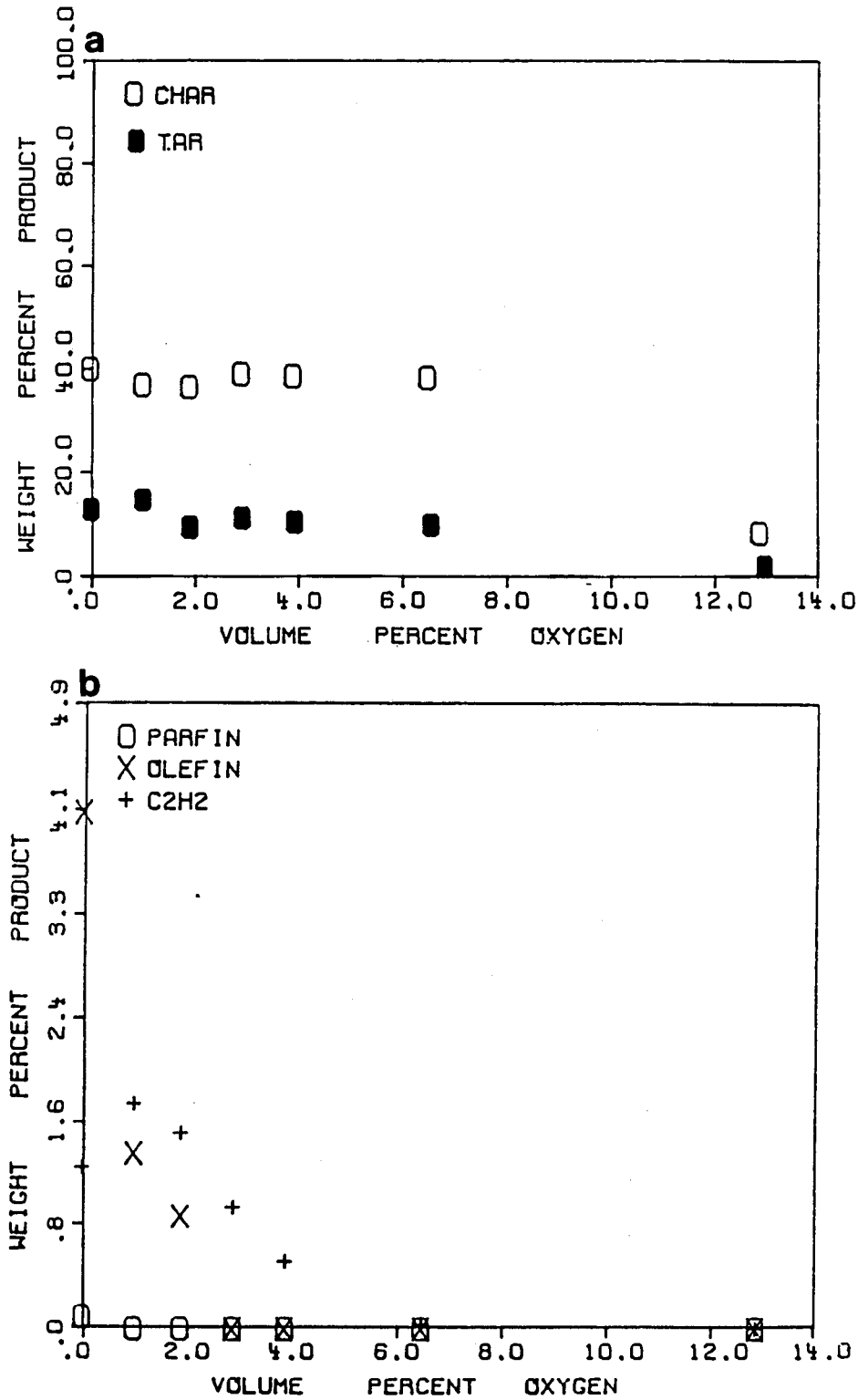

Figure 5-7. Pyrolysis Product Yield (as Weight Percent of DAF Coal) vs Percent Oxygen, in Nitrogen, for a Pittsburgh Seam Coal at 1100°C at Injector Position of 66 cm. a) Char and Tar, b) Paraffin, Olefin and Acetylene.

The other equation is a rupture criterion which predicts cell wall rupture when a critical pressure is reached.

The swelling equation and rupture equations, were incorporated into the pyrolysis code. Computations were made for several cases in which a Pittsburgh #8 bituminous coal was subjected to various heating conditions which resulted in varying amounts of swelling. The results are presented in Table 5-1 where D/D_o is the ratio of the maximum to the original diameter. The agreement between theory and experiment is good.

The parameters of the model are the minimum viscosity and the tensile strength of the coal melt. For the present time we have used 1×10^4 poise for the melt viscosity and a critical stress of 10 atmospheres. These are both reasonable values, but in future work we plan to predict these parameters from the functional group composition of the coal and the molecular weight distribution in the melt.

COUPLING PYROLYSIS, FLUID MECHANICS AND CHEMISTRY

It would be highly desirable to have a computer simulation model capable of predicting the gasification behavior of coals in large-scale gasifiers. Such a computer code would allow informed choices to be made in design, coal feedstocks and operating conditions. At the present time, many components for such a model exist in various stages of development. Comprehensive codes exist for simulating coupled fluid mechanics, heat and mass transfer and chemical reactions in an entrained gasifier. Such codes are in the early stages of validation. These codes require volatile yield and composition, char reactivity and char physical properties as input. As discussed above, the pyrolysis theory can presently predict the volatile yield and composition and has the capability of predicting char reactivity and physical properties, given the time-temperature history of the coal particle.

A completely predictive theory requires obtaining data for the combustion and gasification of the volatiles and coupling the pyrolysis code with comprehensive gasifier simulation codes. Such a coupled code would calculate particle temperature, volatile release, volatile reaction, heat release, swelling, char reactivity and fluid-particle interactions simultaneously. For coals exhibiting heating rate dependent properties, such as swelling and char reactivity, such a model is required.

TABLE 5-1

Comparison of Observed and Predicted Swelling Behavior

CASE	REFERENCE	FURNACE TEMPERATURE	AMBIENT GAS	ESTIMATED HEATING RATE	OBSERVED D/Do	PREDICTED D/Do
1	DOE 4th Quarterly	800°C	Helium	$3x10^{3}$°C/sec	4	3.5
3	DOE 4th Quarterly	1000°C	Helium	$1.0x10^{4}$	1-2	2.0
5	EPRI (Ref.4)	1273°C	Helium	$3x10^{4}$	1	1.1
6	DOE 5th Quarterly	1100°C	Nitrogen	$1x10^{4}$	2	1.5

Section 6

CONCLUSIONS AND RECOMMENDATIONS

1. Coal pyrolysis during the initial stage of gasificaton is extremely important in predicting gasification behavior because the pyrolysis process controls volatile yield and composition, ignition, swelling and char reactivity. The pyrolysis correlations which are being developed have the potential for predicting all of these properties.

2. The experimental reactor and analysis procedures put forth in this study provide data under conditions of temperature and heating rate appropriate to gasification. Temperatures up to 1500°C and heating rates between 10^3 and 10^5°C/sec can be achieved. The experimental facility provides control and measurement of process conditions, has provisions for collecting all pyrolysis products (i.e. char, tar, soot and the following gases: CO, CO_2, H_2O, CH_4, C_2H_2, C_2H_4, C_2H_6, C_3H_6, C_3H_8, C_4H_8, C_6H_6, NH_3, HCN, SO_2, COS, CS_2, CH_3OH, CH_3COOH, CH_3COCH_3), and achieves good material balance. It has optical access to the reaction zone and employs FT-IR for in-situ analysis of gas species and gas temperature. Pyrolysis data for six coals have been obtained. The reactor has also performed successfully with reactive ambient gas compositions to study pyrolysis and char reactivity.

The reactor was designed for only 2 atm. pressure and was operated at 1 atm. It is recommended that a high pressure reactor of similar design be built to study the effect of pressure variations on pyrolysis behavior.

3. The entrained flow reactor has provided pyrolysis yield and kinetic rate data under conditions which are closer to those of a typical gasifier than have previously been available using heated grid techniques. These conditions included higher heating rates than can be obtained with the heated grid and secondary reactions of volatiles which do not occur in the heated grid.

It is recommended that work continue to separate the effects of heat and mass transfer to define more accurate chemical kinetic rates in pyrolysis.

4. The ability to perform in-situ FT-IR measurements of gas species and temperature has been demonstrated. Several comparisons have been made between the in-situ

spectra and the cell spectra to determine whether there are any substantial differences in species concentration due to reactions within the sample collector. For the conditions used so far, no such variations have become appearant but the ability to test this possibility for other species and other conditions is important. The ability to perform gas temperature measurements is proving quite useful in trying to determine particle temperatures (58).

5. The pyrolysis model which employs a rank-independent set of kinetic rate coefficients has been successful when compared with experimental data for all the coals and conditions studied. The functional group compositions (which are the coal-dependent parameters of the model) are reasonable compared to what is expected for coals of similar rank. The model appears capable of predicting thermal decomposition phenomena which are of importance in gasification, but additional work is needed on volatile oxidation, swelling, tar formation, and char reactivity.

It is recommended that models for swelling, tar yield, volatile oxidation and char reactivity be integrated with the basic pyrolysis model.

6. An assessment has been made of the application of the correlations obtained under this program to large scale gasifiers. There are three applications which have been identified. First, the correlations may be used to infer reactor conditions from the composition of chars, tars and gases sampled from the gasifier. Second, given the approximate conditions of the gasifier, predictions can be made for volatile yields, compositions and physical properties and their dependence on variations in coal or operating conditions. Third, the model can be integrated with previously developed comprehensive computer codes for gasifier simulation to provide a truly predictive capability.

It is recommended that work be undertaken to expand the data base to additional coals, particle sizes, temperatures, heating rates and pressure. It is also recommended that the pyrolysis model be combined with codes for fluid mechanics and reaction chemistry to simulate gasifier operations.

Section 7

REFERENCES

1. Howard, J. B., Fundamentals of Coal Pyrolysis and Hydropyrolysis, in Chemistry of Coal Utilization. Second Supplementary Volume. Martin A. Elliot, Editor, Wiley, pg. 665 (1981).

2. Howard, J. B., Peters, W. A. and Serio, M. A., Coal Devolatilization Information for Reactor Modeling. EPRI report AP-1803, April, (1981).

3. Anthony, D. B. and Howard, J. B., Am. Inst. Chem. Eng. J., 22, 625 (1976).

4. Anthony, D. B., Howard, J. B., Meissner, H. P. and Hottel, H. G., Rev. Sci. Instrum., 45, 992 (1974).

5. Anthony, D. B., Howard, J. B., Meissner, H. P. and Hottel, H. G., Fifteenth Symposium (International) on Combustion, 1303, The Combustion Institute, Pittsburgh, PA (1975).

6. Suuberg, E. M., Rapid Pyrolysis and Hydropyrolysis of Coal, Ph.D Thesis, MIT (1977).

7. Suuberg, E. M., Peters, W. A. and Howard, J. B., Ind. Eng. Process Des. Dev., 17, #1, 37 (1978).

8. Suuberg, E. M., Peters, W. A. and Howard, J. B., Seventeenth Symposium (International) on Combustion, 117, The Combustion Institute, Pittsburgh, PA, (1979).

9. Juntgen, H. and van Heek, K. H., Fuel Processing Technology, 2, 26 (1979).

10. Gavalas, G. R. and Oka, M., Fuel 51, 285 (1972).

11. Solomon, P. R. and Colket, M. B., 17th Symposium (International) on Combustion, 131, The Combustion Institute, Pittsburgh, PA (1979).

12. Solomon, P. R., Coal Structure, Advances in Chemistry Series, 192, 95 (1981).

13. Solomon, P. R. and Hamblen, D. G., Chemistry and Physics of Coal Utilization, AIP Conference Proceedings No. 70, Amer, Inst. Phys., New York, (1981), pg. 121.

14. Solomon, P. R., Hamblen, D. G. and Carangelo, R. M., Coal Pyrolysis, AIChE, Symposium on Coal Pyrolysis (Nov., 1981).

15. Solomon, P. R. and Colket, M. B., Fuel, 57, 749 (1978).

16. Goetz, G. J., Nsakala, N.Y., R. L. Patel, T. C. Lao, EPRI Final Report AP-2601, Combustion and Gasification Characteristics of Chars from Four Commercially Significant Coals of Different Rank, Sept., (1982).

17. Badzioch, S. and Hawksley, P. G. W., Ind. Eng. Chem. Process Des. Dev., 9, 521 (1970).

18. Nsakala, N. Y., Essenhigh, R. H. and Walker, P. L., Jr., Combustion Science Technol., 16, 153 (1977).

19. Kobayashi, H., Devolatilization of Pulverized Coal at High Temperatures, Ph.D. Thesis, Dept. of Mechanical Eng., Mass. Institute of Technology, Cambridge, MA (1976).

20. Kobayashi, H., Howard, J. B. and Sarofim, A. F., Sixteenth Symposium (International) on Combustion, The Combustion Institute, Pittsburgh, PA, 411, (1977).

21. Solomon, P. R. and Hamblen, D. G., Characterization of Thermal Decomposition of Coal in Experimental Reactors, EPRI Final Report AP2602, Sept. (1982).

22. Ubhayakar, S. K., Stickler, D. B., von Rosenberg, Jr., C. W. and Gannon, R. E., 16th Symposium (International) Combustion, Combustion Inst., Pittsburgh, PA, 427, (1977).

23. Scaroni, A. W., Walker, Jr., P. L. and Essenhigh, R. H., Fuel, 60, 71, (1981).

24. McLean, W. J., Hardesty, D. R. and Pohl, J. H., 18th Symposium (International), on Combustion, The Combustion Institute, Pittsburgh, PA, 1239 (1981).

25. Samuelson, G. S., Trolinger, J. D., Heap, M. P. and Seeker, W. R., Combust. Flame 38, #3 (1980).

26. Solomon, P. R., Fuel, 60, 3 (1981).

27. Solomon, P. R., Hobbs, R. H., Hamblen, D. G., Chen, W. Y., La Cava, A. and Graff, R. S., Fuel, 60, 342 (1981).

28. Solomon, P. R., New Approaches in Coal Chemistry, ACS Symposium Series, 169, 61 (1981).

29. Solomon, P. R., Characterization of Coal and Coal Thermal Decomposition, Chapter III of EPA Monograph on Coal Combustion, (In Press).

30. Solomon, P. R., Hamblen, D. G., Carangelo, R. M., and Krause, J. L, Coal Thermal Decomposition in an Entrained Flow Reactor; Experiments and Theory, 19th Symposium (International) on Combustion, Haifa, Israel, (1982).

31. Mims, C. A., Neville, M., Quann, R. and Sarofim, A., Laboratory Study of Trace Element Transformation During Coal Combustion, presented at the National 87th AIChE Meeting, Boston, MA, August 19-22 (1979).

32. Haaland, D. M., Easterling. R. G., Applied Spectroscopy, 34, #5, 539 (1980).

33. Herzberg, G., Molecular Spectra and Molecular Structure, I. Spectra of Diatomic Molecules, Van Nostrand Reinhold, New York, (1950).

34. Guelachvii, G., Journal of Molecular Spectroscopy, 75, 251-269, (1979).

35. John, W. and Reischl, G., Journal of the Air Pollution Control Assoc., 872 (1980).

36. Solomon, P. R. and Carangelo, R. M., Fuel, 61, 663, (1982).

37. Solomon, P. R., Hamblen, D. G. and Carangelo, R. M., ACS Symposium Series, 205, Coal and Coal Products: Analytical Characterization Techniques, Am. Chem. Soc., Washington, DC, (1982) pg. 77.

38. Solomon, P. R., The Characterization of Coals During Thermal Decomposition, Fifth EPA Fundamental Combustion Research Workshop, Newport Beach, CA, (1980).

39. Weimer, R. F. and Ngan, D. Y., ACS Div. of Fuel Chemistry Preprints, 24, #3, 129, (1979).

40. Juntgen, H. and van Heek, K. H., An Update of German Non-Isothermal Pyrolysis Work, Fuel Processing Technology, 2, 261, (1979).

41. Fitzgerald, D. and van Krevelen, D. W., Fuel, 38, 17, (1959).

42. Morris, J. P. and Keairns, D. L., Fuel, 58, 465, (1979).

43. Tyler, R. J., Fuel, 59, 218, (1980).

44. Brown, J. K., Dryden, I. G. C., Dunevein D. H., Joy, W. K., and Pankhurst, K. S., J. Inst. Fuels, 31, 259, (1958).

45. Orning, A. A., and Greifer, B., Fuel, 35, 318, (1956).

46. Lahiri, A. and Mazmumdar, B. K., Studies on Dehydrogenation of Coal and Structural Implications, Proceedings of the Symposium on the Science and Technology of Coal, Ottawa, Canada, (1967).

47. van Krevelen, D. W., and Schuyer, J., Coal Science, Elsevier, Amsterdam, (1957).

48. Whitehurst, D. D., Mitchell, T. O., Farcasium M. and Dickert, J. J., Jr., The Nature and Origin of Asphaltenes in Processed Coals, Final Report, Electric Power Research Institute, AF-1298, (Dec., 1979).

49. Derbyshire, F. J., Influence of Polyaromatic Solvent Components in Coal Liquefaction, Electric Power Research Institute, Fifth Annual Coal Liquefaction Contractor's Conference, Palo Alto, CA (May 7-8, 1980).

50. Solomon, P. R. and Carangelo, R. M., Characterization of Wyoming Subbituminous Coals and Liquefaction Products by Fourier Transform Infrared Spectrometry, Final Report, EPRI Contract No. 1604-2, 49, (Sept., 1981). Solomon, P. R., Hamblen, D. G. and Carangelo, R. M., Proceedings of the International Conference on Coal Science, 719, Dusseldorf, Germany, (September, 1981).

51. King, H. H. and Solomon, P.R., Third Quarterly Report for Gas Research Institute, Contract #5081-260-0582, (1982).

52. Unger, P. E. and Suuberg, E.M., Modeling the Devolatilization Behavior of a Softening Bituminous Coal, Eighteenth Symposium (International) on Combustion, 1203, Waterloo, Canada (August 17-22, 1980).

53. Stein, S. E., Golden, D. M. and Benson, S. W., J. Phys. Chem., 81, 314, (1977). Stein S. E. and Barton, B. D., Thermochem. Acta, 44, 265, (1981).

54. Vernon, L. W., Fuel, 59, 102, (1980).

55. Campbell, J. H., Fuel, 57, 217, (1978).

56. Solomon, P.R., Hamblen, D.G. and Best, P.E., Coal Gasification Reactions with On-Line In-Situ FT-IR Analysis, DOE Fourth and Fifth Quarterly Reports, Contract #DE-AC21-81FE05122, (1982).

57. Schneyer, G. P., Cook, J. L., Brownell, D. H. and Blake, T. R.,Dynamic Simulation of a Single-Stage Entrained Flow Gasifier, EPRI Report AP2740, (December,1982).

58. Solomon, P.R. and Hamblen, D.G., An Investigation of Vaporization and Devolatilization of Coal/Water Mixtures DOE Second Quarterly Report, Contract #DE-AC22-82PC50254, (1982).

59. Chiou, M.J. and Levine, H.B., Investigation of Structure Deformation of Coal Particles in Pyrolysis, Report from JAYCOR.

APPENDIX

Illinois #6 Bituminous
(sample from Texaco)

Illinois #6 Bituminous Coal Pyrolyzed in Nitrogen at 1100°C with Injector at 0 cm.

PYROLYSIS SUMMARY REPORT - FUHRUN 424 10 - 6 - 82

RUN CONDITIONS

4310 mg. VACDRY COAL
sec. @ 0 Amps
0 sec. @ 0 Amps
1100 Degrees C. @ 0 torr with ALTUBE grid
762.200 mm. Final Pressure for 77.2410 liters

COAL

Name : ILL6 - 0
% ASH = 13.2100

PYROLYSIS PRODUCT DISTRIBUTION

	Dry Wt. %	DAF Wt. %
Char	01.0348	78.1481
Tar	.88631	1.02121
Gas	3.80767	4.38722
Water	1.80238	2.07672
Missing	12.4688	14.3666

GAS COMPOSITION

	Dry Wt. %	DAF Wt. %	Volume %
Methane	.15017	.17302	1.27770E-2
CO	.56158	.64706	2.73037E-2
Hydrogen	0	0	0
CO2	2.20335	2.53872	.06817
Acetylene	2.55287E-3	2.94143E-3	1.33664E-4
Ethylene	.06724	.07747	3.26924E-3
Ethane	2.58302E-2	2.97618E-2	1.17211E-3
Propylene	.07677	.08846	2.48846E-3
Paraffins	.49009	.56469	7.94263E-3
Olefins	.07700	.08872	1.24001E-3
HCN	2.59860E-2	2.99413E-2	1.31020E-3
Ammonia	4.22966E-3	4.87344E-3	3.38702E-4
COS	6.39197E-3	7.36488E-3	1.45025E-4
CS2	5.30952E-2	6.11767E-2	9.51050E-4
SO2	.06334	.07298	1.34741E-3
Water	1.80238	2.07672	.09437
OTHER	0	0	2.73037E-2
Gas Total:	5.61006	6.46395	

Illinois #6 Bituminous Coal Pyrolyzed in
Nitrogen at 1100°C with Injector at 16 cm

PYROLYSIS SUMMARY REPORT - FUHRUN 425 10 - 6 - 82

RUN CONDITIONS

2010 mg. VACDRY COAL
0 sec. @ 0 Amps
0 sec. @ 0 Amps
1100 Degrees C. @ 0 torr with ALTUBE grid
764.400 mm. Final Pressure for 78.6840 liters

COAL

Name : ILL6 - 4
% ASH = 13.2100

PYROLYSIS PRODUCT DISTRIBUTION

	Dry Wt. %	DAF Wt. %
Char	59.6865	53.5506
Tar	10.9751	12.6456
Gas	16.1237	18.5779
Water	3.81015	4.39008
Missing	9.40438	10.8357

GAS COMPOSITION

	Dry Wt. %	DAF Wt. %	Volume %
Methane	1.44840	1.66886	5.62549E-2
CO	3.56430	4.10680	.07910
Hydrogen	0	0	0
CO2	4.16133	4.79471	5.87718E-2
Acetylene	5.02226E-2	5.78668E-2	1.20037E-3
Ethylene	.96041	1.10659	2.13152E-2
Ethane	.47222	.54409	9.78168E-3
Propylene	.77191	.88941	1.14212E-2
Paraffins	2.22849	2.56769	1.64862E-2
Olefins	2.05594	2.36886	1.52097E-2
HCN	.14621	.16846	3.36525E-3
Ammonia	1.39292E-2	1.60493E-2	5.09177E-4
COS	1.53054E-2	1.77272E-2	1.59349E-4
CS2	.10750	.12386	8.78998E-4
SO2	.12748	.14680	1.23782E-3
Water	3.81015	4.39008	.09106
OTHER	0	0	.07910
Gas Total:	19.9339	22.9679	

Illinois #6 Bituminous Coal Pyrolyzed in
Nitrogen at 1100°C with Injector at 26 cm

PYROLYSIS SUMMARY REPORT -- FUHRUN 423 10 - 6 - 82

RUN CONDITIONS

3880 mg. VACDRY COAL
0 sec. @ 0 Amps
0 sec. @ 0 Amps
1100 Degrees C. @ 0 torr with ALTUBE grid
762.000 mm. Final Pressure for 79.4060 liters

COAL

Name : ILL6 - 8
% ASH = 13.2100

PYROLYSIS PRODUCT DISTRIBUTION

	Dry Wt. %	DAF Wt. %
Char	54.3015	47.3459
Tar	5.62886	6.48561
Gas	17.1934	19.8104
Water	3.51714	4.05247
Missing	19.3589	22.3055

GAS COMPOSITION

	Dry Wt. %	DAF Wt. %	Volume %
Methane	2.04662	2.35813	.15236
CO	4.36490	5.02927	.18568
Hydrogen	0	0	0
CO2	3.75032	4.32115	.10152
Acetylene	.13427	.15470	6.15144E-3
Ethylene	1.24581	1.43543	5.29984E-2
Ethane	.35206	.40565	1.39787E-2
Propylene	.74292	.85600	2.10700E-2
Paraffins	1.59636	1.83934	2.26372E-2
Olefins	2.37643	2.73814	3.36980E-2
HCN	.32566	.37523	1.43672E-2
Ammonia	2.08603E-2	2.40354E-2	1.46164E-3
COS	1.28149E-2	1.47654E-2	2.54410E-4
CS2	.11712	.13495	1.83576E-3
SO2	.10726	.12359	1.99639E-3
Water	3.51714	4.05247	.16113
OTHER	0	0	.18568
Gas Total:	20.7106	23.8629	

Illinois #6 Bituminous Coal Pyrolyzed in Nitrogen at 1100°C with Injector at 36 cm

PYROLYSIS SUMMARY REPORT - FUHRUN 422 10 - 6 - 82

RUN CONDITIONS

4550 mg. VACDRY COAL
0 sec. @ 0 Amps
0 sec. @ 0 Amps
1100 Degrees C. @ 0 torr with ALTUBE grid
763.800 mm. Final Pressure for 79.4060 liters

COAL

Name : ILL6 - 12
% ASH = 13.2100

PYROLYSIS PRODUCT DISTRIBUTION

	Dry Wt. %	DAF Wt. %
Char	53.7186	46.6743
Tar	4.74065	5.46221
Gas	20.0638	23.1176
Water	5.14896	5.93266
Missing	16.3278	18.8130

GAS COMPOSITION

	Dry Wt. %	DAF Wt. %	Volume %
Methane	2.66676	3.07266	.23251
CO	5.80786	6.69186	.28935
Hydrogen	0	0	0
CO2	4.37064	5.03588	.13857
Acetylene	.23285	.26829	1.24937E-2
Ethylene	1.43525	1.65370	.07150
Ethane	.33210	.38265	1.54431E-2
Propylene	.62657	.72194	2.08116E-2
Paraffins	1.05229	1.21245	1.74757E-2
Olefins	2.65222	3.05590	4.40463E-2
HCN	.61479	.70837	3.17649E-2
Ammonia	2.23669E-2	2.57713E-2	1.83542E-3
COS	1.15868E-2	1.33504E-2	2.69390E-4
CS2	.14131	.16282	2.59385E-3
SO2	.09717	.11196	2.11804E-3
Water	5.14896	5.93266	.27626
OTHER	0	0	.28935
Gas Total:	25.2127	29.0503	

Illinois #6 Bituminous Coal Pyrolyzed in Nitrogen at 1100°C with Injector at 46 cm

PYROLYSIS SUMMARY REPORT - FUHRUN 421 10 - 5 - 82

RUN CONDITIONS

4210 mg. VACDRY COAL
0 sec. @ 0 Amps
0 sec. @ 0 Amps
1100 Degrees C. @ 0 torr with ALTUBE grid
762.000 mm. Final Pressure for 79.4060 liters

COAL

Name : ILL6 - 16
% ASH = 13.2100

PYROLYSIS PRODUCT DISTRIBUTION

	Dry Wt. %	DAF Wt. %
Char	53.2992	46.1911
Tar	4.33254	4.99198
Gas	22.4996	25.9242
Water	4.20208	4.84166
Missing	15.6664	18.0509

GAS COMPOSITION

	Dry Wt. %	DAF Wt. %	Volume %
Methane	3.07339	3.54118	.24826
CO	7.12339	8.20762	.32081
Hydrogen	0	0	0
CO2	5.14518	5.92831	.15113
Acetylene	.37986	.43768	1.08831E-2
Ethylene	1.60300	1.84791	.07403
Ethane	.17102	.19706	7.36831E-3
Propylene	.37221	.42886	1.14541E-2
Paraffins	.60641	.69871	9.33064E-3
Olefins	2.62566	3.02530	4.03997E-2
HCN	1.10568	1.27397	5.29280E-2
Ammonia	2.47142E-2	2.84758E-2	1.87895E-3
COS	1.14895E-2	1.32383E-2	2.47497E-4
CS2	.16714	.19258	2.84249E-3
SO2	.08967	.10332	1.81094E-3
Water	4.20208	4.84166	.20888
OTHER	0	0	.32081
Gas Total:	26.7017	30.7659	

Illinois #6 Bituminous Coal Pyrolyzed in
Nitrogen at 1100°C with Injector at 56 cm

PYROLYSIS SUMMARY REPORT - FUHRUN 420 10 - 5 - 82

RUN CONDITIONS

4640 mg. VACORY COAL
0 sec. @ 0 Amps
0 sec. @ 0 Amps
1100 Degrees C. @ 0 torr with ALTUBE grid
763.600 mm. Final Pressure for 82.2940 liters

COAL

Name : ILL6 - 20
% ASH = 13.2100

PYROLYSIS PRODUCT DISTRIBUTION

	Dry Wt. %	DAF Wt. %
Char	51.4224	44.0285
Tar	6.43318	7.41236
Gas	21.2079	24.4358
Water	3.10112	3.57313
Missing	17.8353	20.5500

GAS COMPOSITION

	Dry Wt. %	DAF Wt. %	Volume %
Methane	3.11480	3.58889	.26729
CO	6.96005	8.01942	.34130
Hydrogen	0	0	0
CO2	4.45214	5.12979	.13893
Acetylene	.61990	.71425	3.27365E-2
Ethylene	1.54078	1.77530	.07555
Ethane	.09560	.11015	4.37571E-3
Propylene	.20598	.23734	6.73412E-3
Paraffins	.11175	.12876	1.82671E-3
Olefins	2.37772	2.73963	3.88657E-2
HCN	1.45021	1.67095	.07374
Ammonia	2.66583E-2	3.07158E-2	2.15312E-3
COS	1.20051E-2	1.38324E-2	2.74727E-4
CS2	.15795	.18199	2.85362E-3
SO2	.08231	.09483	1.76587E-3
Water	3.10112	3.57313	.16376
OTHER	0	0	.34130
Gas Total:	24.3090	28.0090	

Illinois #6 Bituminous Coal Pyrolyzed in
Nitrogen at 1100°C with Injector at 66 cm

PYROLYSIS SUMMARY REPORT - FUHRUN 419 10 - 5 - 82

RUN CONDITIONS

5000 mg. VACDRY COAL
0 sec. @ 0 Amps
0 sec. @ 0 Amps
1100 Degrees C. @ 0 torr with ALTUBE grid
762.400 mm. Final Pressure for 88.0688 liters

COAL

Name : ILL6 - 24
% ASH = 13.2100

PYROLYSIS PRODUCT DISTRIBUTION

	Dry Wt. %	DAF Wt. %
Char	51.1339	43.6961
Tar	7.17500	8.26708
Gas	23.3856	26.9451
Water	4.48730	5.17029
Missing	13.8181	15.9213

GAS COMPOSITION

	Dry Wt. %	DAF Wt. %	Volume %
Methane	3.54300	4.08227	.34458
CO	7.76377	8.94547	.43147
Hydrogen	0	0	0
CO2	4.95400	5.70804	.17520
Acetylene	.72554	.83598	4.34241E-2
Ethylene	1.55124	1.78735	.08621
Ethane	2.78007E-2	3.20321E-2	1.44202E-3
Propylene	.16395	.18890	6.07453E-3
Paraffins	.17389	.20036	3.22146E-3
Olefins	2.33226	2.68724	4.32052E-2
HCN	1.80601	2.08089	.10408
Ammonia	2.72422E-2	3.13886E-2	2.49363E-3
COS	1.38717E-2	1.59831E-2	3.59766E-4
CS2	.21905	.25239	4.48519E-3
SO2	.08398	.09676	2.04193E-3
Water	4.48730	5.17029	.26856
OTHER	0	0	.43147
Gas Total:	27.8729	32.1154	

Utah Bituminous
(sample from Texaco)

Utah Bituminous Coal Pyrolyzed in Nitrogen
at 1100°C with Injector at 6 cm
PYROLYSIS SUMMARY REPORT - FUHRUN 445

RUN CONDITIONS

4450 mg. VACDRY COAL
0 sec. @ 0 Amps
0 sec. @ 0 Amps
1100 Degrees C. @ 0 torr with ALTUBE grid
762.400 mm. Final Pressure for 80.8500 liters

COAL

Name : UTAH - 0
% ASH = 8.50000

PYROLYSIS PRODUCT DISTRIBUTION

	Dry Wt. %	DAF Wt. %
Char	80.3348	78.5080
Tar	4.45168	4.86523
Gas	3.65764	3.99742
Water	.90169	.98546
Missing	10.6541	11.6438

GAS COMPOSITION

	Dry Wt. %	DAF Wt. %	Volume %
Methane	.20725	.22651	1.73312E-2
CO	.56268	.61495	2.68872E-2
Hydrogen	0	0	0
CO2	1.16308	1.27113	3.53669E-2
Acetylene	6.80147E-3	7.43330E-3	3.49999E-4
Ethylene	.17537	.19166	8.37994E-3
Ethane	.13853	.15139	6.17819E-3
Propylene	.21369	.23355	6.80753E-3
Paraffins	.61351	.67051	9.77206E-3
Olefins	.55680	.60853	8.86877E-3
HCN	-8.18725E-3	-8.94782E-3	-4.05707E-4
Ammonia	3.66025E-3	4.00027E-3	2.88071E-4
COS	-2.79534E-4	-3.05502E-4	-6.23336E-6
CS2	2.21469E-2	2.42043E-2	3.89887E-4
SO2	2.54196E-3	2.77810E-3	5.31406E-5
Water	.90169	.98546	4.64009E-2
OTHER	0	0	2.68872E-2
Gas Total:	4.55934	4.98288	

Utah Bituminous Coal Pyrolyzed in Nitrogen
at 1100°C with Injector at 16 cm

PYROLYSIS SUMMARY REPORT - FUHRUN 448 10 - 6 - 82

RUN CONDITIONS

4700 mg. VACDRY COAL
0 sec. @ 0 Amps
0 sec. @ 0 Amps
1100 Degrees C. @ 0 torr with ALTUBE grid
764.400 mm. Final Pressure for 80.8500 liters

COAL

Name : UTAH - 4
% ASH = 8.50000

PYROLYSIS PRODUCT DISTRIBUTION

	Dry Wt. %	DAF Wt. %
Char	58.9042	55.0866
Tar	7.21489	7.88512
Gas	11.7073	12.7948
Water	1.70122	1.85925
Missing	20.4723	22.3741

GAS COMPOSITION

	Dry Wt. %	DAF Wt. %	Volume %
Methane	.92577	1.01177	.08182
CO	1.61742	1.76767	.08168
Hydrogen	0	0	0
CO2	2.72695	2.98027	.08764
Acetylene	2.96106E-2	3.23613E-2	1.61054E-3
Ethylene	.76318	.83407	3.85449E-2
Ethane	.28400	.31038	1.33876E-2
Propylene	.76242	.83325	2.56711E-2
Paraffins	2.25803	2.46779	3.80144E-2
Olefins	2.25291	2.46219	3.79282E-2
HCN	2.91670E-2	3.18765E-2	1.52766E-3
Ammonia	6.19688E-3	6.77255E-3	5.15493E-4
COS	6.19189E-4	6.76709E-4	1.45938E-5
CS2	4.62627E-2	5.05603E-2	8.60826E-4
SO2	4.76025E-3	5.20246E-3	1.05183E-4
Water	1.70122	1.85925	.09253
OTHER	0	0	.08168
Gas Total:	13.4085	14.6541	

Utah Bituminous Coal Pyrolyzed in Nitrogen
at 1100°C with Injector at 26 cm

PYROLYSIS SUMMARY REPORT - FUHRUN 450

RUN CONDITIONS

5950 mg. VACDRY COAL
0 sec. @ 0 Amps
0 sec. @ 0 Amps
1100 Degrees C. @ 0 torr with ALTUBE grid
765.400 mm. Final Pressure for 63.5250 liters

COAL

Name : UTAH - 8
% ASH = 8.50000

PYROLYSIS PRODUCT DISTRIBUTION

	Dry Wt. %	DAF Wt. %
Char	53.4151	49.0875
Tar	5.66218	6.18818
Gas	16.3053	17.8200
Water	2.01551	2.20275
Missing	22.6018	24.7014

GAS COMPOSITION

	Dry Wt. %	DAF Wt. %	Volume %
Methane	1.50301	1.64264	.21125
CO	2.50127	2.73363	.20088
Hydrogen	0	0	0
CO2	2.84688	3.11134	.14550
Acetylene	.09436	.10313	8.16181E-3
Ethylene	1.40034	1.53043	.11246
Ethane	.54104	.59130	4.05570E-2
Propylene	1.10574	1.20846	5.92053E-2
Paraffins	2.56452	2.80276	.06865
Olefins	3.55989	3.89059	.09530
HCN	.12240	.13377	1.01951E-2
Ammonia	7.85679E-3	8.58665E-3	1.03932E-3
COS	7.52510E-4	8.22415E-4	2.82042E-5
CS2	5.21660E-2	5.70121E-2	1.54357E-3
SO2	5.02864E-3	5.49578E-3	1.76695E-4
Water	2.01551	2.20275	.17432
OTHER	0	0	.20088
Gas Total:	18.3208	20.0227	

Utah Bituminous Coal Pyrolyzed in Nitrogen
at 1100°C with Injector at 36 cm

PYROLYSIS SUMMARY REPORT - FUHRUN 449 10 - 6 - 82

RUN CONDITIONS

4240 mg. VACDRY COAL
0 sec. @ 0 Amps
0 sec. @ 0 Amps
1100 Degrees C. @ 0 torr with ALTUBE grid
765.200 mm. Final Pressure for 75.0750 liters

COAL

Name : UTAH - 12
% ASH = 8.50000

PYROLYSIS PRODUCT DISTRIBUTION

	Dry Wt. %	DAF Wt. %
Char	49.1108	44.3834
Tar	5.54481	6.05990
Gas	24.9082	27.2221
Water	3.03450	3.31639
Missing	17.4015	19.0181

GAS COMPOSITION

	Dry Wt. %	DAF Wt. %	Volume %
Methane	2.77162	3.02909	.23774
CO	4.88777	5.34183	.23957
Hydrogen	0	0	0
CO2	4.49725	4.91503	.14027
Acetylene	.27672	.30243	1.46076E-2
Ethylene	2.52083	2.75500	.12356
Ethane	.54985	.60093	2.51548E-2
Propylene	1.30850	1.43006	4.27585E-2
Paraffins	1.92522	2.10407	3.14556E-2
Olefins	5.62134	6.14354	.09184
HCN	.46095	.50378	2.34312E-2
Ammonia	1.70375E-2	1.86203E-2	1.37548E-3
COS	5.80395E-5	6.34312E-5	1.32760E-6
CS2	.07100	.07759	1.28219E-3
SO2	3.94200E-5	4.30820E-5	8.45344E-7
Water	3.03450	3.31639	.16018
OTHER	0	0	.23957
Gas Total:	27.9427	30.5385	

Utah Bituminous Coal Pyrolyzed in Nitrogen
at 1100°C with Injector at 46 cm

PYROLYSIS SUMMARY REPORT - FUHRUN 446

RUN CONDITIONS

4670 mg. VACDRY COAL
0 sec. @ 0 Amps
0 sec. @ 0 Amps
1100 Degrees C. @ 0 torr with ALTUBE grid
765.600 mm. Final Pressure for 77.9625 liters

COAL

Name : UTAH - 16
% ASH = 8.50000

PYROLYSIS PRODUCT DISTRIBUTION

	Dry Wt. %	DAF Wt. %
Char	44.7323	39.5981
Tar	5.71948	6.25080
Gas	27.7289	30.3048
Water	2.63620	2.88109
Missing	19.1830	20.9650

GAS COMPOSITION

	Dry Wt. %	DAF Wt. %	Volume %
Methane	4.03366	4.40837	.36432
CO	6.98635	7.63535	.36057
Hydrogen	0	0	0
CO2	4.81871	5.26635	.15826
Acetylene	.58875	.64345	3.27244E-2
Ethylene	2.79594	3.05567	.14430
Ethane	.49838	.54468	2.40077E-2
Propylene	.82401	.90055	2.83525E-2
Paraffins	.83594	.91359	1.43815E-2
Olefins	5.36058	5.85856	.09222
HCN	.89201	.97488	4.77440E-2
Ammonia	2.06469E-2	2.25649E-2	1.75515E-3
COS	-8.42276E-4	-9.20520E-4	-2.02867E-5
CS2	.07904	.08639	1.50310E-3
SO2	-4.26656E-3	-4.66290E-3	-9.63399E-5
Water	2.63620	2.88109	.14652
OTHER	0	0	.36057
Gas Total:	30.3651	33.1859	

Utah Bituminous Coal Pyrolyzed in Nitrogen
at 1100°C with Injector at 56 cm

PYROLYSIS SUMMARY REPORT - FUHRUN 447

RUN CONDITIONS

5890 mg. VACDRY COAL
0 sec. @ 0 Amps
0 sec. @ 0 Amps
1100 Degrees C. @ 0 torr with ALTUBE grid
768.400 mm. Final Pressure for 77.9625 liters

COAL

Name : UTAH - 20
% ASH = 8.50000

PYROLYSIS PRODUCT DISTRIBUTION

	Dry Wt. %	DAF Wt. %
Char	45.9575	40.9372
Tar	5.19864	5.68157
Gas	28.7907	31.4652
Water	4.27633	4.67358
Missing	15.7767	17.2423

GAS COMPOSITION

	Dry Wt. %	DAF Wt. %	Volume %
Methane	4.76959	5.21267	.54501
CO	6.97692	7.62505	.45556
Hydrogen	0	0	0
CO2	4.96207	5.42303	.20618
Acetylene	.70767	.77342	4.97629E-2
Ethylene	2.93299	3.20545	.19151
Ethane	.36120	.39475	2.20126E-2
Propylene	.70779	.77354	3.08108E-2
Paraffins	.79848	.87265	1.73791E-2
Olefins	5.29482	5.78669	.11524
HCN	1.17381	1.28285	.07948
Ammonia	2.59791E-2	2.83925E-2	2.79395E-3
COS	-9.42487E-4	-1.03004E-3	-2.87188E-5
CS2	.08293	.09064	1.99517E-3
SO2	-2.63656E-3	-2.88148E-3	-7.53184E-5
Water	4.27633	4.67358	.30070
OTHER	0	0	.45556
Gas Total:	33.0670	36.1388	

Utah Bituminous Coal Pyrolyzed in Nitrogen
at 1100°C with Injector at 66 cm

PYROLYSIS SUMMARY REPORT - FUHRUN 444

RUN CONDITIONS

3650 mg. VACDRY COAL
0 sec. @ 0 Amps
0 sec. @ 0 Amps
1100 Degrees C. @ 0 torr with ALTUBE grid
765.600 mm. Final Pressure for 93.8440 liters

COAL

Name : UTAH - 24
% ASH = 8.50000

PYROLYSIS PRODUCT DISTRIBUTION

	Dry Wt. %	DAF Wt. %
Char	46.8931	41.9597
Tar	6.63013	7.24605
Gas	31.4493	34.3708
Water	2.90364	3.17338
Missing	12.1237	13.2499

GAS COMPOSITION

	Dry Wt. %	DAF Wt. %	Volume %
Methane	4.46555	4.88038	.26011
CO	9.29487	10.1583	.30938
Hydrogen	0	0	0
CO2	6.19711	6.77280	.13126
Acetylene	1.48233	1.62004	5.31362E-2
Ethylene	2.74031	2.99487	.09121
Ethane	.10764	.11764	3.34425E-3
Propylene	.24920	.27235	5.53000E-3
Paraffins	.08134	.08890	9.02574E-4
Olefins	4.56274	4.98660	5.06247E-2
HCN	2.13784	2.33643	.07379
Ammonia	3.20270E-2	3.50022E-2	1.75584E-3
COS	-2.70047E-3	-2.95134E-3	-4.19474E-5
CS2	.10383	.11348	1.27338E-3
SO2	-2.82473E-3	-3.08714E-3	-4.11352E-5
Water	2.90364	3.17338	.10408
OTHER	0	0	.30938
Gas Total:	34.3529	37.5442	